EQUILIBRIUM STATES FOR A CLASS OF DUAL-SPIN SPACECRAFT

by Thomas W. Flatley

Goddard Space Flight Center
Greenbelt, Md. 20771

NATIONAL AERONAUTICS AND SPACE ADMINISTRATION • WASHINGTON, D. C. • MARCH 1971

1. Report No. NASA TR R-362
2. Government Accession No.
3. Recipient's Catalog No.

4. Title and Subtitle

Equilibrium States for a Class of Dual-Spin Spacecraft

5. Report Date
March 1971
6. Performing Organization Code

7. Author(s)
Thomas W. Flatley

8. Performing Organization Report No.
G-1011
9. Performing Organization Name and Address
10. Work Unit No.

Goddard Space Flight Center
Greenbelt, Maryland 20771

11. Contract or Grant No.
13. Type of Report and Period Covered
Technical Report
12. Sponsoring Agency Name and Address
National Aeronautics and Space Administration
Washington, D.C. 20546
14. Sponsoring Agency Code

15. Supplementary Notes

This report was submitted as a thesis in partial fulfillment of the requirements for the degree of Doctor of Philosophy in Aerospace Engineering, The Catholic University of America, May 1970.

16. Abstract

The attitude motion of a dual-spin spacecraft consisting primarily of two symmetric bodies with a common axis of rotation and a constant relative spin rate is analyzed. Each of the main bodies contains a spring-mass-dashpot damper with a degree of freedom parallel to their common axis. The equations of motion are studied by means of a perturbation analysis in which only the damper masses are assumed small. The problem then becomes the determination of perturbations to a reference motion which is similar to the general precession of the torque-free rigid body in classical mechanics.

One of the key parameters associated with such motion is the nutation angle (or the angle between the nominal spin axis and the inertially-fixed angular momentum vector). By determining the zeroth and first order behavior of this angle for this system, a general analytical stability criterion is established. This criterion not only determines the stability or instability of an arbitrary initial state of the system, but reveals the nature of any instability which might exist. In reduced form, the stability criterion verifies results in the recent literature obtained by Routhian and Floquet analyses of linearized equations representing special cases of this system.

17. Key Words Suggested by Author

Dual-Spin Spacecraft
Spacecraft Attitude Stability
Dynamic Analysis

18. Distribution Statement

Unclassified—Unlimited

19. Security Classif. (of this report)	20. Security Classif. (of this page)	21. No. of Pages	22. Price*
Unclassified	Unclassified	85	$3.00

*For sale by the National Technical Information Service, Springfield, Virginia 22151

CONTENTS

LIST OF SYMBOLS

a	distance of spacecraft damper from spin axis
a'	distance of wheel damper from spin axis
$\mathbf{a}$	damper mass acceleration vector
A	nominal system transverse moment of inertia
A'	integration constant
B'	integration constant
c	spacecraft damper damping coefficient
c'	wheel damper damping coefficient
C	nominal system spin moment of inertia
C_i	integration constants, $i = 1, 2, \ldots, 6$
C'	integration constant
$\delta\mathbf{v}$	$\mathbf{v} - \mathbf{v}_0$
$\delta\mathbf{v}'$	$\mathbf{v}' - \mathbf{v}'_0$
$\mathbf{e}$	unit vector along damper axis
e_i	components of $\mathbf{e}$, $i = 1, 2, 3$
$\mathbf{F}$	total force on damper mass
$\mathbf{F}_0$	total force on caged damper mass
$f(\theta)$	$F(\theta) \sin\theta$
$f'(\theta)$	$df/d\theta$
$F(\theta)$	primary stability function
$\mathbf{H}$	total angular momentum vector

H	$\|\mathbf{H}\|$
H_3	spin component of angular momentum vector
I_1	spacecraft transverse moment of inertia
I_1'	wheel transverse moment of inertia
I_3	spacecraft spin moment of inertia
I_3'	wheel spin moment of inertia
J_3'	spin moment of inertia of wheel, damper, and balance weights
k	spacecraft damper spring constant
k'	wheel damper spring constant
$\mathbf{k}$	unit vector parallel to nominal spin axis
k_1	$\lambda/(\sigma - \lambda)$
K	dimensionless spacecraft damper spring constant
K'	dimensionless wheel damper spring constant
K_1	damper spring constant
l	distance between spacecraft and wheel centers of mass
l_1	distance between spacecraft and nominal system centers of mass
l_2	distance between wheel and nominal system centers of mass
$\mathcal{L}$	the Lagrangian
m	spacecraft damper active mass
m'	wheel damper active mass
m_b	total mass of spacecraft damper, and mass of spacecraft balance weight
m_b'	total mass of wheel damper, and mass of wheel balance weight
M	mass of spacecraft
M'	mass of wheel
M_T	total mass of system
P	energy dissipation rate

$\bar{P}$	average energy dissipation rate
P_S	average energy dissipation rate on spacecraft
P_W	average energy dissipation rate on wheel
q	C/A
q'	J_3'/A
Q_z	generalized force associated with spacecraft damper
Q_z'	generalized force associated with wheel damper
r_Ω	dimensionless spacecraft spin rate
r_σ	dimensionless relative spin rate of the wheel
$\mathbf{r}$	damper active mass position vector
$\mathbf{r}'$	wheel damper active mass position vector
$\mathbf{r}_m$	spacecraft damper active mass position vector
$\mathbf{r}_0$	damper position vector
t	time
T	system kinetic energy
T_i	components of kinetic energy, $i = 0, 1, 2$
$\boldsymbol{\Gamma}$	reaction torque vector
$\boldsymbol{\Gamma}_0$	reaction torque with damper caged
T_s	spin component of $\mathbf{T} - \mathbf{T}_0$ due to spacecraft damper
T_s'	spin component of $\mathbf{T} - \mathbf{T}_0$ due to wheel damper
$\bar{T}_s$	average value of T_s
$\bar{T}_s'$	average value of T_s'
$\mathbf{v}$	velocity of spacecraft damper mass
$\mathbf{v}_0$	velocity of caged spacecraft damper mass
$\mathbf{v}'$	velocity of wheel damper mass
$\mathbf{v}_0'$	velocity of caged wheel damper mass

ν	$\lvert\mathbf{v}\rvert$
ν_0	$\lvert\mathbf{v}_0\rvert$
ν'	$\lvert\mathbf{v}'\rvert$
ν'_0	$\lvert\mathbf{v}'_0\rvert$
V	system potential energy
x	deviation of θ from equilibrium value
x_0	spacecraft damper position coordinate
x'_0	wheel damper position coordinate
z	spacecraft damper displacement coordinate
z'	wheel damper displacement coordinate
$\bar{z}$	coordinate of system center of mass in spacecraft-fixed coordinate system
z_0	spacecraft damper position coordinate
z'_0	wheel damper position coordinate
a	constant forcing function
β	$(\delta/\delta')^{1/2}$
β_1	amplitude of sinusoidal forcing function
γ	frequency of forcing function
δ	ma^2/A
δ'	$m'a'^2/A$
η	$\lvert q\Omega_0 + q'\sigma\rvert$
λ	nutation frequency in spacecraft-fixed coordinate system
λ_0	initial state nutation frequency
Λ	dimensionless nutation frequency
ν	$(M' + 4m'_b)/M_T$
ω_i	spacecraft angular velocity components in spacecraft-fixed coordinate system, $i = 1, 2, 3$
ω	spacecraft transverse angular velocity

$\boldsymbol{\omega}$	spacecraft transverse angular velocity vector
$\boldsymbol{\omega}_T$	spacecraft total angular velocity vector
ω_T	$\lvert\boldsymbol{\omega}_T\rvert$
Ω	spacecraft spin rate
$\boldsymbol{\Omega}$	spacecraft spin vector
Ω_0	initial state spacecraft spin rate
Ω_{01},Ω_{02}	spacecraft spin rates for initial states inverted relative to one another
φ	third Euler angle
φ_1	phase angle of forcing function
ψ	angle between spacecraft-fixed and wheel-fixed coordinate systems
ψ_1	first Euler angle
$\dot{\psi}_1$	system precession rate
ρ	m/M_T
ρ'	m'/M_T
$\boldsymbol{\rho}$	damper displacement vector
ρ_1	spacecraft damper displacement coordinate
ρ_1'	wheel damper displacement coordinate
σ	relative spin rate of wheel
$\sigma_1,\sigma_2,\sigma_{cr}$	critical values of σ
θ	nutation or cone angle, second Euler angle
θ_0	particular value of cone angle
τ	time constant
ζ	$\rho z + \rho' z'$

EQUILIBRUM STATES FOR A CLASS OF DUAL-SPIN SPACECRAFT*

by
Thomas W. Flatley
Goddard Space Flight Center

CHAPTER 1

INTRODUCTION

Since the dramatic and unexpected attitude instability experienced by the first United States artificial satellite (Reference 1), now a textbook example (Reference 2) of the possible effects of energy dissipation on "torque-free rigid body" motion, a design rule of thumb for gyroscopically stabilized spacecraft has been that such a body must spin about its maximum moment of inertia axis. Recently, however, a control concept that promises to relieve this increasingly burdensome constraint, while keeping much of the basic simplicity of the simple spinners, has emerged. It is known as *dual-spin* stabilization and in its simplest form features a rotor mounted on the nominal spin axis of the spacecraft and some type of passive damper.

The basic idea had its beginning in the largely intuitive work of Vernon Landon in 1962. Unfortunately, his early claims were greeted with great skepticism, and his first attempt to publish his results was rejected. The dual-spin principle reached the open literature in 1963 (Reference 3) and 1964 (Reference 4) and has been the subject of intensive research and frequent publication over the second half of the 1960's. In fact, a symposium (Reference 5) held in El Segundo, California, in 1967 was devoted entirely to this subject.

Understandably, published analyses have focused almost exclusively on the stability of pure rotations about the nominal spin axis. A variety of approaches to this problem are found in the literature, most of which involve linearization of equations of motion (derived either heuristically or exactly for specific systems) and analysis by informal averaging, "energy sink" approaches, and the more rigorous Routhian, Floquet, and Lyapunov methods. In some of these papers, one of the bodies is assumed to be completely despun.

*This report was submitted as a thesis in partial fulfillment of the requirements for the degree of Doctor of Philosophy in Aerospace Engineering, The Catholic University of America, May 1970.

However, the nature of dual-spin instabilities has been largely ignored in the literature. The subject has been mentioned, notably by Fang (References 6 and 7) and Cloutier (References 8 and 9), but mostly in connnection with possible small system principal-axis shifts and equilibrium states involving damper masses displaced from their nominal positions. Cloutier (Reference 10) also discusses possible instabilities in the motion of a specific type of damper whose behavior is governed by Mathieu-type equations.

A general analysis of dual-spin instabilities is not available, however. The research reported here addresses this problem by analyzing the detailed nonlinear equations of motion for a particular but fairly general dual-spin system by a perturbation analysis in which only the damper masses are assumed small and which involves variations in a general precessional motion of the system with an arbitrarily large cone angle.

Among the various papers listed as references at the end of this report, the work of Mingori (Reference 11) is particularly pertinent to the research reported here. The particular system chosen for detailed analysis is basically that studied in his paper, the notation used is similar to his, and the results obtained are frequently compared to those presented in the referenced publication.

The basic objective of this work is to develop a better understanding of the physical principles involved in dual-spin stabilization by seeking equilibrium states for a dual-spin system (analogous to the "flat-spin" or "tumble" condition for single-spin bodies) which represent final states for unstable dual-spin configurations.

Terminology can sometimes be a problem in applied mechanics, particularly in the area of rotational dynamics. Imprecisely or inconsistently defined terms and colloquial expressions can often be confusing. A brief review of the general motion of a torque-free symmetric rigid body will serve to define the various terms as they are used herein.

In Figure 1.1, the 3-axis is the axis of symmetry for the cylindrical body shown and will be referred to as the *nominal spin axis.* That component of the angular velocity vector parallel to this axis will be called the *spin rate*; terms such as *spin component* and *spin moment of inertia* will refer to the nominal spin axis. The word *transverse* will imply a direction normal to the nominal spin axis (e.g., transverse angular velocity, transverse moment of inertia, and so forth).

The angle θ between the inertially fixed angular momentum vector **H** and the nominal spin axis is the *nutation angle*, or *cone angle.* In the strict sense, nutation involves variations in this angle; but, in accordance with popular usage and for lack of a better word, the rate at which the transverse angular velocity vector rotates in a body-fixed coordinate system will be referred to as the *nutation rate.*

The motion of the nominal spin axis around the angular momentum vector is *precession*, and the corresponding rate is the *precession rate.* One source of confusion is the fact that this phenomenon is observable only when there is a nutation angle, i.e., if the angular momentum vector and the nominal spin axis are not coincident. In this case, the motion is popularly referred to by various authors as *precession*, *nutation*, *coning*, or *wobble.*

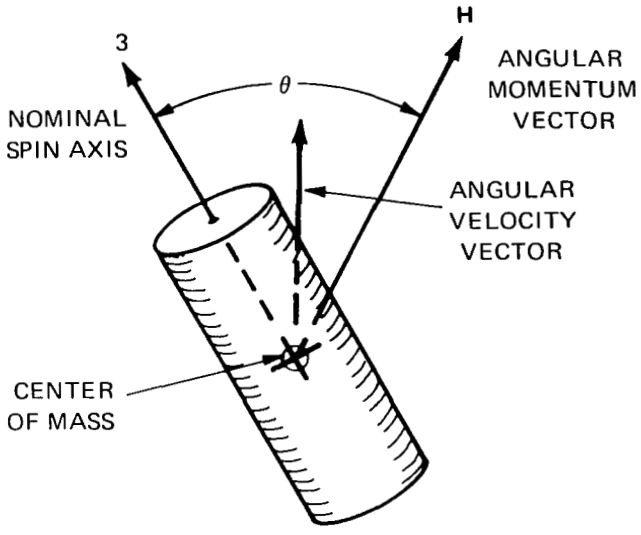

Figure 1.1—Symmetric rigid body.

For a symmetric body, the total angular velocity vector and the nominal spin axis are coplanar with the angular momentum vector and rotate about it at the precession rate.

With a rigid body, all of the above-mentioned quantities are constants of the motion. It is now well known, however, that inevitable energy dissipation in real systems (i.e., quasi-rigid bodies) can drastically change the characteristics of the motion. The effect is critically dependent on the moment-of-inertia ratio $q = C/A$, where C and A are the spin and transverse moments of inertia, respectively. For $q > 1$, any coning is damped out, and an eventual pure rotation about the nominal spin axis is attained. With $q < 1$, the nutation angle increases with time toward a stable equilibrium value of 90°, reaching what is commonly called a *flat spin* or *tumble*. In any case, the final state is a minimum-energy state for the system consistent with the amount of angular momentum present.

CHAPTER 2

SYSTEM DEFINITION AND EQUATIONS OF MOTION

The particular dual-spin system to be analyzed consists of two primary bodies with a common axis of rotation and a motor that maintains an arbitrary but constant relative spin rate σ. For convenience, these bodies will be referred to herein as a *spacecraft* and a *wheel*, although the relative size, weight, and moments of inertia of the two parts are unrestricted. Each is basically symmetric with respect to its common axis, which will be called the nominal spin axis. Schematically, they will be represented as bodies of revolution (Figure 2.1). The spacecraft has a mass M, a spin moment of inertia I_3, and a transverse moment of inertia I_1. Corresponding properties of the wheel are M', I'_3, and I'_1. The centers of mass of the two bodies are a fixed distance l apart.

Attached to each of the primary bodies is a spring-mass-dashpot damper with a single degree of freedom parallel to the nominal spin axis. The spacecraft damper is at a distance a from the spin axis in a plane containing the center of mass. It has a total mass m_b, an active mass m, a spring constant k, a damping coefficient c, and a displacement coordinate z. The wheel damper is similarly specified by the constants a', m'_b, m', k', and c' and a displacement coordinate z'.

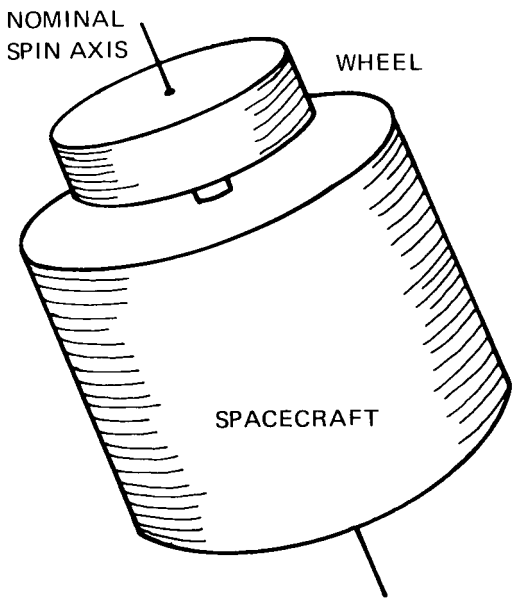

Figure 2.1—Dual-spin system.

To provide static and dynamic balance of the system when the active masses of the dampers are at rest (i.e., $z = z' = 0$), six balance weights, three each of masses m_b and m'_b, are added as shown in Figure 2.2. This figure also shows a set of transverse principal axes for each of the bodies, arbitrarily chosen such that the l- and l'-axes pass through the dampers.

Figure 2.3 shows a complete description of the system to be analyzed.

The equations of motion for this system are presented, without derivation, by Mingori in Reference 11. They are rederived in Appendix I and agree in every detail with those in the literature. They form a seventh-order, nonlinear, nonautonomous set, inconveniently coupled even in the highest derivatives.

In essence, the first three equations (2.1 through 2.3) govern the basic attitude behavior of the system and are

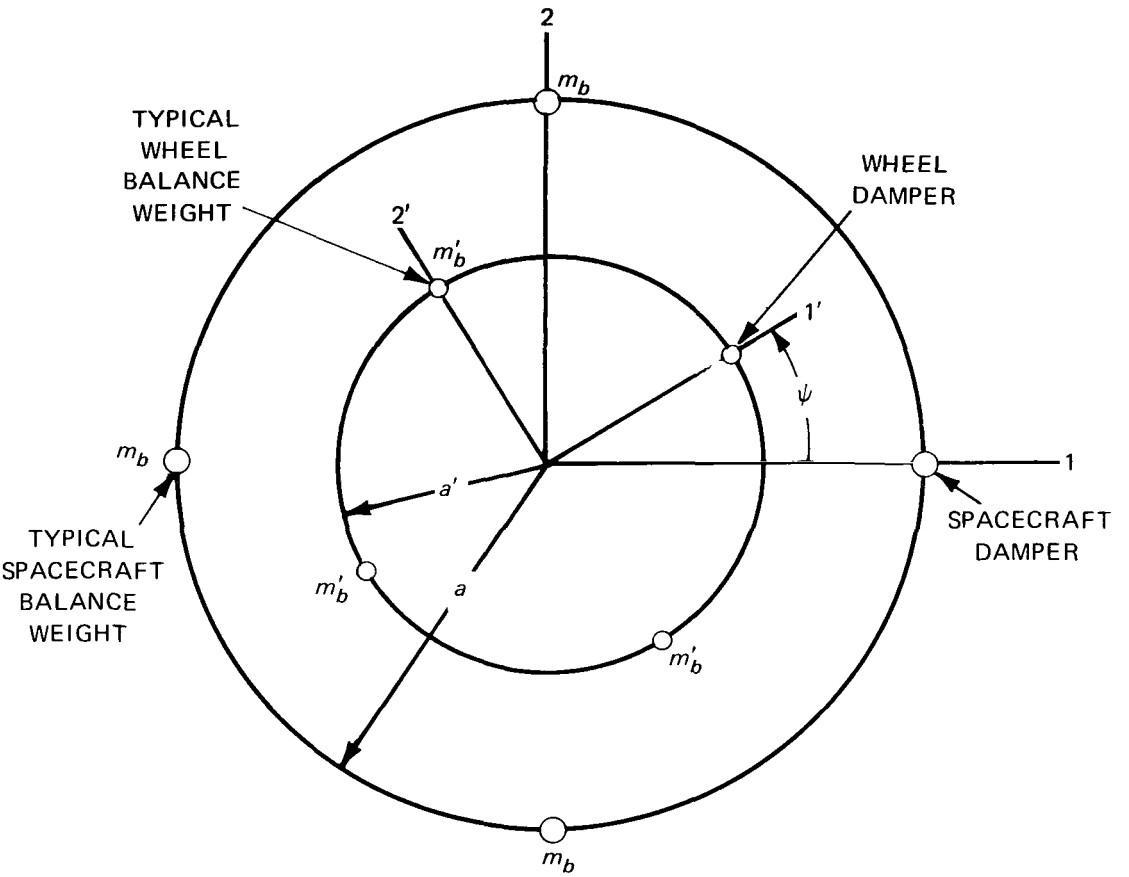

Figure 2.2—Balance weights and transverse principal axes.

analogous to the classical Euler equations of motion for a rigid body. Equations 2.4 and 2.5 are second-order equations which primarily determine the motion of the active masses of the dampers.

In spite of the complex nature of the system of equations, we are assured *a priori* of the existence of a first integral of the motion corresponding to the total angular momentum. In principle, this fact could be used to reduce the order of the system by one, but of more interest here is the fact that the lack of external torques guarantees that the total angular momentum vector will be a constant of the motion. We will take advantage of both the constant magnitude of this vector and the inertially fixed reference direction it provides.

$$
\begin{aligned}
&[A + M_T\zeta^2 + mz^2 - 2m(\zeta + l_2)z + m'z'^2 - 2m'(\zeta - l_1)z']\dot{\omega}_1 - (maz + m'a'z'\cos\psi)\dot{\omega}_3 \pm m'a'\sin\psi\,\ddot{z}' \\
&\quad = (A - C)\omega_2\omega_3 - J'_3\sigma\omega_2 - 2M_T\zeta\dot{\zeta}\omega_1 + M_T\zeta^2\omega_2\omega_3 + 2m(\zeta + l_2)(\dot{z}\omega_1 - z\omega_2\omega_3) \\
&\quad + mz(2\dot{\zeta}\omega_1 - 2\dot{z}\omega_1 + z\omega_2\omega_3 + a\omega_1\omega_2) + 2m'(\zeta - l_1)(\dot{z}'\omega_1 - z'\omega_2\omega_3) \\
&\quad + m'z'(2\dot{\zeta}\omega_1 - 2\dot{z}'\omega_1 + z'\omega_2\omega_3 + a'\cos\psi\,\omega_1\omega_2) - m'a'z'\sin\psi\,[(\omega_3 + \sigma)^2 - \omega_2^2]\,, \qquad (2.1)
\end{aligned}
$$

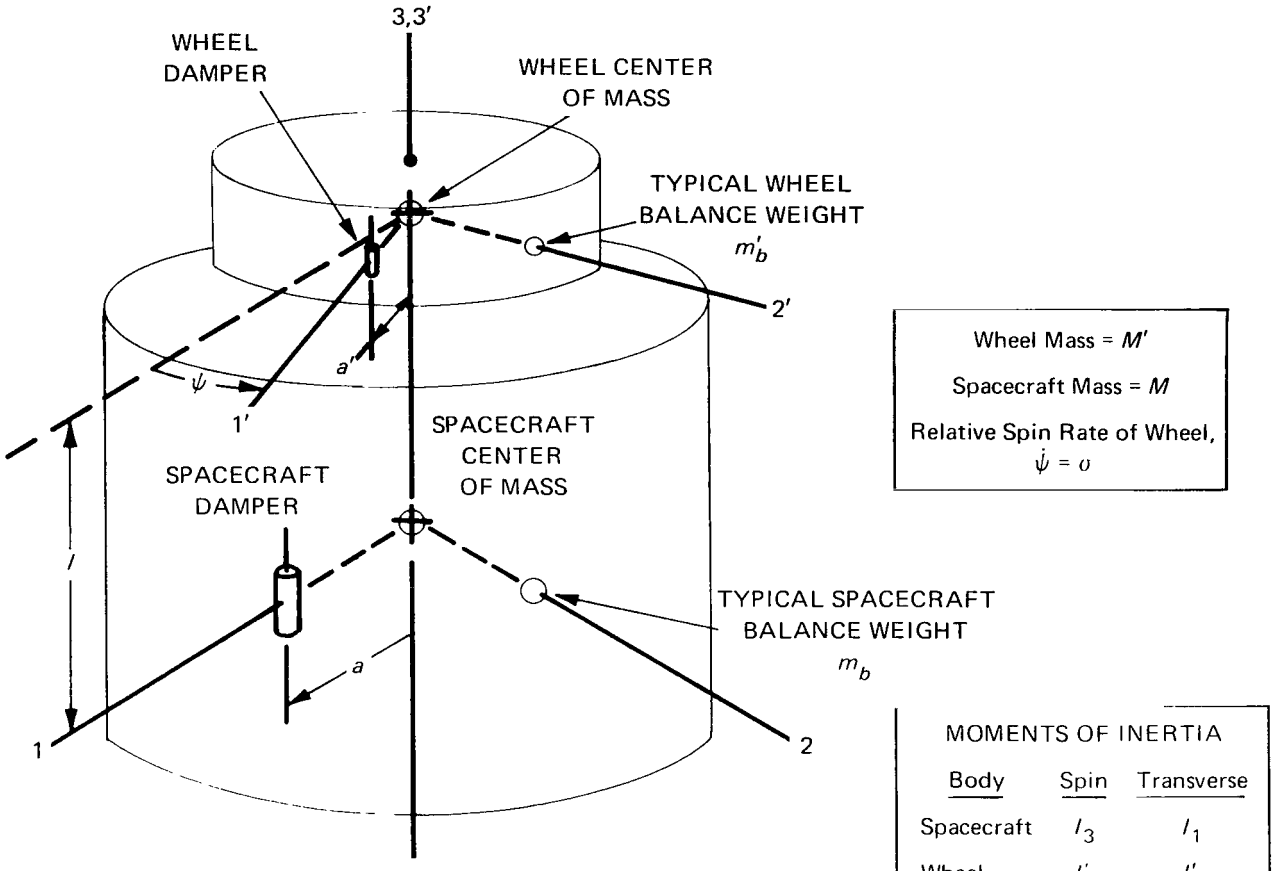

Wheel Mass = M'

Spacecraft Mass = M

Relative Spin Rate of Wheel, $\dot{\psi} = \sigma$

MOMENTS OF INERTIA

Body	Spin	Transverse
Spacecraft	I_3	I_1
Wheel	I'_3	I'_1

DAMPER PROPERTIES

Property	Spacecraft	Wheel
Total Mass	m_b	m'_b
Active Mass	m	m'
Spring Constant	k	k'
Damping Coefficient	c	c'
Displacement Coordinate	z	z'

TYPICAL DAMPER SCHEMATIC

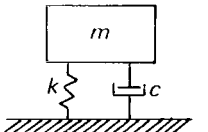

Figure 2.3—Definition of specific dual-spin system.

$$[A + M_T\xi^2 + mz^2 - 2m(\xi + l_2)z + m'z'^2 - 2m'(\xi - l_1)z']\dot{\omega}_2 - m'a'z' \sin\psi\ \dot{\omega}_3 - ma\ddot{z} - m'a' \cos\psi\ \ddot{z}'$$
$$= (C - A)\omega_1\omega_3 + J'_3\sigma\omega_1 - 2M_T\xi\dot{\xi}\omega_2 - M_T\xi^2\omega_1\omega_3 + 2m(\xi + l_2)(\dot{z}\omega_2 + z\omega_1\omega_3)$$
$$+ mz(2\dot{\xi}\omega_2 - 2\dot{z}\omega_2 - z\omega_1\omega_3) + maz(\omega_3^2 - \omega_1^2) + 2m'(\xi - l_1)(z'\omega_1\omega_3 + \dot{z}'\omega_2)$$
$$+ m'z'(2\dot{\xi}\omega_2 - 2\dot{z}'\omega_2 - z'\omega_1\omega_3) + m'z'[(\omega_3 + \sigma)^2 - \omega_1^2]a' \cos\psi - m'a' \sin\psi\ z'\omega_1\omega_2\ , \quad (2.2)$$

$$-(maz + m'a'z' \cos\psi)\dot{\omega}_1 - m'a' \sin\psi\, z'\dot{\omega}_2 + C\dot{\omega}_3$$

$$= ma(2\dot{z}\omega_1 - z\omega_2\omega_3) + m'a' \sin\psi(2\dot{z}'\omega_2 + z'\omega_1\omega_3) + m'a' \cos\psi(2\dot{z}'\omega_1 - z'\omega_2\omega_3)\,, \quad (2.3)$$

$$-ma\dot{\omega}_2 + m(1-\rho)\ddot{z} - m'\rho\ddot{z}' = -ma\omega_1\omega_3 + m(\omega_1^2 + \omega_2^2)[z(1-\rho) - l_2 - \rho'z'] - c\dot{z} - kz\,, \quad (2.4)$$

and

$$m'a' \sin\psi\, \dot{\omega}_1 - m'a' \cos\psi\, \dot{\omega}_2 - m\rho'\ddot{z} + m'(1-\rho')\ddot{z}'$$

$$= -m'a'[\sin\psi\, \omega_2(\omega_3 + 2\sigma) + \cos\psi\, \omega_1(\omega_3 + 2\sigma)]$$

$$+ m'(\omega_1^2 + \omega_2^2)[z'(1-\rho') + l_1 - \rho z] - c'\dot{z}' - k'z'\,. \quad (2.5)$$

These equations are written in terms of the following useful combinations of constants and variables in order to reduce the number of terms:

$$M_T = M + M' + 4m_b + 4m_b'\,,$$

$$\rho = \frac{m}{M_T}\,,$$

$$\rho' = \frac{m'}{M_T}\,,$$

$$\zeta = \rho z + \rho' z'$$

$$l_1 = \frac{l(M + 4m_b)}{M_T}\,,$$

$$l_2 = \frac{l(M' + 4m_b')}{M_T}\,,$$

$$A = I_1 + I_1' + 2m_b a^2 + 2m_b' a'^2 + (M + 4m_b)(M' + 4m_b')\frac{l^2}{M_T}\,,$$

$$C = I_3 + I_3' + 4m_b a^2 + 4m_b' a'^2\,,$$

and

$$J_3' = I_3' + 4m_b' a'^2\,.$$

The constant M_T is the total mass of the system, A is the combined transverse moment of inertia of the system about the center of mass with the damper masses at rest, and C is the combined spin moment of inertia, which includes J_3' (the spin moment of inertia of the wheel, its damper, and its balance weights).

CHAPTER 3

PERTURBATION ANALYSIS, PART I: UNPERTURBED MOTION OF THE SYSTEM AND FIRST-ORDER DAMPER MOTION

An approximate solution of the equations of motion will be carried out with the assumption that the effects of the dampers are a small perturbation on the general "rigid body" motion of the system. The "zeroth-order" equations (which represent the unperturbed state, or the reference motion, of the system) are easily obtained if the masses m and m' are allowed to vanish in Equations 2.1, 2.2, and 2.3. The resulting set of equations is as follows:

$$A\dot{\omega}_1 + (C - A)\omega_2\omega_3 + J'_3\sigma\omega_2 = 0 , \tag{3.1}$$

$$A\dot{\omega}_2 - (C - A)\omega_1\omega_3 - J'_3\sigma\omega_1 = 0 , \tag{3.2}$$

and

$$C\dot{\omega}_3 = 0 . \tag{3.3}$$

Equation 3.3 has the obvious solution ω_3 = constant, and we will label that constant Ω. Substituting this solution into Equations 3.1 and 3.2 reduces them to a pair of constant-coefficient linear equations with an elementary solution:

$$\dot{\omega}_1 + \lambda\omega_2 = 0$$

and

$$\dot{\omega}_2 - \lambda\omega_1 = 0 ,$$

where

$$A\lambda = (C - A)\Omega + J'_3\sigma .$$

Thus, ω_1 and ω_2 are sinusoidal functions with a constant amplitude ω and frequency λ. Without loss of generality, we can select a reference time when $\omega_2 = 0$ and write these solutions as

$$\omega_1 = \omega \cos \lambda t$$

and

$$\omega_2 = \omega \sin \lambda t ,$$

where ω is the amplitude of ω_1 at $t = 0$.

A. Characteristics of Reference Motion

The equations above show that the unperturbed motion of the dual-spin system being studied is very similar to the general precessional motion of the torque-free, symmetric, rigid body in classical mechanics. Figure 3.1 is a representation of the behavior of the angular velocity vector in the spacecraft-fixed coordinate system.

The 3-component (or the spacecraft spin rate) is constant with a magnitude of Ω, and the transverse component is of fixed magnitude ω but rotates around the 3-axis (or nominal spin axis) at a rate λ.

Figure 3.2 shows the motion of the angular momentum vector in the same reference frame, the spin and transverse components of angular momentum, and the cone angle θ.

The quantities ω, Ω, λ, H, and θ are constants of the unperturbed motion of the system. The actual motion of the nominal spin axis (Figure 3.3) is a steady precession on a cone of half-angle θ around a fixed angular momentum vector. This would be the motion seen by an outside observer, and the precession rate is given by $\dot{\psi}_1 = H/A$, obviously another constant of the motion.

Qualitatively, this motion is exactly that of the classical, torque-free, symmetric, rigid body, but there are quantitative differences due to the presence of the wheel. The nutation rate λ and precession rate $\dot{\psi}_1$ are given by

$$\lambda = \left(\frac{C}{A} - 1\right)\Omega + \frac{J_3'}{A}\sigma$$

and

$$\dot{\psi}_1 = \frac{C\Omega + J_3'\sigma}{A\cos\theta}.$$

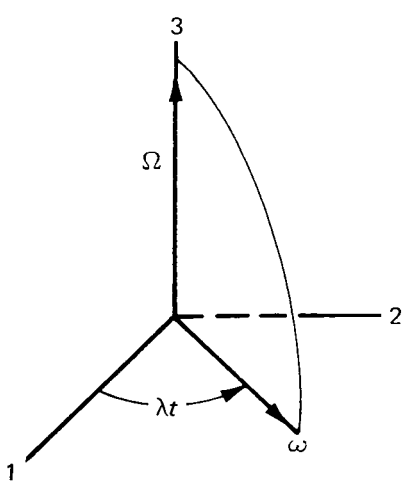

Figure 3.1—Angular velocity vector in body coordinates.

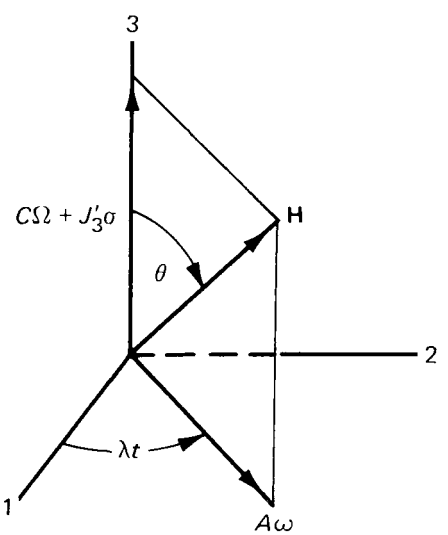

Figure 3.2—Angular momentum vector in body coordinates.

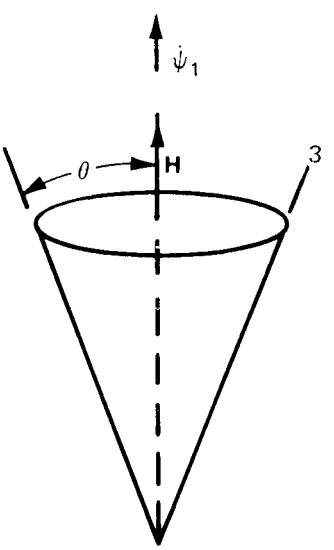

Figure 3.3—Actual motion of nominal spin axis.

When $\sigma = 0$, the system is reduced to exactly the classical rigid body with the familiar expressions

$$\lambda = \left(\frac{C}{A} - 1\right)\Omega$$

and

$$\dot{\psi}_1 = \frac{C\Omega}{A\cos\theta} \approx \frac{C}{A}\Omega \quad \text{for} \quad \theta \ll 1 .$$

B. First-Order Damper Motion

To find a first approximation for the motion of the active masses in the two dampers, we turn to Equations 2.4 and 2.5, retain all terms linear in the damper masses m and m', and substitute the zeroth-order angular velocities determined above. The resulting equations are

$$m\ddot{z} + c\dot{z} + (k - m\omega^2)z = ma\omega(\lambda - \Omega)\cos\lambda t - m\omega^2 l_2 \tag{3.4}$$

and

$$m'\ddot{z}' + c'\dot{z}' + (k' - m'\omega^2)z' = m'a'\omega(\lambda - \Omega - 2\sigma)\cos(\sigma - \lambda)t + m'\omega^2 l_1 . \tag{3.5}$$

Equations 3.4 and 3.5 are similar in form and are simply representations of classical forced, damped, harmonic oscillations. Their steady-state solutions can be written as

$$z = C_1 + C_2 \sin\lambda t + C_3 \cos\lambda t$$

and

$$z' = C_4 + C_5 \sin(\sigma - \lambda)t + C_6 \cos(\sigma - \lambda)t ,$$

where the constants C_i can easily be shown to be

$$C_1 = \frac{\omega^2 l_2}{\omega^2 - \frac{k}{m}} ,$$

$$C_2 = \frac{a\frac{c}{m}\lambda\omega(\lambda - \Omega)}{\left(\frac{k}{m} - \omega^2 - \lambda^2\right)^2 + \left(\frac{c}{m}\lambda\right)^2} ,$$

$$C_3 = \frac{a\omega(\lambda - \Omega)\left(\frac{k}{m} - \omega^2 - \lambda^2\right)}{\left(\frac{k}{m} - \omega^2 - \lambda^2\right)^2 + \left(\frac{c}{m}\lambda\right)^2} ,$$

$$C_4 = \frac{\omega^2 l_1}{\frac{k'}{m'} - \omega^2} ,$$

$$C_5 = \frac{a' \frac{c'}{m'} \omega(\sigma - \lambda)(\lambda - \Omega - 2\sigma)}{\left[\frac{k'}{m'} - \omega^2 - (\lambda - \sigma)^2\right]^2 + \left[\frac{c'}{m'}(\sigma - \lambda)\right]^2},$$

and

$$C_6 = \frac{a'\omega(\lambda - \Omega - 2\sigma)\left[\frac{k'}{m'} - \omega^2 - (\sigma - \lambda)^2\right]}{\left[\frac{k'}{m'} - \omega^2 - (\lambda - \sigma)^2\right]^2 + \left[\frac{c'}{m'}(\sigma - \lambda)\right]^2}.$$

Thus far, we have determined the unperturbed motion of the dual-spin system and, in effect, have assumed that this basic motion drives the two dampers. Having found the steady-state response of the damper masses to the precessional excitation, we now seek the effect of their oscillatory motions on the attitude motion of the system.

CHAPTER 4

PERTURBATION ANALYSIS, PART II: ATTITUDE DISTURBANCE AND STABILITY CONSIDERATIONS

Since the physical system under consideration is free of external torques, the total angular momentum vector will be a constant of the motion. The magnitude of this vector, $H = |\mathbf{H}|$, will be a first integral of the exact equations of motion The fixed direction of the angular momentum vector provides a useful inertial reference line, and in consideration of the attitude behavior of the system, it is convenient to concentrate attention on the motion of the nominal spin axis relative to this fixed line.

The cone angle $0 \leqslant \theta \leqslant \pi$ between the angular momentum vector and the nominal spin axis is a key parameter relative to the stability of possible motions. Knowledge of its behavior as a function of time is the usual objective in stability analyses for spin-stabilized spacecraft.

Now, if the constant angular momentum vector is decomposed into components perpendicular and parallel to the nominal spin axis (the 3-axis in Figure 4.1), the magnitude of the latter vector will obviously be

$$H_3 = H \cos\theta \,. \tag{4.1}$$

For the system under consideration, however, this component of the angular momentum can also be shown to be

$$H_3 = C\omega_3 + J'_3\sigma - maz\omega_1 - m'a'z'(\omega_1 \cos\psi + \omega_2 \sin\psi) \,. \tag{4.2}$$

Thus,

$$H \cos\theta = C\omega_3 + J'_3\sigma - maz\omega_1 - m'a'z'(\omega_1 \cos\psi + \omega_2 \sin\psi) \,.$$

Differentiating both sides of this equation with respect to time and eliminating $\dot{\omega}_3$ by use of Equation 2.3 yields an exact relationship:

$$\begin{aligned} -H \sin\theta\,\dot{\theta} = {} & ma(\dot{z}\omega_1 - z\omega_2\omega_3) + m'a'z'(\omega_3 + \sigma)(\omega_1 \sin\psi - \omega_2 \cos\psi) \\ & + m'a'\dot{z}'(\omega_1 \cos\psi + \omega_2 \sin\psi) \,. \end{aligned} \tag{4.3}$$

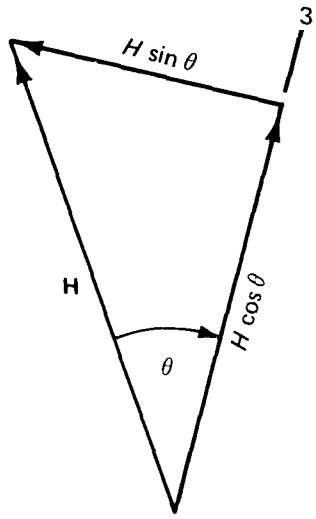

Figure 4.1—Decomposition of angular momentum vector.

Equation 4.3 represents an exact equation of motion for the system cone angle θ. The right side of this equation contains the small parameters m and m'. If $m = m' = 0$, the cone angle is a constant of the motion (as seen also in Chapter 3).

To determine the first-order perturbation of the cone angle, we substitute the approximate expressions for the body rates and the damper motions found in Chapter 3, repeated here for convenience:

$$\omega_1 = \omega \cos \lambda t ,$$

$$\omega_2 = \omega \sin \lambda t ,$$

$$\omega_3 = \Omega ,$$

and

$$z = C_1 + C_2 \sin \lambda t + C_3 \cos \lambda t ,$$

$$z' = C_4 + C_5 \sin (\sigma - \lambda)t + C_6 \cos (\sigma - \lambda)t .$$

Substituting first for the body rates, assuming, without loss of generality, that $\psi(0) = 0$ we obtain

$$-H \sin \theta \, \dot{\theta} = ma\omega(\dot{z} \cos \lambda t - z\Omega \sin \lambda t) + m'a'\omega[z'(\Omega + \sigma) \sin (\sigma - \lambda)t + \dot{z}' \cos (\sigma - \lambda)t] . \quad (4.4)$$

Now, substituting for z and z' would produce sin, cos, $\sin^2$, and $\cos^2$ terms with arguments λt and $(\sigma - \lambda)t$. Through use of trigonometric identities, the squared terms may be eliminated, and the resulting equation would contain only constants and sinusoidal oscillatory terms. In the spirit of the method of averaging (Reference 12), then, the systematic change of θ is considered to be controlled by the constant terms, with the periodic terms contributing only small oscillations of θ about some average value.

With only the constant terms retained, the secular behavior of the cone angle is found to be governed by the equation

$$-H \sin \theta \, \dot{\theta} = ma\omega(\lambda - \Omega) \frac{C_2}{2} + m'a'\omega(2\sigma - \lambda + \Omega) \frac{C_5}{2} . \quad (4.5)$$

Substituting the calculated values of C_2 and C_5 from Chapter 3 and approximating the transverse momentum $H \sin \theta$ by the transverse angular momentum of the unperturbed motion $A\omega$ yields

$$\dot{\theta} = -\frac{H \sin \theta}{2A^2} \left\{ \frac{a^2 c \lambda (\lambda - \Omega)^2}{\left(\frac{k}{m} - \omega^2 - \lambda^2\right)^2 + \left(\frac{c}{m}\lambda\right)^2} - \frac{a'^2 c' (\sigma - \lambda)(2\sigma - \lambda + \Omega)^2}{\left[\frac{k'}{m'} - \omega^2 - (\sigma - \lambda)^2\right]^2 + \left[\frac{c'}{m'}(\sigma - \lambda)\right]^2} \right\} . \quad (4.6)$$

Now, each term within the brackets above is either a fixed constant or a constant of the unperturbed motion of the system. These latter constants can be expressed explicitly in terms of the cone angle θ as follows:

$$\omega = \frac{H \sin\theta}{A},$$

$$\Omega = \frac{H \cos\theta - J_3'\sigma}{C},$$

and

$$\lambda = \frac{(C - A)H \cos\theta + AJ_3'\sigma}{AC}.$$

Equation 4.6 is thus of the form $\dot{\theta} = f(\theta)$, and for a first-order differential equation such as this, questions of stability are almost trivial. Equilibrium will obviously be possible whenever $f(\theta) = 0$, and the stability of any equilibrium point depends on the value of a derivative of $f(\theta)$, usually the first, at that point. Figure 4.2 shows this in graphical form.

The labels U, M, and S identify points of unstable, metastable, and stable equilibrium, respectively; the arrows show the direction of motion along the phase plane trajectory. Stable equilibrium at $\theta = \theta_0$ is seen to require $f(\theta_0) = 0$ and $f'(\theta_0) < 0$.

Equation 4.6 is rather remarkable in that it represents a single first-order differential equation that determines the overall attitude behavior of a seventh-order, nonlinear, nonautonomous system with arbitrary initial conditions. Plotting the function $f(\theta)$ for any particular dual-spin configuration would immediately reveal the stability characteristics of the system, indicate "zones of attraction" for particular stable equilibrium points, and show the "time constant" associated with cone-angle buildup or decay near equilibrium states.

The time constant τ is given by the inverse of the slope of $f(\theta)$ at the equilibrium point, as shown below:

With

$$\dot{\theta} = f(\theta)$$

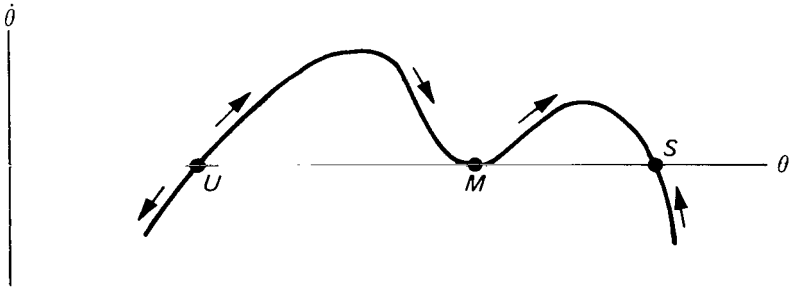

Figure 4.2—Equilibrium and stability if $f(\theta) = 0$.

and

$$f(\theta_0) = 0 ,$$

let

$$\theta = \theta_0 + x .$$

Then,

$$\dot{\theta} = \dot{x}$$

and

$$f(\theta) = f(\theta_0 + x) \approx f(\theta_0) + xf'(\theta_0) ,$$

so

$$\dot{x} \approx xf'(\theta_0) .$$

Thus,

$$\frac{dx}{x} = f'(\theta_0)\, dt ,$$

and the solution can be written as

$$x = x(0)e^{f'(\theta_0)t} .$$

Since such exponential behavior is conventionally written as

$$x = x(0)e^{t/\tau} ,$$

we have

$$\tau = \frac{1}{f'(\theta_0)} .$$

It is convenient to let $\dot{\theta} = F \sin\theta$, where

$$F = \frac{H}{2A^2}\left\{ - \frac{a^2 c\lambda(\lambda - \Omega)^2}{\left(\frac{k}{m} - \omega^2 - \lambda^2\right)^2 + \left(\frac{c}{m}\lambda\right)^2} + \frac{a'^2 c'(\sigma - \lambda)(2\sigma - \lambda + \Omega)^2}{\left[\frac{k'}{m'} - \omega^2 - (\sigma - \lambda)^2\right]^2 + \left[\frac{c'}{m'}(\sigma - \lambda)\right]^2} \right\} .$$

In this problem, $0 \leqslant \theta \leqslant \pi$. Equilibrium always exists at 0° and 180° and possibly exists at intermediate angles if F vanishes. It follows that the dual-spin system is stable—

(1) at $\theta = 0°$ if $F(0) < 0$.

(2) at $\theta = 180°$ if $F(\pi) > 0$.

(3) at $\theta = \theta_0$ if $F(\theta_0) = 0$ and $F'(\theta_0) < 0$.

An immediate example will clarify these concepts. Consider the special case where there is a damper on the spacecraft only. Then,

$$F = -\frac{H}{2A^2}\left[\frac{a^2 c\lambda(\lambda - \Omega)^2}{\left(\frac{k}{m} - \omega^2 - \lambda^2\right)^2 + \left(\frac{c}{m}\lambda\right)^2}\right],$$

and since only the sign of F is significant, the positive constants, the term $(\lambda - \Omega)^2$ in the numerator, and the entire denominator can be factored out. Thus, $F \propto -\lambda$, so that $\dot{\theta} \propto -\lambda \sin\theta$.

Now,

$$\lambda = \frac{(C - A)H \cos\theta + AJ'_3\sigma}{AC}.$$

Hence, $\lambda(\theta)$ is a biased cosine function. In the special case of $\sigma = 0$ (i.e., no relative motion of the wheel) and $C > A$, the function $\dot{\theta}(\theta)$ would be of the form shown by the solid line in Figure 4.3.

Note the stability at 0° and 180°; since the wheel has been despun and the system reduced to an ordinary spinning spacecraft, this result is in agreement with the well-known fact that rotation about the nominal spin axis is stable if the moment-of-inertia ratio is "favorable" (i.e., if $C > A$). If the case $C < A$ had been considered, the function $\dot{\theta}(\theta)$ would be the mirror image of that shown by the solid line and there would be unstable equilibrium at 0° and 180° and stable equilibrium at $\theta = 90°$. This latter point would represent a flat-spin condition, the famous minimum-energy state for spinning satellites with "unfavorable" moment-of-inertia ratios.

The dashed lines in Figure 4.2 show the effect of the addition of a positive relative wheel rate to the system. The unstable equilibrium point is moved to the right monotonically as the spin is increased, eventually reaching 180° as a critical rate σ_{cr} is attained. For $\sigma \geqslant \sigma_{cr}$, only one stable equilibrium angle (0°) exists, and the 180° point becomes unstable. An initial condition of $\theta = 180°$ would then result in an eventual complete inversion of the system; i.e., the spacecraft would literally turn upside

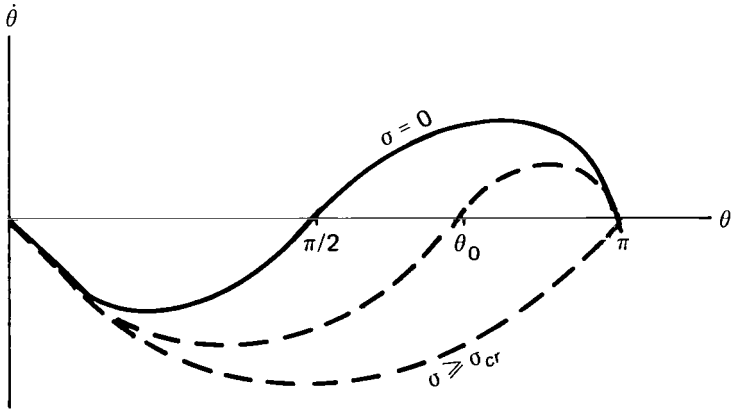

Figure 4.3–$\dot{\theta}(\theta)$, Damping on spacecraft only and $C > A$.

down in reaching a stable equilibrium state. σ_{cr} can be calculated by setting $\lambda = 0$ and $\cos\theta = -1$ in the equation for λ above; i.e.,

$$\sigma_{cr} = \frac{(C - A)H}{AJ'_3} .$$

CHAPTER 5

ANALYSIS OF RESULTS

A. The Fundamental Result Restated

The primary result obtained in the preceding chapters can be summarized briefly as follows: The condition $\theta = \theta_0$ represents a state of stable equilibrium (or a stable steady-state cone angle) if $f(\theta_0) = 0$ and $f'(\theta_0) < 0$, where

$$f(\theta) = \sin\theta \; F(\theta) \, ,$$

$$F(\theta) = \frac{H}{2A^2}\left\{ \frac{a^2 c\lambda(\lambda - \Omega)^2}{\left(\frac{k}{m} - \omega^2 - \lambda^2\right)^2 + \left(\frac{c}{m}\lambda\right)^2} + \frac{a'^2 c'(\sigma - \lambda)(2\sigma - \lambda + \Omega)^2}{\left[\frac{k'}{m'} - \omega^2 - (\sigma - \lambda)^2\right]^2 + \left[\frac{c'}{m'}(\sigma - \lambda)\right]^2} \right\}, \tag{5.1}$$

$$\Omega = \frac{H\cos\theta - J'_3\sigma}{C} \, ,$$

$$\lambda = \frac{(C - A)H\cos\theta + AJ'_3\sigma}{AC} \, ,$$

and

$$\omega = \frac{H\sin\theta}{A} \, .$$

The function F represented by Equation 5.1 is a function of 14 variables, 11 of which would be fixed constants for a given spacecraft configuration (the moments of inertia C, A, and J'_3, and the damper parameters m, k, c, a, m', k', c', and a'). The other independent variables are the angular momentum H, the wheel rate σ (constants of the motion in this analysis), and the cone angle θ. The variables Ω, λ, and ω are not independent, and they are given explicitly above.

The most important quality of F, however, is its sign, and the various terms involved are predominantly positive. The only terms possibly negative are λ and $(\sigma - \lambda)$ in the numerators of the two fractions. In terms of the independent variables, these quantities are

$$\lambda = \frac{(C - A)H\cos\theta + AJ'_3\sigma}{AC} \tag{5.2}$$

and

$$\sigma - \lambda = \frac{(A - C)H \cos\theta + A(C - J_3')\sigma}{AC} \quad . \tag{5.3}$$

Also, in the special cases of damping on one body only, the sign of F is determined by (1) the sign of $(-\lambda)$ for spacecraft damper only, and (2) the sign of $(\sigma - \lambda)$ for wheel damper only.

In what follows, *initial states* of the system will be considered to be characterized by a pure rotation about the nominal spin axis, with an initial spacecraft spin rate of Ω_0 and a wheel rate of σ. An $\Omega_0\sigma$-plane then contains points representing all possible initial states for a particular system. The angular momentum corresponding to a particular point in this plane will be given by $H = |C\Omega_0 + J_3'\sigma|$, and since $C\Omega_0 + J_3'\sigma = H \cos\theta_0$, an initial state for which $C\Omega_0 + J_3'\sigma > 0$ will represent an initial cone angle of 0°. Likewise, if $C\Omega_0 + J_3'\sigma < 0$, the initial cone angle will be 180°. The line $C\Omega_0 + J_3'\sigma = 0$ thus divides the $\Omega_0\sigma$-plane into two parts, as shown in Figure 5.1.

B. Special Case I: Damper on Spacecraft Only

The stability of an arbitrary initial state, with damping on the spacecraft only, is determined according to the following conditions:

(1) 0° is stable if λ_0 is positive.

(2) 180° is stable if λ_0 is negative.

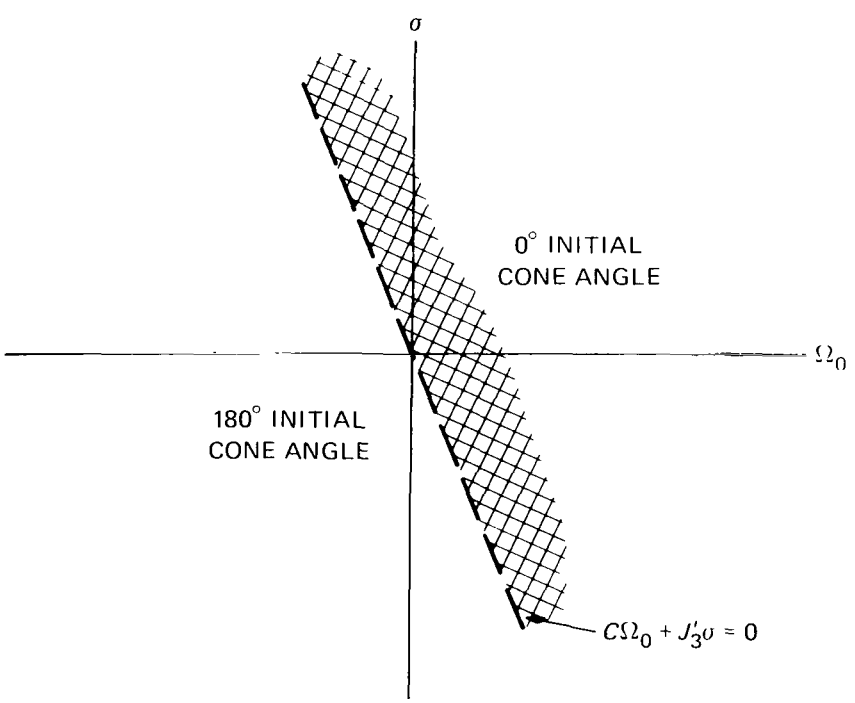

Figure 5.1—Possible initial states and corresponding cone angles.

In both cases, λ_0 is calculated from Equation 5.2, with the appropriate values of H and $\cos\theta$, as follows:

$$\lambda_0 = \frac{(C-A)(C\Omega_0 + J_3'\sigma) + AJ_3'\sigma}{AC}$$

$$= \frac{C-A}{A}\Omega_0 + \frac{J_3'}{A}\sigma .$$

The line $\lambda_0 = 0$, or $\sigma/\Omega_0 = (A - C)/J_3'$, then divides the initial state plane into regions of $\lambda_0 > 0$ and $\lambda_0 < 0$, as shown in Figure 5.2.

Combining Figures 5.1 and 5.2 and recalling the stability criterion above yields Figure 5.3, a stability diagram for the system with damping on the spacecraft only. Regions marked S and U are stable and unstable, respectively.

A useful alternate form of this stability diagram can be constructed in terms of dimensionless parameters. Let $q = C/A$ and $q' = J_3'/A$. The stability boundaries above then become the lines $q + q'(\sigma/\Omega_0) = 0$ and $q + q'(\sigma/\Omega_0) = 1$. Figure 5.4 shows the new stability diagram. The only values of q that are physically meaningful lie between the limits q' and 2.

Figure 5.4 verifies a result obtained by Mingori (Reference 11) through a Routhian analysis of linearized equations of motion representing this special case and pure spins about the nominal spin axis.

Turning now to the nature of possible instabilities, we recall that stable equilibrium states can exist at intermediate cone angles ($0 < \theta_0 < \pi$) if $F(\theta_0) = 0$. Thus, in the special case at hand we are interested in the possibility of λ vanishing, where, in terms of dimensionless parameters,

$$\lambda = \frac{(q-1)\dfrac{H\cos\theta}{A} + q'\sigma}{q}, \tag{5.4}$$

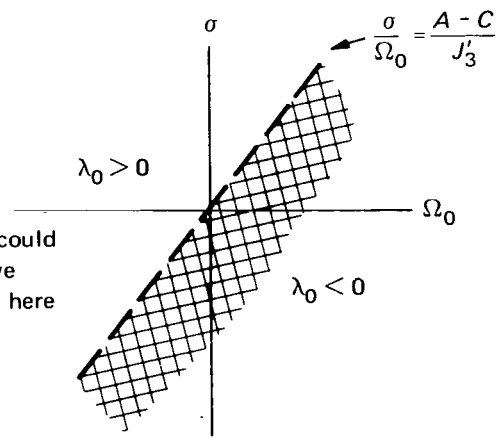

Note: The line $\lambda_0 = 0$ could have positive or negative slope. It is represented here for the case $A > C$.

Figure 5.2—The sign of λ_0.

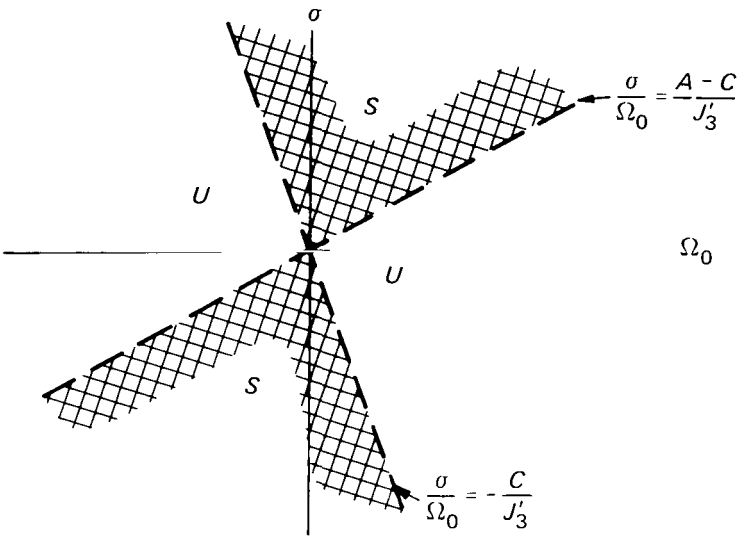

Figure 5.3—Stability diagram with damping on the spacecraft only.

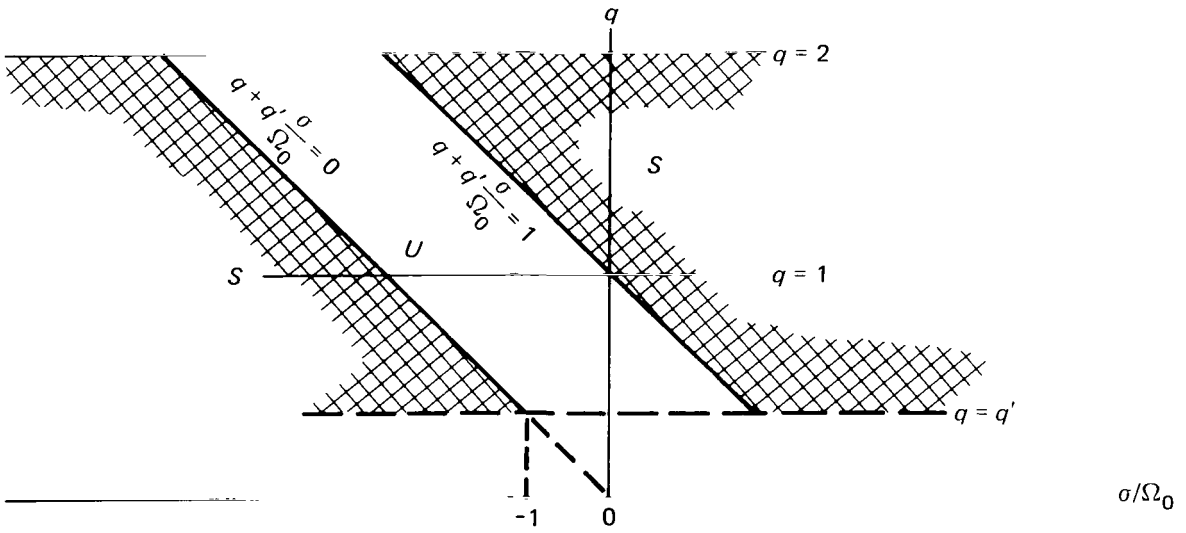

Figure 5.4—Alternate form of stability diagram with damping on the spacecraft only.

where

$$\frac{H}{A} = |q\Omega_0 + q'\sigma| .$$

Now, λ is seen to be a biased cosine function of the cone angle θ, and by inspection of Equation 5.4 the following may be deduced:

(1) For $\sigma = 0$, λ will vanish at $\theta = \pi/2$ and will have a slope at that point determined by the sign of $(q - 1)$.

(2) Introducing $\sigma \neq 0$ monotonically raises or lowers the curve, moving the point where λ vanishes to the right or left and eventually eliminating the possibility of λ vanishing for a real θ. Critical values of σ are determined from Equation 5.4 with $\lambda = 0$ and $\cos\theta = \pm 1$.

These critical values, σ_1 and σ_2, are calculated as follows:

$$(q-1)(q\Omega_0 + q'\sigma_1) + q'\sigma_1 = 0 ,$$

or

$$\frac{\sigma_1}{\Omega_0} = \frac{1-q}{q'} . \tag{5.5}$$

$$(1-q)(q\Omega_0 + q'\sigma_2) + q'\sigma_2 = 0 ,$$

or

$$\frac{\sigma_2}{\Omega_0} = \frac{q(1-q)}{q'(q-2)} . \tag{5.6}$$

Since $f(\theta) = F(\theta)\sin\theta$, the function $f(\theta)$ will take on one of the four characteristic shapes shown in Table 5.1, depending on the magnitude of the wheel rate σ and the sign of $(q-1)$. In this table, stable equilibrium states are marked by an arrow ($\swarrow$) and comments are added concerning conditions that produce the various possibilities.

Class I behavior includes as a special case the "favorable" single-spin spacecraft, which is stable right side up ($\theta = 0°$) or upside down ($\theta = 180°$). Note that only in Class II can a stable intermediate cone angle exist. The "unfavorable" single-spin spacecraft is a special case of this type of behavior, where $\theta_0 = 90°$. Equation 5.4 can be used to calculate the value of the stable intermediate angle in general, with the result being

$$\cos\theta_0 = \frac{q'\sigma}{(1-q)|q\Omega_0 + q'\sigma|} . \tag{5.7}$$

For Class II, all pure spins about the nominal spin axis are unstable. Classes III and IV include the possibility of a heretofore unreported type of instability, a complete inversion of the system. Unstable pure spins about the nominal spin axis will change to stable pure spins about the nominal spin axis, with the spacecraft turning upside down in the process.

Table 5.1 shows that only stable initial states and inversions are possible if $q > 1$ or, equivalently, if $C > A$. A complete stability diagram for this case is shown in Figure 5.5.

For $q < 1$, two types of initial-state instabilities are possible—inversion, and a steady-state intermediate cone angle. One obvious observation is that if $\sigma = 0$, the latter possibility will occur and the steady cone angle will be 90°. In general, for $q < 1$, Table 5.1 shows that stable intermediate angles exist if

$$\frac{q(1-q)}{q'(q-2)} < \frac{\sigma}{\Omega_0} < \frac{1-q}{q'} .$$

Table 5.1—Four classes of possible behavior for $f(\theta)$.

Class	$f(\theta)$	Stable Cone Angles	Conditions
I	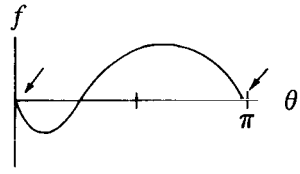	0°, 180°	$q > 1$ $\sigma_1 < \sigma < \sigma_2$*
II	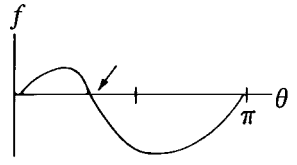	$0° < \theta_0 < 180°$	$q < 1$ $\sigma_2 < \sigma < \sigma_1$
III	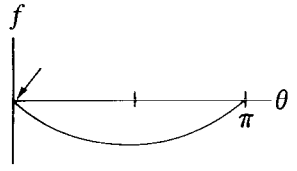	0° only	$q > 1, \sigma > \sigma_2$ or $q < 1, \sigma > \sigma_1$
IV	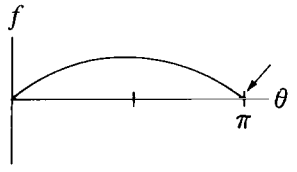	180° only	$q > 1, \sigma < \sigma_1$ or $q < 1, \sigma < \sigma_2$

*The terms σ_1 and σ_2 are given by Equations 5.5 and 5.6, respectively.

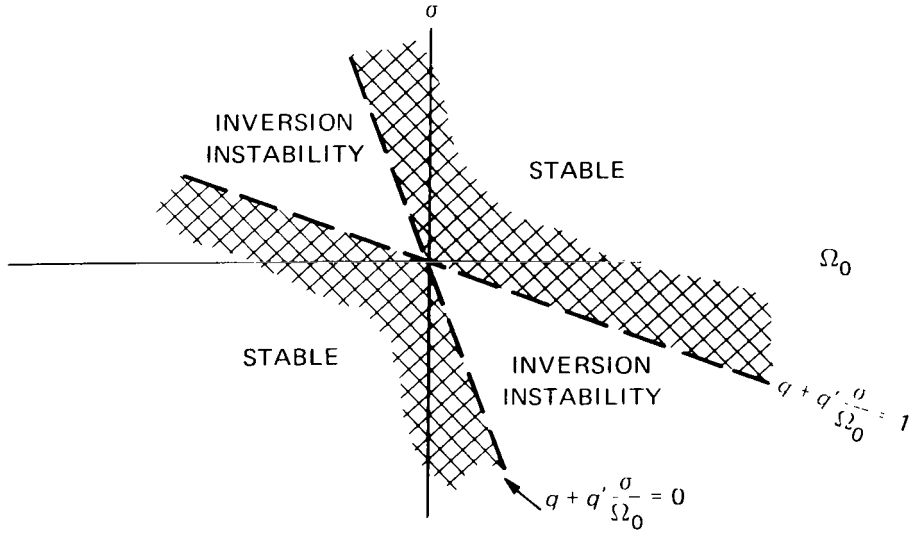

Figure 5.5—Complete stability diagram with damper on the spacecraft only and $C > A$.

The upper bound here is actually the line $q + q'(\sigma/\Omega_0) = 1$, which has been found to separate stable and unstable initial states. The lower bound represents a new line,

$$\frac{\sigma}{\Omega_0} = \frac{q(1-q)}{q'(q-2)},$$

which divides the previously shown unstable regions into two parts corresponding to the two possible types of instability. Intermediate cone-angle values can be calculated from Equation 5.7, and the loci of points representing fixed values of θ_0 will be straight lines in the $\Omega_0\sigma$, initial-state plane. Figure 5.6 shows a complete stability diagram for the case of $q < 1$.

Presenting the above information in the alternate form [in σ/Ω_0, q-space] has disadvantages and compensating advantages. Many of the straight lines in Figure 5.6 become curved, and the distinction between supplementary cone angles (i.e., θ and $\pi - \theta$) is lost, but the effect of the parameter q is more

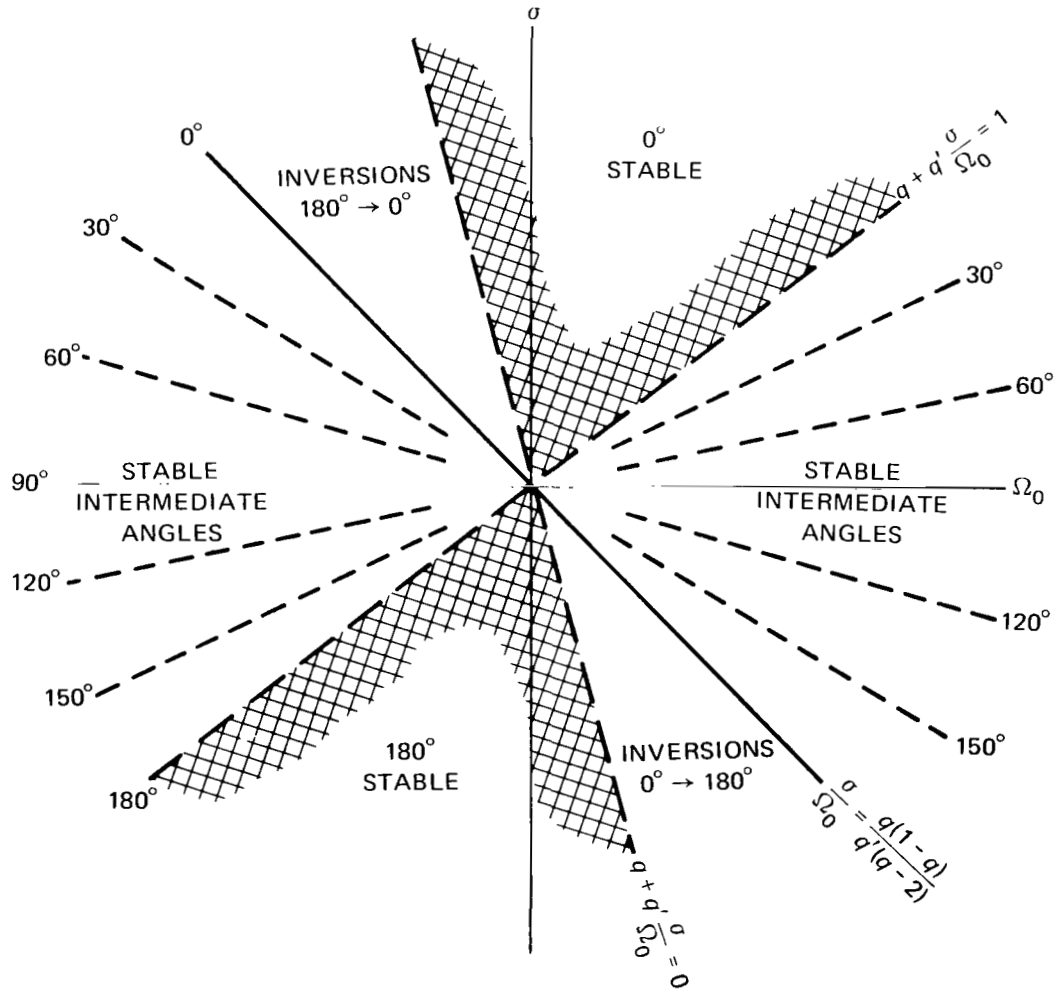

Figure 5.6—Complete stability diagram for damper on the spacecraft only and $q < 1$.

clearly seen. For definiteness of cone angle only, it is assumed in the construction of Figure 5.7 that $\Omega_0 > 0$. For clarity, only that portion of the stability diagram involving the two types of instability is shown. Refer to Figure 5.4 for the overall view.

C. Special Case II: Damper on Wheel Only

The stability of an arbitrary initial state, with damping on the wheel only, is determined according to the following conditions:

(1) 0° is stable if $\lambda_0 - \sigma$ is positive.

(2) 180° is stable if $\lambda_0 - \sigma$ is negative.

In these conditions, $\lambda_0 - \sigma$ is calculated from Equation 5.2 with appropriate values of H and $\cos\theta$ as follows:

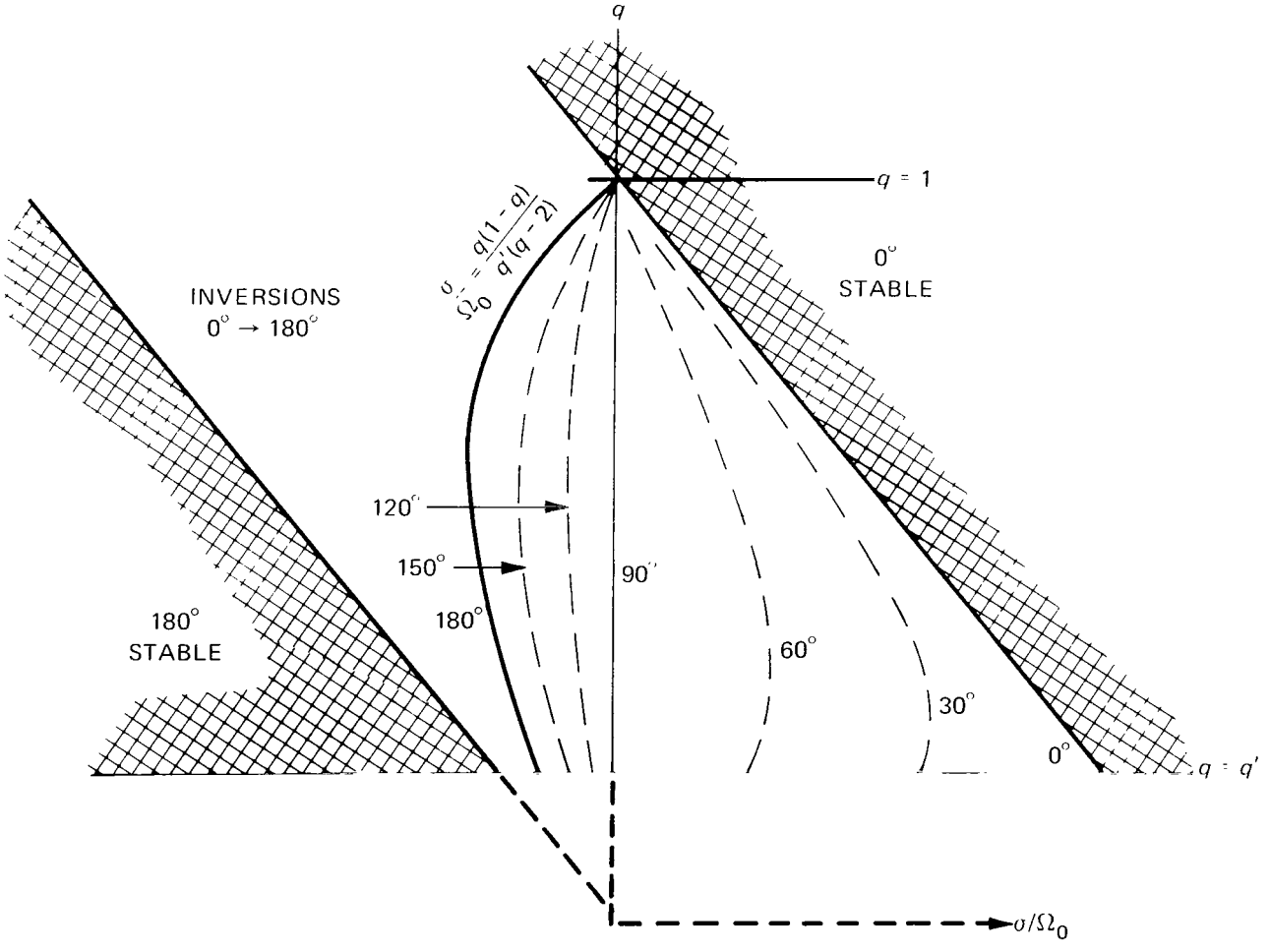

Figure 5.7—Portion of stability diagram in alternate form, damping on spacecraft only and $\Omega_0 > 0$.

$$\lambda_0 - \sigma = \frac{(C-A)(C\Omega_0 + J_3'\sigma) + A(J_3' - C)\sigma}{AC}$$

$$= \frac{C-A}{A}\Omega_0 + \frac{J_3' - A}{A}\sigma .$$

The line $\lambda_0 - \sigma = 0$, or

$$\frac{\sigma}{\Omega_0} = \frac{C-A}{A-J_3'},$$

then divides the initial-state plane into regions of $\lambda_0 - \sigma > 0$ and $\lambda_0 - \sigma < 0$, as shown in Figure 5.8.

Combining Figures 5.1 and 5.8 and recalling the stability criterion above yields a stability diagram for damping on the wheel only, shown in Figure 5.9. Regions marked *S* and *U* are stable and unstable, respectively.

Again, a useful alternate form of this stability diagram can be constructed in terms of dimensionless parameters. With $q = C/A$ and $q' = J_3'/A$, the stability boundaries above become the straight lines

$$q + q'\frac{\sigma}{\Omega_0} = 0$$

and

$$q + q'\frac{\sigma}{\Omega_0} = 1 + \frac{\sigma}{\Omega_0}.$$

This alternate stability diagram, Figure 5.10, verifies a result obtained by Mingori (Reference 11) with a Routhian analysis of linearized equations of motion representing this special case and pure spins about the nominal spin axis.

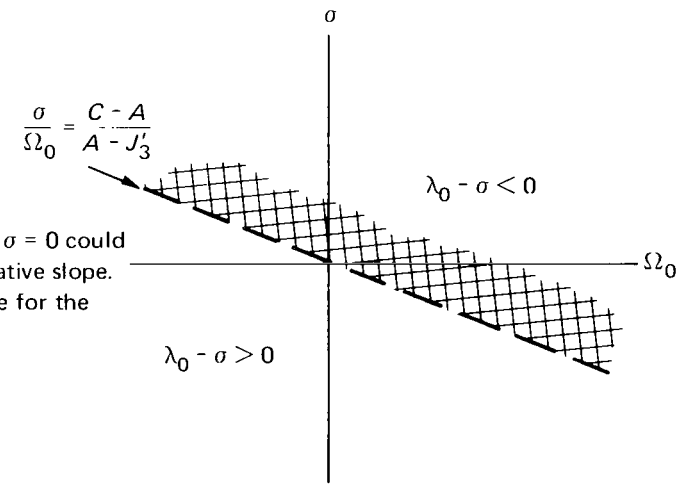

Figure 5.8—The sign of $\lambda_0 - \sigma$.

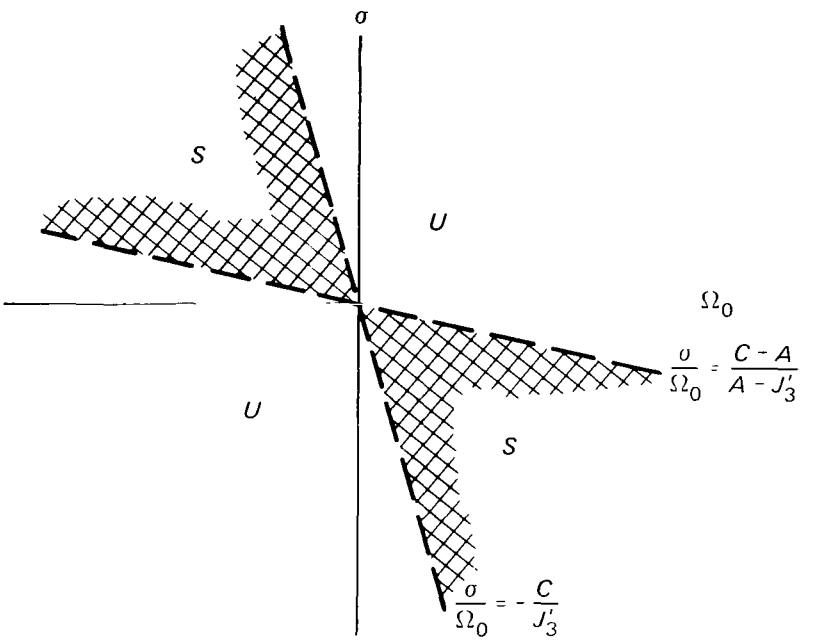

Figure 5.9—Stability diagram with damping on the wheel only.

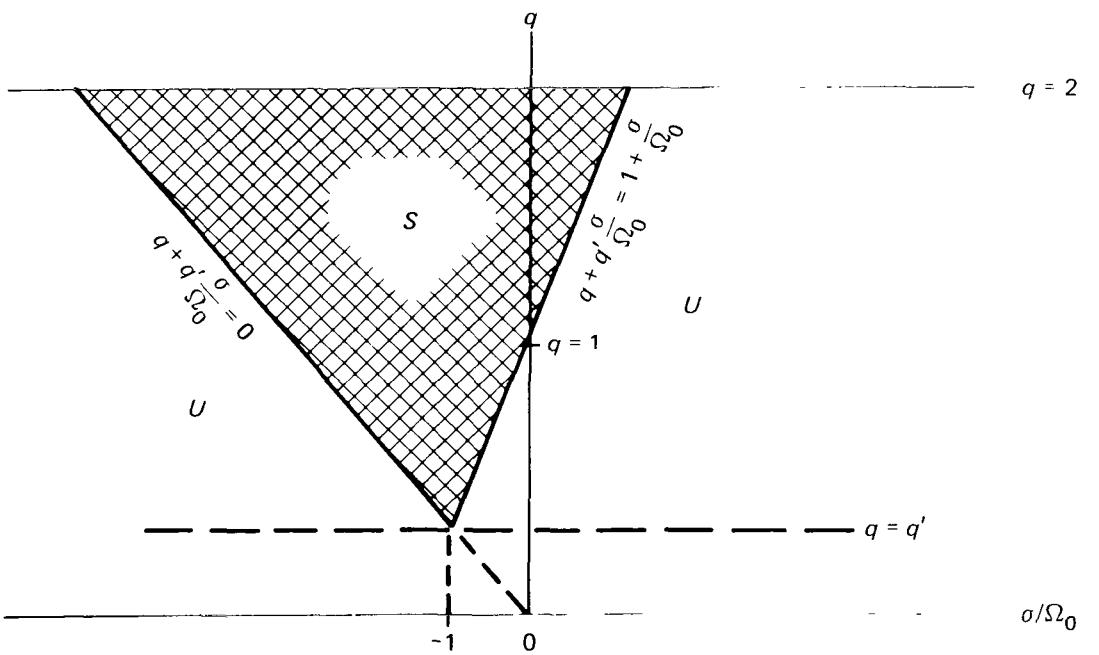

Figure 5.10—Alternate form of stability diagram with damping on the wheel only.

Turning now to the nature of possible instabilities, we recall that stable equilibrium states can exist at intermediate cone angles ($0 < \theta_0 < \pi$) if $F(\theta_0) = 0$. Thus, in the special case at hand we are interested in the possibility of $\lambda - \sigma$ vanishing, where, in terms of the dimensionless parameters,

$$\lambda - \sigma = \frac{(q-1)\frac{H}{A}\cos\theta + (q'-q)\sigma}{q} \tag{5.8}$$

and

$$\frac{H}{A} = |q\Omega_0 + q'\sigma| .$$

An analysis of Equation 5.8 would closely parallel the earlier analysis of Equation 5.4. Each is a biased cosine function of the cone angle θ which vanishes at $\theta = 90°$ if $\sigma = 0$; its slope is determined by the sign of $q - 1$, and the bias level is a monotonic function of σ. However, critical values of σ are now determined for $\lambda - \sigma = 0$ in Equation 5.8, with $\cos\theta = \pm 1$.

$$(q-1)(q\Omega_0 + q'\sigma_1) + (q'-q)\sigma_1 = 0 ,$$

or

$$\frac{\sigma_1}{\Omega_0} = \frac{q-1}{1-q'} . \tag{5.9}$$

$$(1-q)(q\Omega_0 + q'\sigma_2) + (q'-q)\sigma_2 = 0 ,$$

or

$$\frac{\sigma_2}{\Omega_0} = \frac{q(1-q)}{q + qq' - 2q'} . \tag{5.10}$$

The discussion of the behavior of the function $f(\theta)$ with damping on the spacecraft only is appropriate for this special case as well. The four classes of behavior represented in Table 5.1 are again possible. The conditions producing these classes are different, however. Table 5.2 shows the appropriate inequalities involved.

All comments in the previous section concerning the various classes of behavior apply here also, except that in Class II, the value of the stable intermediate cone angle is determined from Equation 5.8 to be

$$\cos\theta_0 = \frac{(q'-q)\sigma}{(1-q)|q\Omega_0 + q'\sigma|} . \tag{5.11}$$

Table 5.2 shows that only stable initial states and inversions are possible if $q > 1$. A complete stability diagram for this case is shown in Figure 5.11.

For $q < 1$, we again have two possible types of instability—inversion, and a steady-state intermediate cone angle. The latter possibility (Class II of Table 5.2) occurs when

$$\frac{q-1}{1-q'} < \frac{\sigma}{\Omega_0} < \frac{q(1-q)}{q + qq' - 2q'} .$$

The lower bound here is seen to be the line which has previously been found to separate regions of stability and instability in the initial-state plane above. The upper bound is a new line which

Table 5.2–Four classes of possible behavior for $f(\theta)$.

Class	$f(\theta)$	Stable Cone Angles	Conditions
I	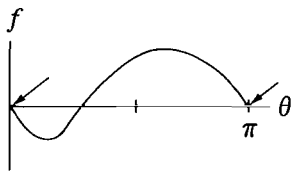	0°, 180°	$q > 1$ $\sigma_2 < \sigma < \sigma_1$*
II	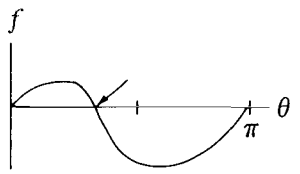	$0° < \theta_0 < 180°$	$q < 1$ $\sigma_1 < \sigma < \sigma_2$
III	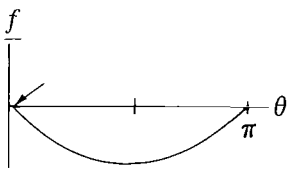	0° only	$q > 1, \sigma < \sigma_2$ or $q < 1, \sigma < \sigma_1$
IV	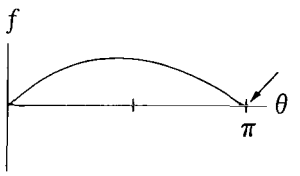	180° only	$q < 1, \sigma > \sigma_1$ or $q > 1, \sigma > \sigma_2$

*The terms σ_1 and σ_2 are given by Equations 5.9 and 5.10, respectively.

divides the unstable region in Figure 5.9 into two parts, corresponding to the two possible types of instability.

Appropriate values of intermediate cone angles can be determined from Equation 5.11, and the loci of points representing constant values of θ_0 will be straight lines in the $\Omega_0\sigma$-plane. Figure 5.12 shows the complete stability diagram for the case of $q < 1$.

The above information can also be presented in an alternate form (in the σ/Ω_0, q-space) as shown in Figure 5.13. Again, for definiteness of cone angle only, the assumption is made that $\Omega_0 > 0$. Note the singularity in the boundary separating inversions from the intermediate angles. It occurs when the denominator of the expression

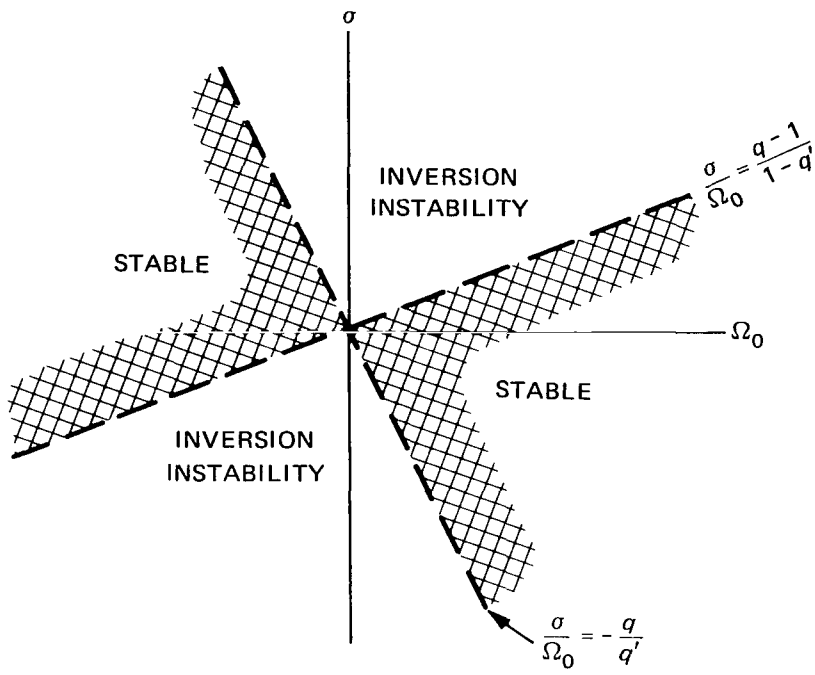

Figure 5.11—Complete stability diagram with damper on the wheel only and $q > 1$.

$$\frac{\sigma}{\Omega_0} = \frac{q(1-q)}{q + qq' - 2q'}$$

vanishes, or when

$$q = \frac{2q'}{1-q'}.$$

Figure 5.13 shows only that portion of the $(\sigma/\Omega_0)q$ plane of most interest here. (Refer to Figure 5.10 for the overall view.)

D. General Case With Tuned Dampers

For the special cases considered so far, specific damper parameters have not been important. We have been concerned only with the moments of inertia C, A, and J_3', the angular velocities Ω and ω, and the cone angle θ. The general case, however, involves eight additional variables which appear in the function F (Equation 5.1)—m, k, c, and a and m', k', c', and a'. However, the stability characteristics of a particular configuration can easily be determined by a numerical evaluation of the function $F(\theta)$ and an examination of the results in light of the basic stability criteria we have been using.

In order to simplify the analysis of the general case, we make the following assumptions, which reduce the number of independent parameters:

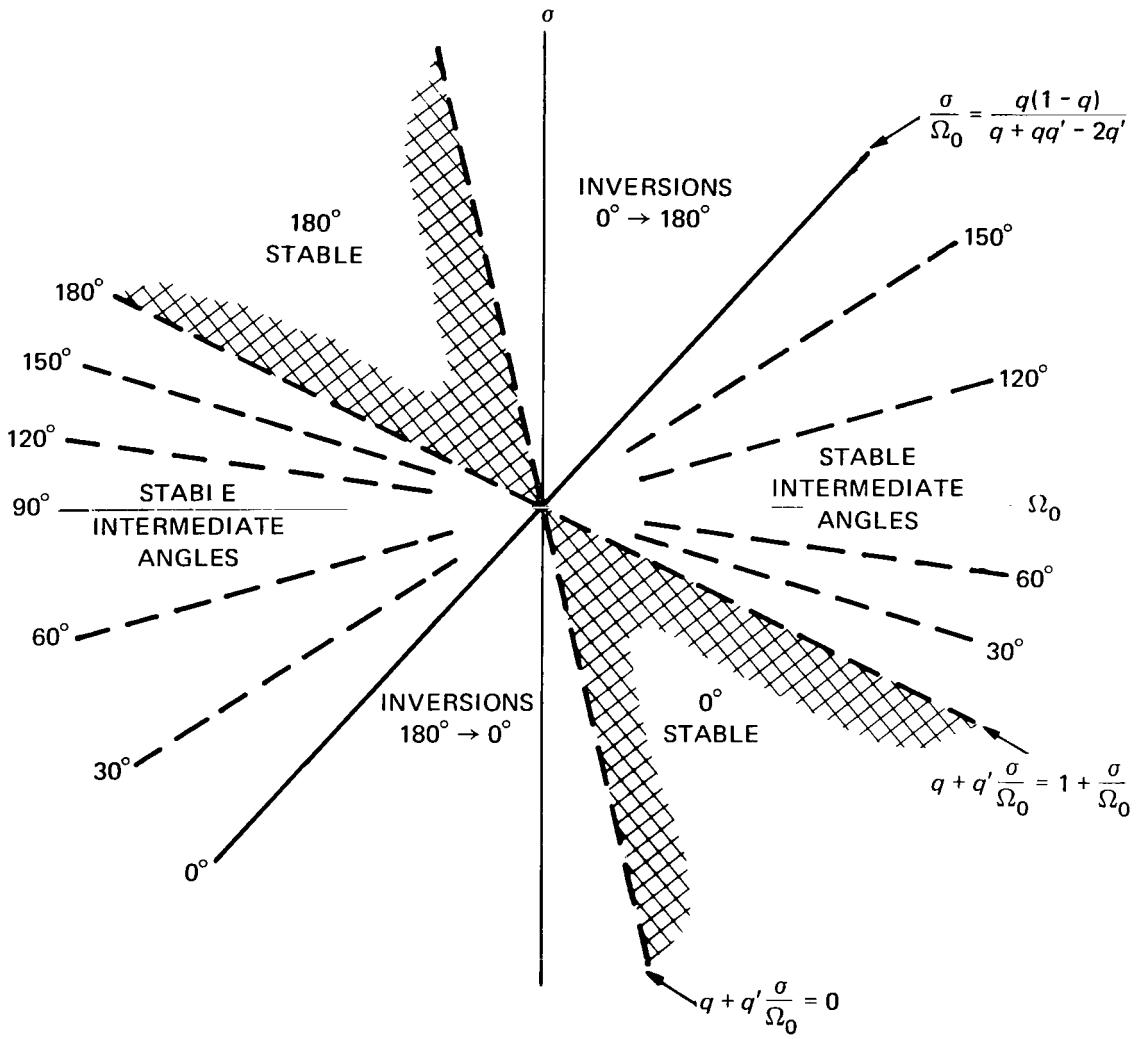

Figure 5.12—Complete stability diagram for damper on the wheel only and $q < 1$.

(1) Each of the dampers is "tuned" such that its natural frequency matches its excitation frequency with the spacecraft in its initial state. Let λ_0 be the corresponding value of λ. We thus require $k/m = \lambda_0^2$ and $k'/m' = (\sigma - \lambda_0)^2$.

(2) The damping in each is "0.1 critical," that is, $c = 0.2m|\lambda_0|$ and $c' = 0.2m'|\sigma - \lambda_0|$.

Combining these assumptions with Equation 5.1 produces the following expression for $F(\theta)$:

$$F(\theta) = \frac{5H}{2A}\left[-\delta\frac{(\lambda_0 - \Omega_0)^2}{\lambda_0|\lambda_0|} + \delta'\frac{(2\sigma - \lambda_0 + \Omega_0)^2}{(\sigma - \lambda_0)|\sigma - \lambda_0|}\right], \tag{5.12}$$

where

$$\delta = \frac{ma^2}{A}$$

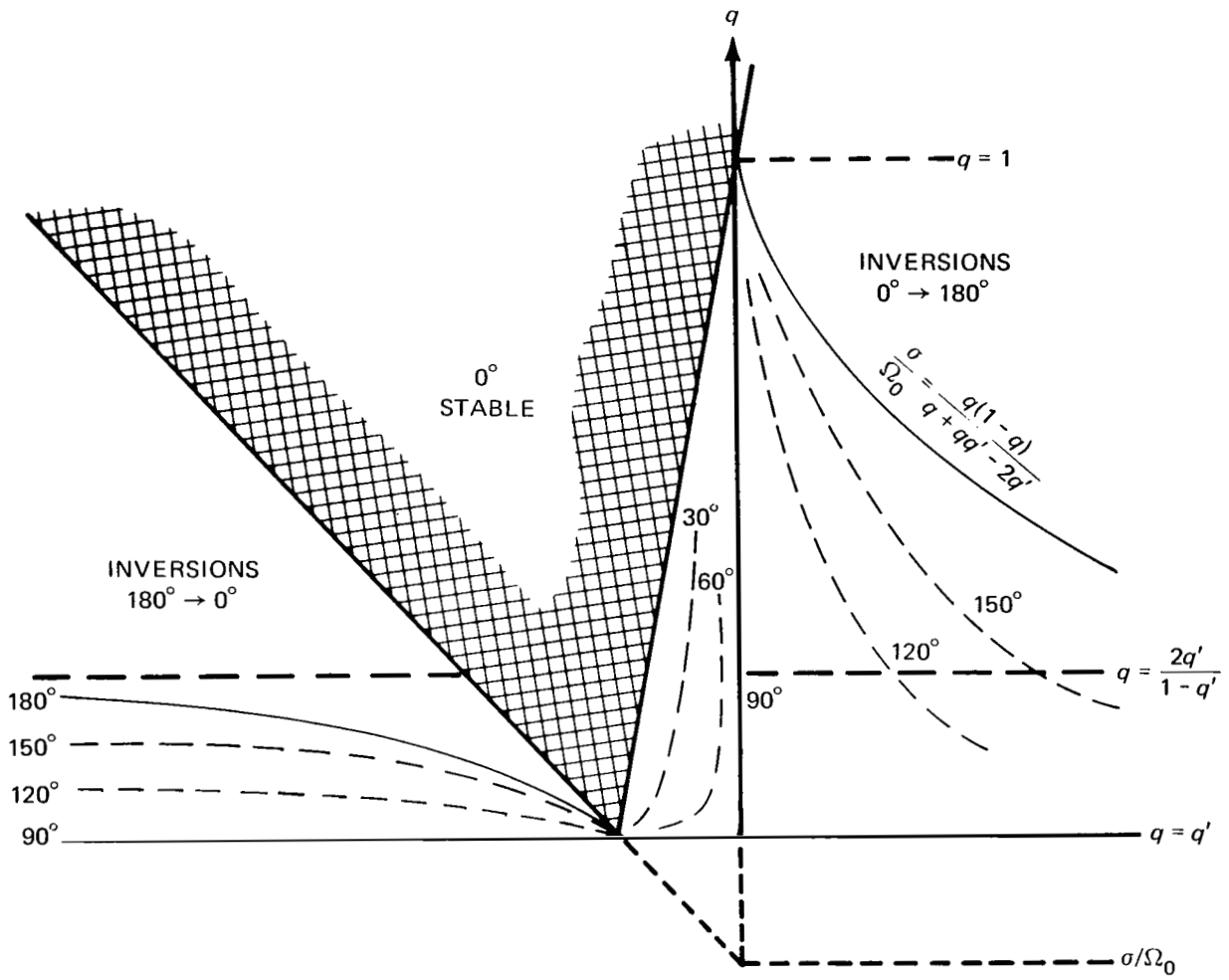

Figure 5.13—Portion of stability diagram in alternate form, with damping on wheel only and $\Omega_0 > 0$.

and

$$\delta' = \frac{m'a'^2}{A} .$$

We have seen several times that the stability of initial states is determined according to the following conditions:

(1) 0° is stable if $F(\theta) < 0$.

(2) 180° is stable if $F(\pi) > 0$.

These requirements can be reduced to one, viz., an arbitrary initial state is stable if $F(\theta_0) \cos\theta_0 < 0$, where $\cos\theta_0 = \text{sgn}(q\Omega_0 + q'\sigma)$. Thus, for stability of an initial state, it is required that

$$(q\Omega_0 + q'\sigma)\left[\delta\frac{(\lambda_0 - \Omega_0)^2}{\lambda_0|\lambda_0|} - \delta'\frac{(2\sigma - \lambda_0 + \Omega_0)^2}{(\sigma - \lambda_0)|\sigma - \lambda_0|}\right] > 0\,,$$

or, equivalently,

$$\left(q + q'\frac{\sigma}{\Omega_0}\right)\left[\delta\frac{\left(\frac{\lambda_0}{\Omega_0} - 1\right)^2}{\frac{\lambda_0}{\Omega_0}\left|\frac{\lambda_0}{\Omega_0}\right|} - \delta'\frac{\left(2\frac{\sigma}{\Omega_0} - \frac{\lambda_0}{\Omega_0} + 1\right)^2}{\left(\frac{\sigma}{\Omega_0} - \frac{\lambda_0}{\Omega_0}\right)\left|\frac{\sigma}{\Omega_0} - \frac{\lambda_0}{\Omega_0}\right|}\right] > 0\,. \tag{5.13}$$

Examination of Equation 5.13 reveals that there exist four possible situations, which are shown in Table 5.3.

Mingori (Reference 11) studied linearized equations representing the special case being considered here, with five particular combinations of the parameters q, q', and σ/Ω_0. These equations had periodic coefficients, and he explored a $\delta\delta'$-space at various isolated points by a numerical, computerized Floquet analysis, producing a total of 125 data points, to which the results obtained here can now be compared.

Table 5.3—Initial state stability, damping on both bodies.

$\left(q + q'\frac{\sigma}{\Omega_0}\right)\frac{\lambda_0}{\Omega_0}$	$\left(q + q'\frac{\sigma}{\Omega_0}\right)\left(\frac{\sigma}{\Omega_0} - \frac{\lambda_0}{\Omega_0}\right)$	Requirement for Stability
+	+	$\frac{\delta}{\delta'} > \left[\frac{\left(\frac{\lambda_0}{\Omega_0}\right)\left(2\frac{\sigma}{\Omega_0} - \frac{\lambda_0}{\Omega_0} + 1\right)}{\left(\frac{\lambda_0}{\Omega_0} - 1\right)\left(\frac{\sigma}{\Omega_0} - \frac{\lambda_0}{\Omega_0}\right)}\right]^2$
	−	Always stable
−	+	Never stable
	−	$\frac{\delta}{\delta'} < \left[\frac{\left(\frac{\lambda_0}{\Omega_0}\right)\left(2\frac{\sigma}{\Omega_0} - \frac{\lambda_0}{\Omega_0} + 1\right)}{\left(\frac{\lambda_0}{\Omega_0} - 1\right)\left(\frac{\sigma}{\Omega_0} - \frac{\lambda_0}{\Omega_0}\right)}\right]^2$

Table 5.4 shows the particular combinations of parameters examined by Mingori and the corresponding stability criteria deduced from the analytical results obtained here.

Figure 5.14 shows comparative results for Cases 1, 2, and 3 of Table 5.4, in which an analytical stability boundary is predicted. Nearly total agreement occurs, with the exception of single points in Cases 1 and 2. (These particular points will be discussed later.)

Results for Case 4 are not shown; however, they agree with Mingori's results, which yielded instability at each point tested.

In Case 5, Mingori found instability at over half of the points tested (Figure 5.15), a result apparently in gross disagreement with the stability criteria reported here. To assess the significance of this disagreement, we digress to consider the work of Mingori in some detail.

Recall that this result comes from a Floquet analysis, which was necessary because the linearized equations of motion had periodic coefficients with damping on each of the bodies. However, Mingori also presented the results of a Routhian analysis for the special cases of damping on one body only, which can be used to investigate the stability of the particular configurations examined on the δ- and δ'-axes, i.e., when δ or δ' vanishes. Appendix II contains a detailed discussion of the behavior of the system on these axes and shows damper size limitations which arise when the dampers are tuned.

Briefly, the Routhian analyses produce five inequalities that are necessary and sufficient for stability in the special cases to which they are applicable. Two of these are trivially satisfied for physically realistic systems; a third represents that criterion which has been shown to be in agreement with the results obtained here, i.e., the stability diagrams presented earlier for those special cases.

The other two inequalities pertain to the sizes of the damper masses, and Table 5.5 shows the damper size limitations imposed by these inequalities for the special combinations of variables examined by Mingori. The headings II-15, II-16, and so forth refer to equations in Appendix II.

Of particular interest in this table are the very low limits on the size of the spacecraft damper in Case 5. Spacecraft damping has been found to be stabilizing in this instance, yet instability is indicated for $\delta > 0.008$.

Table 5.4—Mingori's particular combinations of q, q', and σ/Ω_0.

Case	q	q'	$\frac{\sigma}{\Omega_0}$	$q + q'\frac{\sigma}{\Omega_0}$	$\frac{\lambda_0}{\Omega_0}$*	$\frac{\sigma}{\Omega_0} - \frac{\lambda_0}{\Omega_0}$	Requirements for Stability
1	0.8	0.2	4	1.6	0.6	3.4	$\delta/\delta' > 13.7$
2	0.8	0.2	-6	-0.4	-1.4	-4.6	$\delta/\delta' > 1.48$
3	0.8	0.2	-2	0.4	-0.6	-1.4	$\delta/\delta' < 0.414$
4	0.8	0.2	0.5	0.9	-0.1	0.6	Never stable
5	1.5	0.2	-1.5	1.2	0.2	-1.7	Always stable

*$\lambda_0/\Omega_0 = q + q'(\sigma/\Omega_0) - 1$.

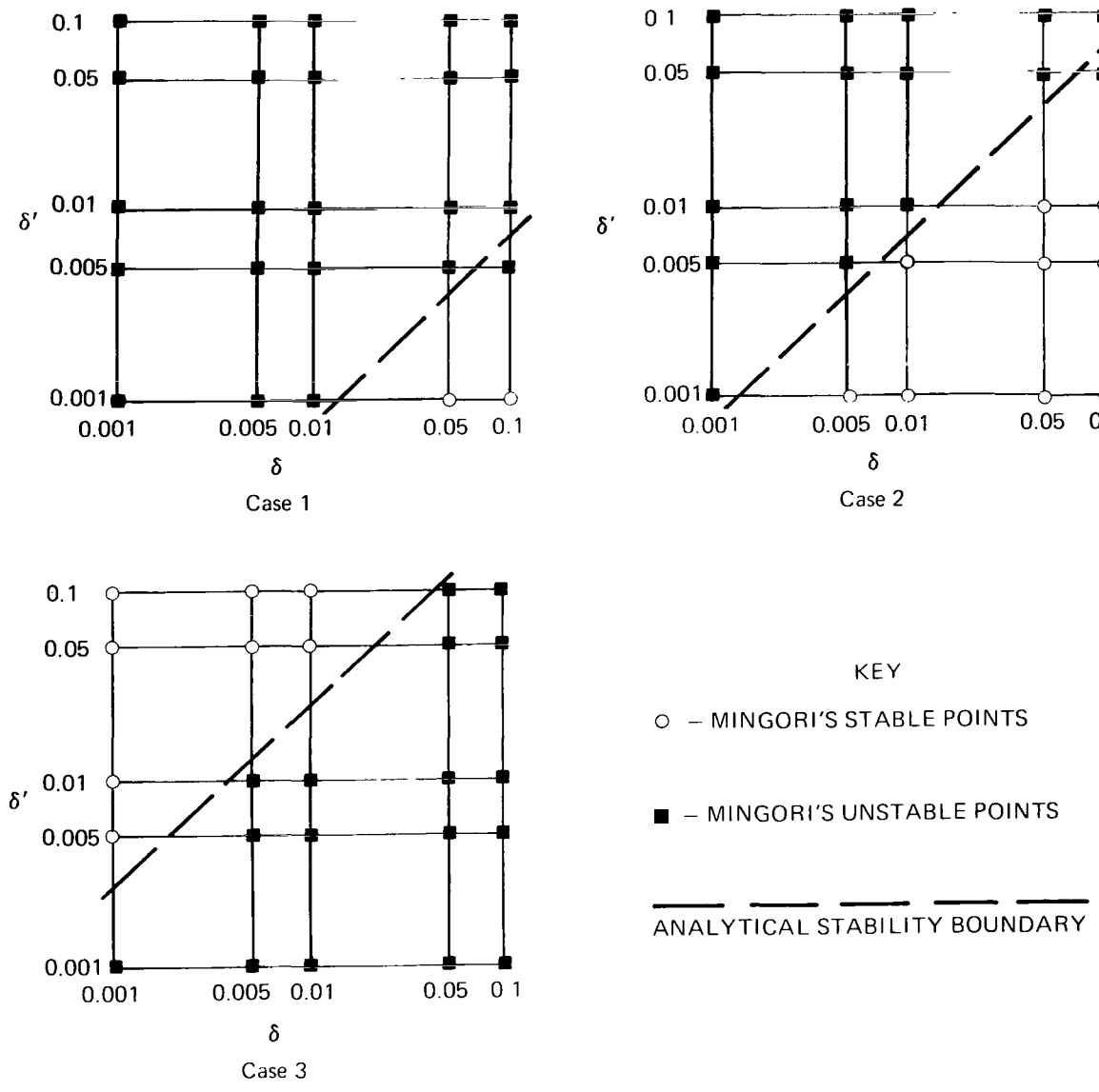

Figure 5.14—Comparison of results, Cases 1, 2, and 3.

The inequalities involved in these low limits (derived in Appendix II) are repeated here for convenience:

$$\lambda_0^2 - \delta\Omega_0(\Omega_0 + \lambda_0) > 0$$

and

$$\lambda_0^4 - \delta\lambda_0(\lambda_0^3 + \Omega_0^3) > 0 .$$

In an effort to find the physical significance of these inequalities, the appropriate linearized equations in Reference 11 were examined. Terms extraneous to our purpose here were removed for clarity, and the following set of equations was found to possess possible pertinent types of instabilities:

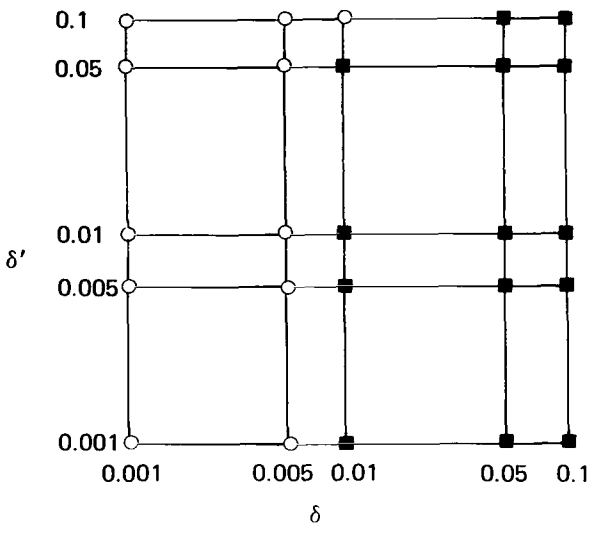

Figure 5.15—Mingori's Case 5 results.

$$\dot{\omega}_1 + \lambda_0 \omega_2 = 0 , \tag{5.14}$$

$$\dot{\omega}_2 - \lambda_0 \omega_1 = \frac{ma}{A} \Omega_0^2 z , \tag{5.15}$$

and

$$m\ddot{z} + kz = ma(\dot{\omega}_2 - \Omega_0 \omega_1) . \tag{5.16}$$

Substituting Equation 5.15 into Equation 5.16 produces

$$\ddot{z} + \left(\frac{k}{m} - \delta\Omega_0^2\right) z = a(\lambda_0 - \Omega_0)\omega_1 . \tag{5.17}$$

Note that the "effective spring constant" in Equation 5.17 involves δ, and in order for this to be positive, it is necessary that $\delta < k/m\Omega_0^2$.

If the damper is tuned to its excitation frequency, i.e., if $k/m = \lambda_0^2$, this inequality becomes $\lambda_0^2 > \delta\Omega_0^2$, or equivalently, $\lambda_0^2 - \delta\Omega_0^2 < 0$. This latter inequality is seen to be similar to the first Routhian inequality above.

If a fourth-order equation in z is formed, equivalent to the set of Equations 5.14 through 5.16, it is found that the linear term has the coefficient $\lambda_0^2(k/m) - \delta\lambda_0\Omega_0^3$. Requiring this "spring constant" to be positive implies $k/m > \delta\Omega_0^3/\lambda_0$. If the damper is again tuned to its excitation frequency, this requirement becomes $\lambda_0^2 > \delta\Omega_0^2/\lambda_0$, or equivalently, $\lambda_0^4 - \delta\lambda_0\Omega_0^3 > 0$. This inequality resembles the other Routhian inequality listed above.

Physically, then, these inequalities involve effective spring constants which are characteristic of the coupled equations. In the perturbation analysis reported here, the equations of motion are uncoupled, and these types of instabilities could not be detected.

Since the inequalities involved depend on the size of the dampers, it seems reasonable to consider them as representative of second-order effects beyond the scope of this perturbation analysis. The

Table 5.5—Special case limits on damper sizes.

Case	q	q'	$\frac{\sigma}{\Omega_0}$	δ_{max}		δ'_{max}	
				II.15	II.16	II.17	II.18
1	0.8	0.2	4	0.225	0.178	1.45	No limit
2	0.8	0.2	-6	No limit	1.57	10.6	No limit
3	0.8	0.2	-2	0.900	No limit	No limit	1.56
4	0.8	0.2	0.5	0.011	No limit	0.267	No limit
5	1.5	0.2	-1.5	0.033	0.008	4.83	1.03

above inequalities show that tuning the dampers to low excitation frequencies can greatly enhance these effects and severely limit the size of the damper. This is the problem encountered here.

If Table 5.5 is used as an indicator of the range of applicability of our first-order perturbation analysis, the following conclusions may be drawn:

(1) None of the wheel damper size limitations (δ'_{max}) are of any consequence. They are all remote from the range of primary interest (0.001 to 0.1), except for Case 4 and Equation II.17, which is not important since there is first-order instability in that case.

(2) The limitations on δ in Cases 2 and 3 are probably remote enough from 0.1 to be inconsequential, and the low limit (0.011) in Case 4 is not significant because of the first-order instability in that case.

(3) Both of the δ-limitations in Case 1 lie just beyond the range investigated by Mingori, so that the second-order effects may have destabilized the point of disagreement mentioned earlier.

(4) In Case 5, the line $\delta = 0.008$ cuts through the middle of the stability diagram shown in Figure 5.14. The stability at all points to the left of this line is in agreement with the stability criterion developed here. At one point, the stabilizing wheel damping was efficient enough to stabilize the system even though δ exceeded 0.008.

The point of disagreement in Case 2 remains unexplained. A situation similar to that of Case 1 exists here, but the second-order instability boundary is further away (at $\delta = 1.57$). An alternate explanation of the disagreement at this point may lie in a sign error in a very small term in one of the matrices worked with by Mingori.* This error appears in two published versions of his work (References 5 and 11), but may or may not be significant.**

E. Transformation of the Stability Diagram

The stability criteria developed here for the case of tuned dampers with 0.1 critical damping on each body can be used to trace the transformation of the stability diagram as energy dissipation capability is gradually shifted from one of the bodies to the other. The extreme cases would be the diagrams shown in Figures 5.4 and 5.10 for damping on the spacecraft only and wheel only, respectively.

Recall that the stability criteria for initial states, given by Equation 5.13, involved the signs of the quantities

$$q + q' \frac{\sigma}{\Omega_0},$$

*The term $W_1(4,3)$ should be negative.

**In a recent personal communication, Mingori acknowledged the presence of this error in his published equations and in his computer program. He also brought to the writer's attention, however, a paper by Lindh and Likins ["Infinite Determinant Methods for Stability Analysis of Periodic-Coefficient Differential Equations," *AIAA J* 8(4), p. 680, 1970] in which results in total agreement with his are presented. He added that the same error is present in the equations in this paper but *not* in the computer program which produced the results.

$$\frac{\lambda_0}{\Omega_0} = q + q' \frac{\sigma}{\Omega_0} - 1 ,$$

and

$$\frac{\sigma}{\Omega_0} - \frac{\lambda_0}{\Omega_0} = (1 - q') \frac{\sigma}{\Omega_0} - q + 1 .$$

Figures 5.16, 5.17, and 5.18 show which regions of the $(\sigma/\Omega_0)q$-, initial-state plane represent positive and negative areas for these quantities.

Inspection of Table 5.3 reveals that the relative amount of damping on the two bodies is unimportant if λ_0/Ω_0 and $\sigma/\Omega_0 - \lambda_0/\Omega_0$ have opposite signs, i.e., all initial states are either stable or unstable. Figure 5.19 shows the regions of the initial-state plane to which this situation applies.

In other areas of this plane, the sign of the function $F(\theta_0)$ given by Equation 5.12 will be important, and stability boundaries (or places where F changes sign) will be characterized by the vanishing of the bracketed quantity in Equation 5.13. Since we are now interested strictly in cases where λ_0/Ω_0 and $\sigma/\Omega_0 - \lambda_0/\Omega_0$ have the same sign, we can thus concentrate on satisfying the relationship

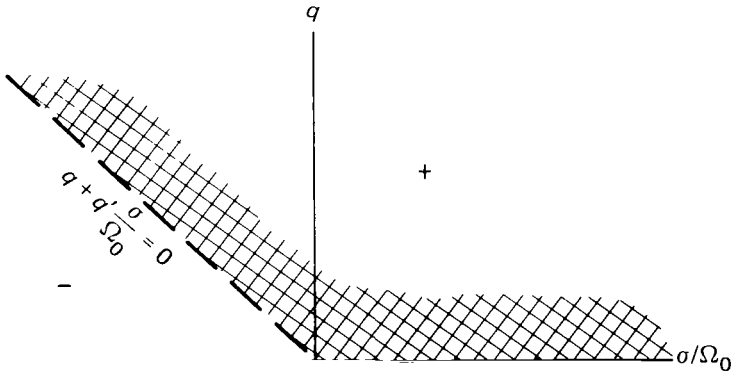

Figure 5.16—The sign of $q + q'(\sigma/\Omega_0)$.

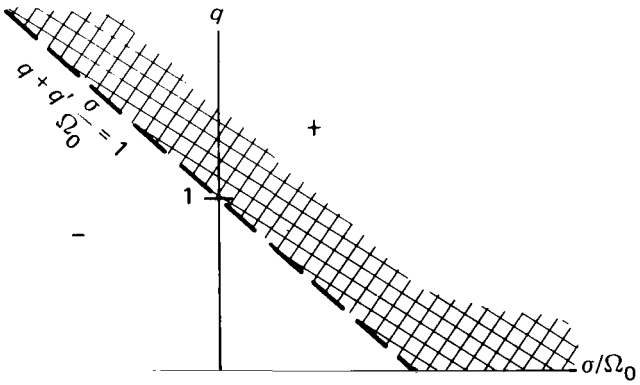

Figure 5.17—The sign of λ_0/Ω_0.

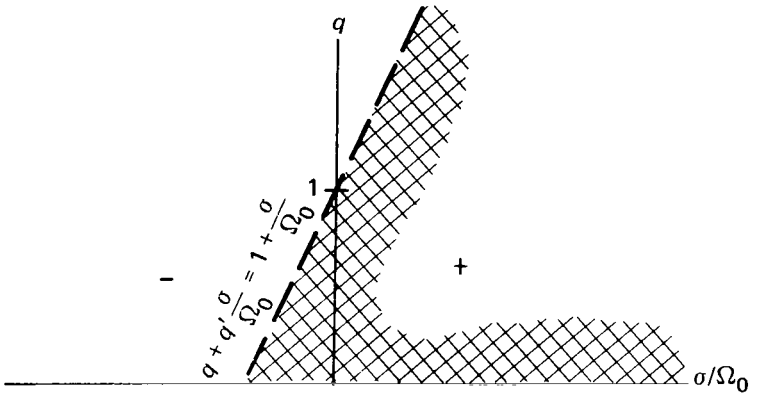

Figure 5.18—The sign of $\sigma/\Omega_0 - \lambda_0/\Omega_0$.

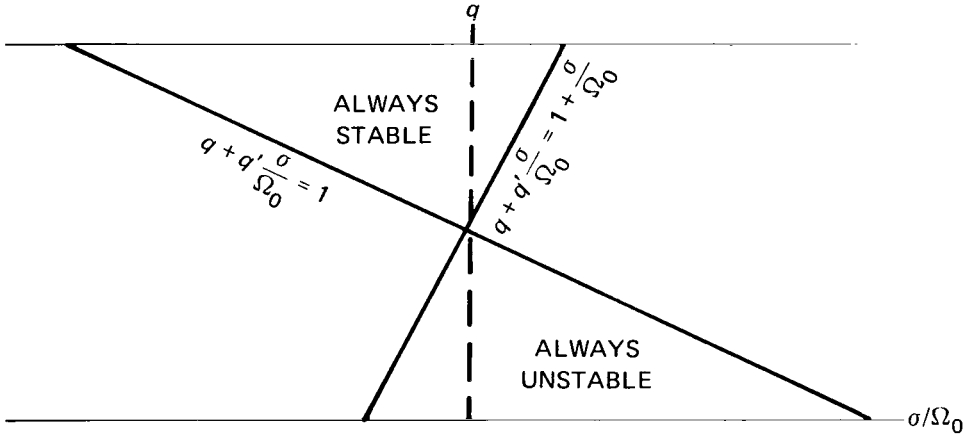

Figure 5.19—Special regions of the initial-state plane.

$$\frac{\delta}{\delta'} = \left[\frac{\lambda_0(2\sigma - \lambda_0 + \Omega_0)}{(\lambda_0 - \Omega_0)(\sigma - \lambda_0)}\right]^2 .$$

With $\beta = (\delta/\delta')^{1/2}$, solutions are sought for the equation

$$\lambda_0(2\sigma - \lambda_0 + \Omega_0) = \pm\beta(\lambda_0 - \Omega_0)(\sigma - \lambda_0) .$$

With the substitution $\lambda_0 = (q - 1)\Omega_0 + q'\sigma$, this equation becomes a quadratic function in σ/Ω_0 that can be solved analytically for lines along which F vanishes. Appendix III shows a derivation of the general quadratic and the particular form it takes when q' is arbitrarily selected to be 0.2. This particular case is used for illustrative purposes. The function F, referred to several times below, is repeated here for convenience:

$$F \propto -\delta\frac{(\lambda_0 - \Omega_0)^2}{\lambda_0|\lambda_0|} + \delta'\frac{(2\sigma - \lambda_0 + \Omega_0)^2}{(\sigma - \lambda_0)|\sigma - \lambda_0|} .$$

Study of the transformation of the stability diagram is begun with an examination of the behavior of the function F with damping on the wheel only. The initial stability diagram is shown in Figure 5.10 and is repeated in Figure 5.20. Two important lines corresponding to $\lambda_0 = 0$ and $2\sigma - \lambda_0 + \Omega_0 = 0$ are also shown. Near the first of these lines, a small amount of spacecraft damping will strongly affect the function F; near the second, the stabilizing effect of the wheel damper is weak (i.e., $F \approx 0$).

Now, the addition of a small amount of damping on the spacecraft splits both the stable and unstable regions along the dashed lines in Figure 5.20. The result is shown qualitatively in Figure 5.21.

The spacecraft damping has changed the sign of F in two regions, stabilizing one and destabilizing the other. A further increase in spacecraft damping causes these new regions to grow, completely eliminating the leftmost stable area above when $\beta = 1$. Adding still more damping causes the leftmost $F = 0$ line to sweep to the left, leaving stable area behind, as shown in Figure 5.22. This moving line eventually stabilizes the remainder of the left half-plane and then begins to approach from infinity on the right, leaving stable area behind again. As the spacecraft damping becomes more and more dominant, the stability diagram takes on the appearance of Figure 5.23.

The final state, as the transformation is completed, is shown in Figure 5.24. Lines corresponding to $\lambda_0 - \Omega_0 = 0$ and $\sigma - \lambda_0 = 0$ have been added to this figure, indicating places where the stabilizing effect of the spacecraft damper is weak (i.e., $F \approx 0$) and where the effect of a small amount of damping on the wheel is strong, respectively.

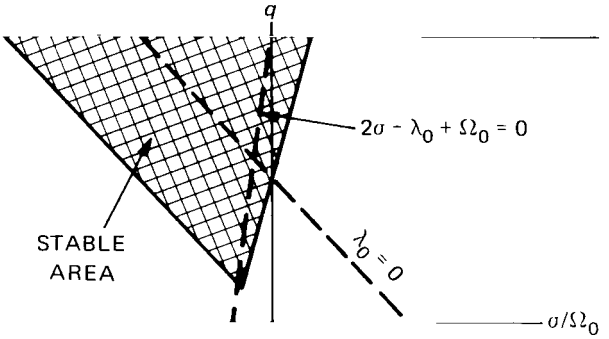

Figure 5.20—Initial stability diagram.

Figure 5.25 shows the progressive steps of the transformation for the special case of $q' = 0.2$. In order to show the complete transformation on one fairly simple figure, many lines have been omitted and the figure appears somewhat abstract, but the information shown is quantitatively accurate.

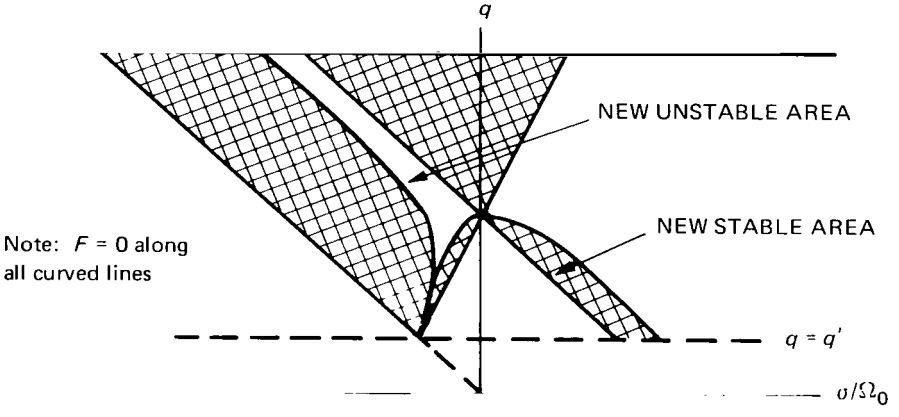

Figure 5.21—First intermediate stability diagram.

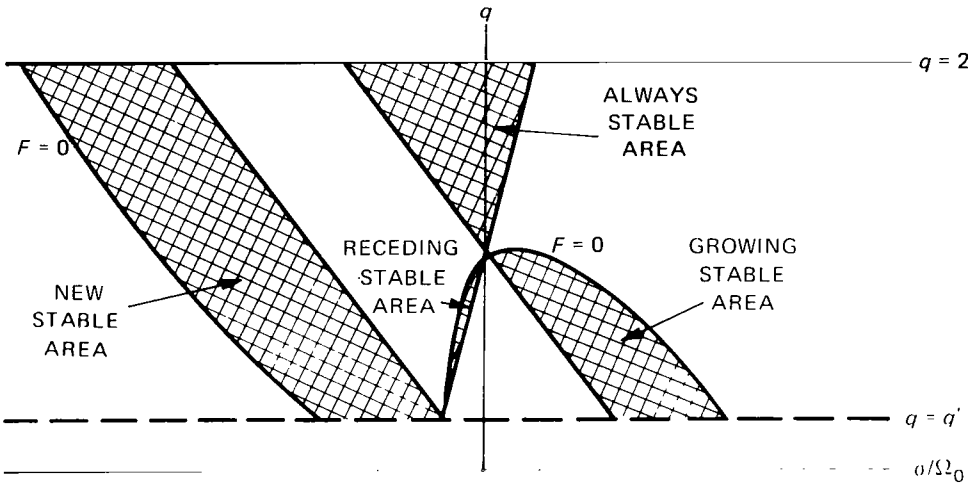

Figure 5.22—Second intermediate stability diagram.

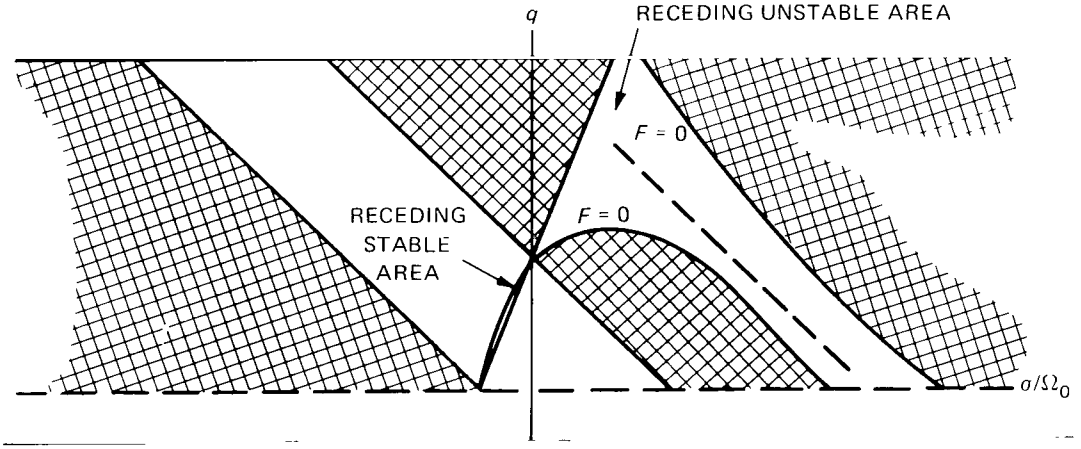

Figure 5.23—Third intermediate stability diagram.

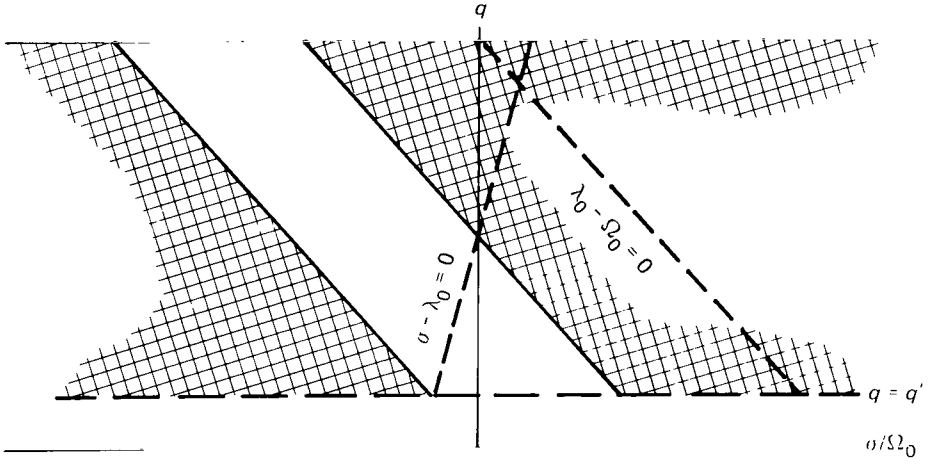

Figure 5.24—Final stability diagram.

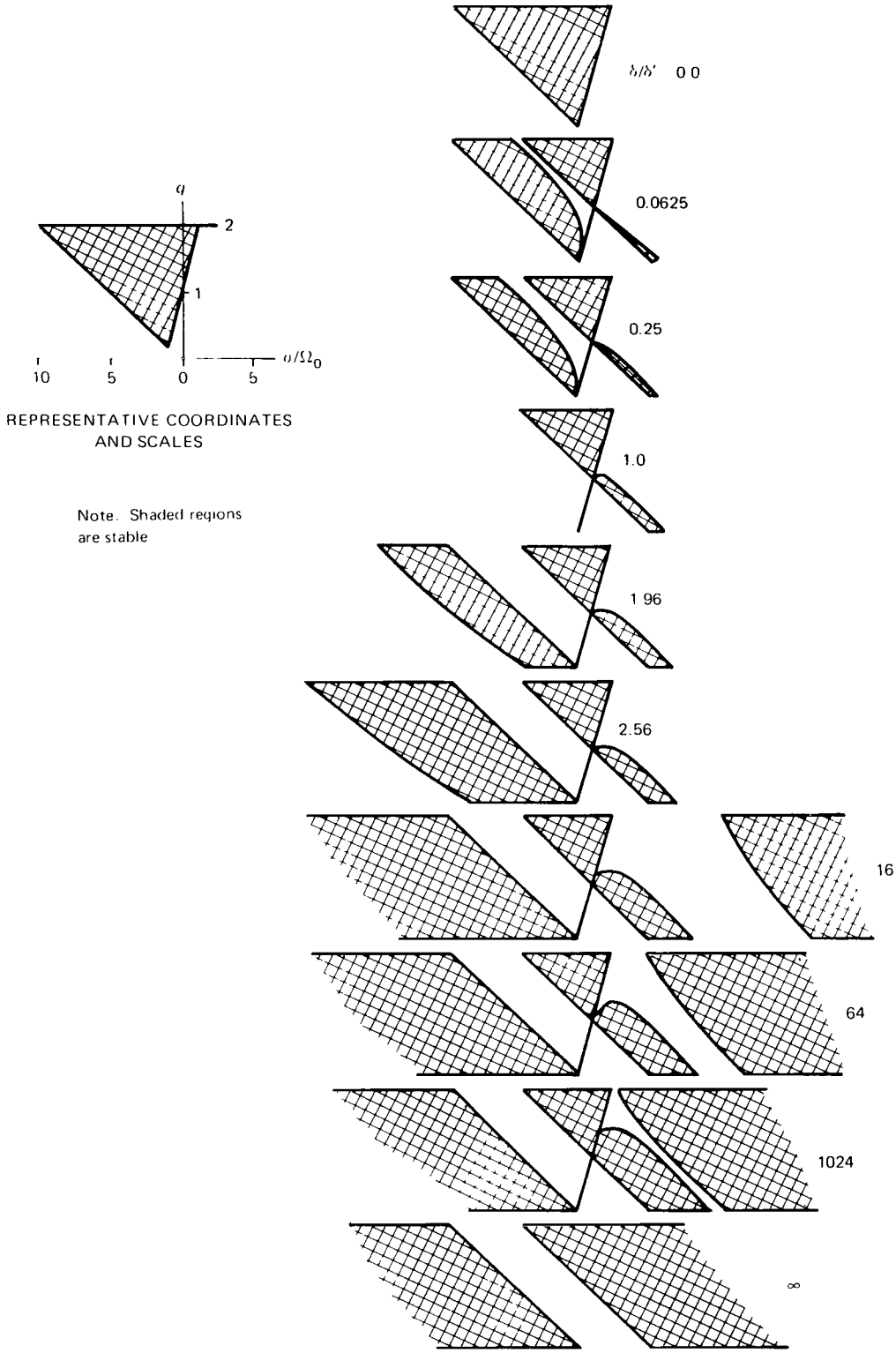

Figure 5.25—Transformation of stability diagram.

CHAPTER 6

POSSIBLE GENERALIZATIONS

In Chapter 3, it was said that, in effect, the unperturbed motion of the system was determined by letting the damper masses vanish; that motion was allowed to drive the dampers, and then their steady-state response to the excitation was found. In Chapter 4 it was shown that, for small damper masses, the spin component of the system angular momentum can be written as

$$H \cos\theta \approx C\omega_3 + J'_3\sigma ,$$

so that

$$-H \sin\theta\, \dot{\theta} \approx C\dot{\omega}_3 .$$

Thus, cone-angle behavior is intimately related to spacecraft spin-rate changes.

The damper motion mentioned above generates reaction torques on the spacecraft; in particular, it generates a spin torque that can change the spacecraft spin rate. From the sign of the average spin component of the reaction torque, the sign of $\dot{\omega}_3$, and consequently the sign of $\dot{\theta}$, can be determined.

In order to assess the significance of the specific damper orientation chosen in this analysis and in the hope of expanding the generality of the results obtained, we consider here the effects of a generalized spring-mass-dashpot damper (arbitrarily positioned with respect to the center of mass and arbitrarily oriented relative to the nominal spin axis) on the motion of a symmetric dual-spin system, using the above-mentioned heuristic approach to the dynamics.

The basic system consists of a symmetric spacecraft and a symmetric wheel driven at a constant relative angular velocity. Figure 6.1 shows this system and gives several pertinent parameter definitions.

A. Unperturbed Motion of the System

The characteristics of the unperturbed motion of the system are given by the solution of the well-known Euler equations:

$$\frac{d}{dt}\mathbf{H} + \boldsymbol{\omega}_T \times \mathbf{H} = 0 ,$$

where

$$\mathbf{H} = A\boldsymbol{\omega} + (C\Omega + J'_3\sigma)\mathbf{k}$$

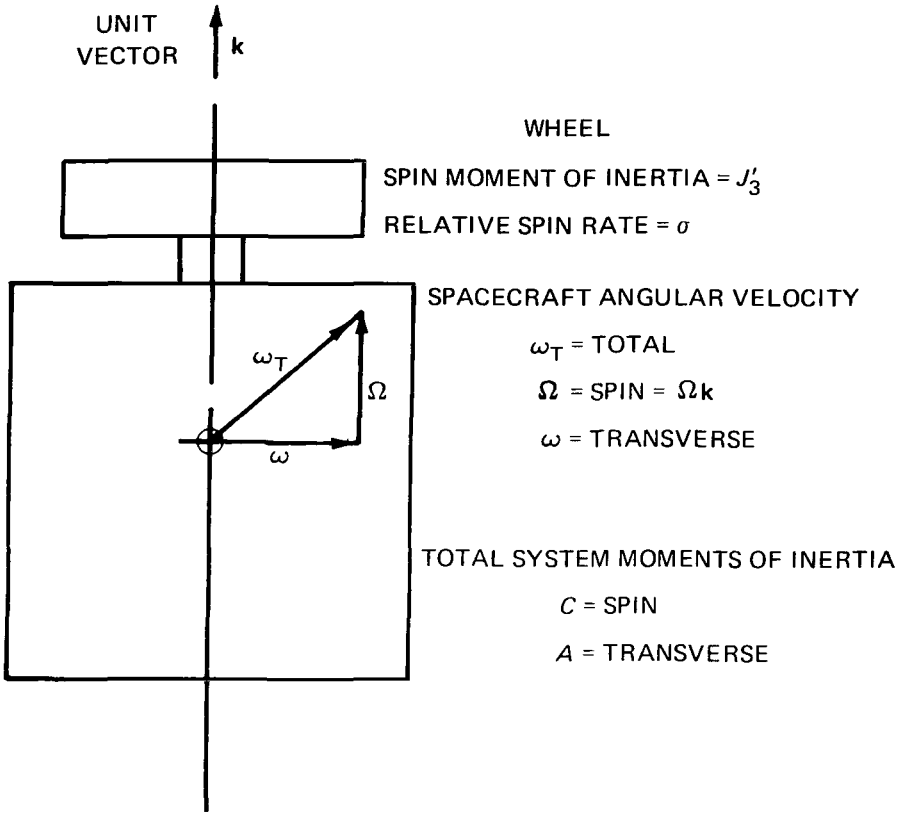

Figure 6.1—Basic dual-spin system.

is the total angular momentum vector and all vectors are measured in a spacecraft-fixed reference frame with origin at the center of mass and one axis along the nominal spin axis.

With the appropriate substitutions and differentiation,

$$A\dot{\omega} + C\dot{\Omega}\mathbf{k} + (\omega + \Omega\mathbf{k}) \times [A\omega + (C\Omega + J_3'\sigma)\mathbf{k}] \simeq 0 ,$$

or

$$A\dot{\omega} + (C\Omega + J_3'\sigma - A\Omega)\omega \times \mathbf{k} = 0$$

and

$$C\dot{\Omega} = 0 .$$

Thus

$$\Omega = \text{constant} \quad \text{and} \quad \dot{\omega} = \lambda\mathbf{k} \times \omega , \tag{6.1}$$

where

$$\lambda = \frac{(C - A)\Omega + J_3'\sigma}{A} ,$$

which is a constant.

If $\omega = (\omega_1, \omega_2, 0)$, Equation 6.1 has the elementary solution $\omega = (\omega \cos \lambda t, \omega \sin \lambda t, 0)$, where ω is a constant of the motion and we have chosen $\omega_2(0) = 0$ without loss of generality.

B. Location and Orientation of the Damper

Let $\mathbf{r}_0$ and $\mathbf{e}$ specify the location and orientation, respectively, of a small, single-axis, spring-mass-dashpot damper with a spring constant k and a damping coefficient c. If ρ locates the active mass of the damper relative to its undeflected position, the actual position of the damper mass is given by $\mathbf{r} = \mathbf{r}_0 + \rho$, where $\rho = \rho_1 \mathbf{e}$. Without loss of generality, we can set one of the components of $\mathbf{r}_0$ equal to zero. We will then be working with the vectors

$$\mathbf{r}_0 = \begin{pmatrix} x_0 \\ 0 \\ y_0 \end{pmatrix},$$

$$\mathbf{e} = \begin{pmatrix} e_1 \\ e_2 \\ e_3 \end{pmatrix},$$

$$\rho = \rho_1 \begin{pmatrix} e_1 \\ e_2 \\ e_3 \end{pmatrix},$$

and

$$\mathbf{r} = \begin{pmatrix} x_0 + \rho_1 e_1 \\ \rho_1 e_2 \\ z_0 + \rho_1 e_3 \end{pmatrix}.$$

C. Damper Equation of Motion

The motion of the active mass of the damper will be given by the solution of the vector equation $m\mathbf{a} = \mathbf{F}$, where m is the mass, $\mathbf{a}$ is the total acceleration, and $\mathbf{F}$ is the total force. In terms of the above vectors, this becomes

$$\begin{aligned} \mathbf{F} &= m[\ddot{\mathbf{r}} + 2\omega_T \times \dot{\mathbf{r}} + \dot{\omega}_T \times \mathbf{r} + \omega_T \times (\omega_T \times \mathbf{r})] \\ &= m[\ddot{\rho} + 2\omega_T \times \dot{\rho} + \dot{\omega} \times \mathbf{r} + \omega_T \times (\omega_T \times \mathbf{r})] \\ &= m[\ddot{\rho} + 2\omega_T \times \dot{\rho} + \lambda(\mathbf{k} \times \omega) \times \mathbf{r} + \omega_T(\omega_T \cdot \mathbf{r}) - \mathbf{r}(\omega_T^2)] \end{aligned}$$

$$= m[\ddot{\boldsymbol{\rho}} + 2\boldsymbol{\omega}_T \times \dot{\boldsymbol{\rho}} + \lambda\boldsymbol{\omega}(\mathbf{r}\cdot\mathbf{k}) - \lambda\mathbf{k}(\mathbf{r}\cdot\boldsymbol{\omega}) + \boldsymbol{\omega}_T(\boldsymbol{\omega}_T\cdot\mathbf{r}) - \mathbf{r}(\omega_T^2)]\,. \tag{6.2}$$

The equation for the axial motion of the mass is obtained from the scalar product of each side of Equation 6.2 and the vector **e**, with the right side becoming $-k\rho_1 - c\dot{\rho}_1$. Thus,

$$m[\ddot{\rho}_1 + \lambda(\mathbf{e}\cdot\boldsymbol{\omega})(\mathbf{r}\cdot\mathbf{k}) - \lambda e_3(\mathbf{r}\cdot\boldsymbol{\omega}) + (\mathbf{e}\cdot\boldsymbol{\omega}_T)(\boldsymbol{\omega}_T\cdot\mathbf{r}) - \omega_T^2(\mathbf{e}\cdot\mathbf{r})] + c\dot{\rho}_1 + k\rho_1 = 0\,. \tag{6.3}$$

D. Spin Component of Reaction Torque on Spacecraft

A reaction force $-\mathbf{F}$ acts at **r**, so the resulting torque on the spacecraft is $\mathbf{T} = \mathbf{F}\times\mathbf{r}$. The system is assumed to be balanced such that this torque vanishes when the damper is caged, i.e., when $\rho_1 = \dot{\rho}_1 = 0$. If $\mathbf{F}_0$ is the corresponding force, it is required that $\mathbf{T}_0 = \mathbf{F}_0\times\mathbf{r}_0 = 0$. Of primary concern is the spin component of the torque $\mathbf{T} - \mathbf{T}_0$, or

$$T_S = \mathbf{k}\cdot(\mathbf{F}\times\mathbf{r} - \mathbf{F}_0\times\mathbf{r}_0)$$

$$= \mathbf{k}\cdot[\mathbf{F}\times\boldsymbol{\rho}_1 - \mathbf{r}_0\times(\mathbf{F}-\mathbf{F}_0)]\,,$$

where **F** is given by Equation 6.2 and

$$\mathbf{F} - \mathbf{F}_0 = m[\ddot{\boldsymbol{\rho}} + 2\boldsymbol{\omega}_T\times\dot{\boldsymbol{\rho}} + \lambda\boldsymbol{\omega}(\boldsymbol{\rho}\cdot\mathbf{k}) - \lambda\mathbf{k}(\boldsymbol{\rho}\cdot\boldsymbol{\omega}) + \boldsymbol{\omega}_T(\boldsymbol{\omega}_T\cdot\boldsymbol{\rho}) - \boldsymbol{\rho}\omega_T^2]\,.$$

Appendix IV gives the derivation of the final result:

$$T_S = m\{-e_2x_0\ddot{\rho}_1 + \dot{\rho}_1[2e_3(\mathbf{r}\cdot\boldsymbol{\omega}_T) - 2\Omega(\rho_1 + \mathbf{r}_0\cdot\mathbf{e})]$$

$$- \rho_1(e_1\omega_2 - e_2\omega_1)[\lambda(z_0 + \rho_1e_3) + \boldsymbol{\omega}_T\cdot\mathbf{r}] - \rho_1x_0\omega_2(\lambda e_3 + \boldsymbol{\omega}_T\cdot\mathbf{e})\}\,. \tag{6.4}$$

E. Special Case I: Damper Parallel to Nominal Spin Axis

We now let $e_1 = e_2 = 0$ and $e_3 = 1$. The resulting equations are

$$\ddot{\rho}_1 + \frac{c}{m}\dot{\rho}_1 + \left(\frac{k}{m} - \omega^2\right)\rho_1 = (\lambda - \Omega)x_0\omega\cos\lambda t + z_0\omega^2$$

and

$$T_S = mx_0\omega[2\dot{\rho}_1\cos\lambda t - \rho_1(\lambda + \Omega)\sin\lambda t]\,. \tag{6.5}$$

The first of these equations is identical to Equation 3.4, produced by the perturbation analysis. The variables ρ_1, x_0, and y_0 are the same quantities labelled z, a, and $-l_2$ previously. This equation can be solved in closed form, and if the steady-state solution is substituted into the second of Equations 6.5, an average value of T_S can be determined in a way analogous to that which produced an average value of $\dot{\theta}$ in Chapter 4.

The equations above can be manipulated to represent the motion and effect of a damper on the wheel as follows. The angular velocity vector for the wheel, in a reference frame rotating with the wheel, has the components $\omega \cos(\lambda - \sigma)t$, $\omega \sin(\lambda - \sigma)t$, and $\Omega + \sigma$. Comparing these with corresponding terms in the total angular velocity vector used in the derivation above ($\omega \cos \lambda t$, $\omega \sin \lambda t$, Ω) shows that the wheel damper equations can be produced by changing the variables λ and Ω such that $\lambda \rightarrow \lambda - \sigma$ and $\Omega \rightarrow \Omega + \sigma$. Thus,

$$\ddot{\rho}'_1 + \frac{c}{m}\dot{\rho}'_1 + \left(\frac{k'}{m'} - \omega^2\right)\rho'_1 = (\lambda - \Omega - 2\sigma)x'_0\omega \cos(\lambda - \sigma)t + z'_0\omega^2$$

and (6.6)

$$T'_S = m'x'_0\omega[2\dot{\rho}'_1 \cos(\lambda - \sigma)t - \rho'_1(\lambda + \Omega) \sin(\lambda - \sigma)t] .$$

In Equations 6.6 and in what follows, primed quantities are used for parameters associated with wheel dampers. Except for the difference in notation (ρ'_1, x'_0, and z'_0 become z', a', and l_1), the first of Equations 6.6 compares favorably with Equation 3.5, derived earlier. These equations can also be analyzed to obtain an average value of T'_S in a straightforward manner.

For this particular damper orientation, then, we can find the average spin torque produced by the steady-state damper response to excitation arising from the general precessional motion of the system with an arbitrarily large cone angle. We now turn to other possible orientations of the dampers.

F. Special Case II: Damper Normal to Spin Axis and Radius Vector

In this case, let $e_1 = e_3 = 0$ and $e_2 = 1$. Equations 6.3 and 6.4 then reduce to

$$\ddot{\rho}_1 + \frac{c}{m}\dot{\rho}_1 + \left[\frac{k}{m} - \omega^2(1 - \sin^2 \lambda t) - \Omega^2\right]\rho_1 = -(\Omega + \lambda)z_0\omega \sin \lambda t - \frac{x_0\omega^2}{2} \sin 2\lambda t$$

and (6.7)

$$T_S = m\left[-x_0\ddot{\rho}_1 - 2\rho_1\dot{\rho}_1\Omega + \rho_1 z_0(\lambda + \Omega)\omega \cos \lambda t + \frac{\rho_1 x_0\omega^2}{2} \cos 2\lambda t + \frac{\rho_1^2\omega^2}{2} \sin 2\lambda t\right] .$$

For a damper on the wheel, these equations become

$$\ddot{\rho}'_1 + \frac{c'}{m'}\dot{\rho}'_1 + \left\{\frac{k'}{m'} - \omega^2[1 - \sin^2(\lambda - \sigma)t] - (\Omega + \sigma)^2\right\}\rho'_1$$

$$= -(\Omega + \lambda)z'_0\omega \sin(\lambda - \sigma)t - \frac{x'_0\omega^2}{2} \sin 2(\lambda - \sigma)t$$

and (6.8)

$$T'_S = m'\left[-x'_0\ddot{\rho}'_1 - 2\rho'_1\dot{\rho}'_1(\Omega + \sigma) + \rho'_1 z'_0(\lambda + \Omega)\omega \cos(\lambda - \sigma)t\right.$$

$$\left. + \frac{\rho'_1 x'_0\omega^2}{2} \cos 2(\lambda - \sigma)t + \frac{\rho'^2_1\omega^2}{2} \sin 2(\lambda - \sigma)t\right] .$$

G. Special Case III: Damper Radial

In the case where $e_1 = 1$ and $e_2 = e_3 = 0$, the damper and torque equations become

$$\ddot{\rho}_1 + \frac{c}{m}\dot{\rho}_1 + \left[\frac{k}{m} - \omega^2(1 - \cos^2 \lambda t) - \Omega^2\right]\rho_1 = -z_0(\lambda + \Omega)\omega \cos \lambda t + x_0(\omega^2 \sin^2 \lambda t + \Omega^2)$$

and (6.9)

$$T_S = m\left[-2\dot{\rho}_1(\rho_1 + x_0)\Omega - \rho_1 z_0(\lambda + \Omega)\omega \sin \lambda t - \frac{\rho_1 \omega^2}{2}(2x_0 + \rho_1) \sin 2\lambda t\right] .$$

For a damper on the wheel, these equations become

$$\ddot{\rho}'_1 + \frac{c'}{m'}\dot{\rho}'_1 + \left\{\frac{k'}{m'} - \omega^2[1 - \cos^2 (\lambda - \sigma)t] - (\Omega + \sigma)^2\right\}\rho'_1$$

$$= -z'_0(\lambda + \Omega)\omega \cos (\lambda - \sigma)t + x'_0[\omega^2 \sin^2 (\lambda - \sigma)t + (\Omega + \sigma)^2]$$

and (6.10)

$$T'_S = m'\left[-2\dot{\rho}'_1(\rho'_1 + x'_0)(\Omega + \sigma) - \rho'_1 z'_0(\lambda + \Omega)\omega \sin (\lambda - \sigma)t\right.$$

$$\left. - \frac{\rho'_1 \omega^2}{2}(2x'_0 + \rho'_1) \sin 2(\lambda - \sigma)t\right] .$$

The damper equations obtained for Special Cases II and III are clearly more complicated in general than those associated with Special Case I. They involve periodic coefficients and are similar in form to Mathieu equations with sinusoidal forcing functions of two frequencies. For small angles (ω^2 small), however, they reduce to tractable constant-coefficient equations, and they will be analyzed on that basis.

The average spin-axis torque arising from the steady-state motion of the various dampers considered above will now be determined, with the assumption of small-angle motion for the system.

H. Small-Angle Analysis of the Special Cases

Spacecraft Damper of Case I

For Case I, the appropriate spacecraft damper equation of motion is

$$\ddot{\rho}_1 + \frac{c}{m}\dot{\rho}_1 + \frac{k}{m}\rho_1 = (\lambda - \Omega)x_0\omega \cos \lambda t ,$$

with a steady-state solution

$$\rho_1 = B' \sin \lambda t + C' \cos \lambda t .$$

The spin torque is given by

$$T_S = mx_0\omega[2\dot{\rho}_1 \cos\lambda t - \rho_1(\lambda + \Omega) \sin\lambda t] ,$$

so that the average torque will be

$$\bar{T}_S = mx_0\omega[B'\lambda - \tfrac{1}{2}B'(\lambda + \Omega)]$$

$$= \frac{mx_0\omega}{2} B'(\lambda - \Omega) .$$

Since

$$B' = \frac{\begin{vmatrix} 0 & -\lambda\frac{c}{m} \\ (\lambda - \Omega)x_0\omega & \frac{k}{m} - \lambda^2 \end{vmatrix}}{\begin{vmatrix} \frac{k}{m} - \lambda^2 & -\lambda\frac{c}{m} \\ \lambda\frac{c}{m} & \frac{k}{m} - \lambda^2 \end{vmatrix}} ,$$

we have

$$\bar{T}_S = \frac{\tfrac{1}{2}cx_0^2\omega^2\lambda(\lambda - \Omega)^2}{\left(\frac{k}{m} - \lambda^2\right)^2 + \left(\lambda\frac{c}{m}\right)^2} . \qquad (6.11)$$

Wheel Damper of Case I

For Case I, the appropriate wheel damper equation of motion is

$$\ddot{\rho}_1' + \frac{c'}{m'}\dot{\rho}_1' + \frac{k'}{m'}\rho_1 = (\lambda - \Omega - 2\sigma)x_0\omega \cos(\lambda - \sigma)t ,$$

with a steady-state solution

$$\rho_1' = B' \sin(\lambda - \sigma)t + C' \cos(\lambda - \sigma)t .$$

The spin torque is given by

$$T_S' = m'x_0'\omega[2\dot{\rho}_1' \cos(\lambda - \sigma)t - \rho_1'(\lambda + \Omega) \sin(\lambda - \sigma)t] ,$$

so that the average torque will be

$$\bar{T}'_S = m'x'_0\omega[B'(\lambda - \sigma) - \tfrac{1}{2}B'(\lambda + \Omega)]$$

$$= \frac{m'x'_0\omega}{2}B'(\lambda - 2\sigma - \Omega) .$$

Since

$$B' = \frac{\begin{vmatrix} 0 & -(\lambda-\sigma)\dfrac{c'}{m'} \\ (\lambda - \Omega - 2\sigma)x_0\omega & \dfrac{k'}{m'} - (\lambda-\sigma)^2 \end{vmatrix}}{\begin{vmatrix} \dfrac{k'}{m'} - (\lambda-\sigma)^2 & -(\lambda-\sigma)\dfrac{c'}{m'} \\ (\lambda-\sigma)\dfrac{c'}{m'} & \dfrac{k'}{m'} - (\lambda-\sigma)^2 \end{vmatrix}} ,$$

we have

$$\bar{T}'_S = \frac{\tfrac{1}{2}c'x'^2_0\omega^2(\lambda-\sigma)(2\sigma - \lambda + \Omega)^2}{\left[\dfrac{k'}{m'} - (\lambda-\sigma)^2\right]^2 + \left[(\lambda-\sigma)\dfrac{c'}{m'}\right]^2} . \tag{6.12}$$

Spacecraft Damper of Case II

For Case II, the appropriate spacecraft damper equation of motion is

$$\ddot{\rho}_1 + \frac{c}{m}\dot{\rho}_1 + \left(\frac{k}{m} - \Omega^2\right)\rho_1 = -(\Omega + \lambda)z_0\omega \sin\lambda t ,$$

with a steady-state solution

$$\rho_1 = B' \sin\lambda t + C' \cos\lambda t .$$

The spin torque is given by

$$T_S = m[-x_0\ddot{\rho}_1 - 2\rho_1\dot{\rho}_1\Omega + \rho_1 z_0(\lambda + \Omega)\omega \cos\lambda t] ,$$

so that the average torque will be

$$\bar{T}_S = \frac{mz_0\omega C'(\lambda + \Omega)}{2} .$$

Since

$$C' = \frac{\begin{vmatrix} \frac{k}{m} - \Omega^2 - \lambda^2 & -(\Omega + \lambda) z_0 \omega \\ \frac{c}{m}\lambda & 0 \end{vmatrix}}{\begin{vmatrix} \frac{k}{m} - \Omega^2 - \lambda^2 & -\frac{c}{m}\lambda \\ \frac{c}{m}\lambda & \frac{k}{m} - \Omega^2 - \lambda^2 \end{vmatrix}},$$

we have

$$\overline{T}_S = \frac{\frac{1}{2} c z_0^2 \omega^2 \lambda (\lambda + \Omega)^2}{\left(\frac{k}{m} - \Omega^2 - \lambda^2\right)^2 + \left(\frac{c}{m}\lambda\right)^2} . \tag{6.13}$$

Wheel Damper of Case II

For Case II, the appropriate wheel damper equation of motion is

$$\ddot{\rho}'_1 + \frac{c'}{m'}\dot{\rho}'_1 + \left[\frac{k'}{m'} - (\Omega + \sigma)^2\right]\rho'_1 = -(\Omega + \lambda) z'_0 \omega \sin(\lambda - \sigma)t ,$$

with a steady-state solution

$$\rho'_1 = B' \sin(\lambda - \sigma)t + C' \cos(\lambda - \sigma)t .$$

The spin torque is given by

$$T'_S = m'[-x'_0 \ddot{\rho}'_1 - 2\rho'_1 \dot{\rho}'_1 (\Omega + \sigma) + \rho'_1 z'_0 (\lambda + \Omega)\omega \cos(\lambda - \sigma)t] ,$$

so that the average torque will be

$$\overline{T}'_S = \tfrac{1}{2} m' z'_0 \omega (\lambda + \Omega) C' .$$

Since

$$C' = \frac{\begin{vmatrix} \frac{k'}{m'} - (\Omega + \sigma)^2 - (\lambda - \sigma)^2 & -(\Omega + \lambda) z'_0 \omega \\ (\lambda - \sigma)\frac{c'}{m'} & 0 \end{vmatrix}}{\begin{vmatrix} \frac{k'}{m'} - (\Omega + \sigma)^2 - (\lambda - \sigma)^2 & -(\lambda - \sigma)\frac{c'}{m'} \\ (\lambda - \sigma)\frac{c'}{m'} & \frac{k'}{m'} - (\Omega + \sigma)^2 - (\lambda - \sigma)^2 \end{vmatrix}},$$

we have

$$\overline{T}'_S = \frac{\frac{1}{2}c'z_0'^2\omega^2(\lambda - \sigma)(\Omega + \lambda)^2}{\left[\frac{k'}{m'} - (\Omega + \sigma)^2 - (\lambda - \sigma)^2\right]^2 + \left[(\lambda - \sigma)\frac{c'}{m'}\right]^2} . \tag{6.14}$$

Spacecraft Damper of Case III

For Case III, the appropriate spacecraft damper equation of motion is

$$\ddot{\rho}_1 + \frac{c}{m}\dot{\rho}_1 + \left(\frac{k}{m} - \Omega^2\right)\rho_1 = -z_0(\lambda + \Omega)\omega \cos \lambda t + x_0\Omega^2 ,$$

with a steady-state solution

$$\rho_1 = A' + B' \sin \lambda t + C' \cos \lambda t .$$

The spin torque is given by

$$T_S = m[-2\dot{\rho}_1(\rho_1 + x_0)\Omega - \rho_1 z_0(\lambda + \Omega)\omega \sin \lambda t] ,$$

so that the average torque will be

$$\overline{T}_S = -\frac{1}{2}mz_0\omega(\lambda + \Omega)B' .$$

Since

$$B' = \frac{\begin{vmatrix} 0 & -\frac{c}{m}\lambda \\ -z_0(\lambda + \Omega)\omega & \frac{k}{m} - \Omega^2 - \lambda^2 \end{vmatrix}}{\begin{vmatrix} \frac{k}{m} - \Omega^2 - \lambda^2 & -\frac{c}{m}\lambda \\ \frac{c}{m}\lambda & \frac{k}{m} - \Omega^2 - \lambda^2 \end{vmatrix}} ,$$

we have

$$\overline{T}_S = \frac{\frac{1}{2}cz_0^2\omega^2\lambda(\lambda + \Omega)^2}{\left(\frac{k}{m} - \Omega^2 - \lambda^2\right)^2 + \left(\frac{c}{m}\lambda\right)^2} . \tag{6.15}$$

Wheel Damper of Case III

For Case III, the appropriate wheel damper equation of motion is

$$\ddot{\rho}'_1 + \frac{c'}{m'}\dot{\rho}'_1 + \left[\frac{k'}{m'} - (\Omega + \sigma)^2\right]\rho'_1 = -z'_0(\lambda + \Omega)\omega \cos(\lambda - \sigma)t + x'_0(\Omega + \sigma)^2 ,$$

with a steady-state solution

$$\rho'_1 = A' + B' \sin(\lambda - \sigma)t + C' \cos(\lambda - \sigma)t .$$

The spin torque is given by

$$T'_S = m'[-2\dot{\rho}'_1(\rho'_1 + x'_0)(\Omega + \sigma) - \rho'_1 z'_0(\lambda + \Omega)\omega \sin(\lambda - \sigma)t] ,$$

so that the average torque will be

$$\bar{T}'_S = -\tfrac{1}{2}m'z'_0\omega(\lambda + \Omega)B' .$$

Since

$$B' = \frac{\begin{vmatrix} 0 & -\frac{c'}{m'}(\lambda - \sigma) \\ -z'_0(\lambda + \Omega)\omega & \frac{k'}{m'} - (\Omega + \sigma)^2 - (\lambda - \sigma)^2 \end{vmatrix}}{\begin{vmatrix} \frac{k'}{m'} - (\Omega + \sigma)^2 - (\lambda - \sigma)^2 & -\frac{c'}{m'}(\lambda - \sigma) \\ \frac{c'}{m'}(\lambda - \sigma) & \frac{k'}{m'} - (\Omega + \sigma)^2 - (\lambda - \sigma)^2 \end{vmatrix}} ,$$

we have

$$\bar{T}'_S = \frac{\tfrac{1}{2}m'z'^2_0\omega^2(\lambda - \sigma)(\lambda + \Omega)^2}{\left[\frac{k'}{m'} - (\Omega + \sigma)^2 - (\lambda - \sigma)^2\right]^2 + \left[\frac{c'}{m'}(\lambda - \sigma)\right]^2} . \tag{6.16}$$

I. General Observations

Equations 6.11 through 6.16 are similar in many ways. Of particular interest is the preponderance of positive terms. Although the various equations differ in detail, it can easily be seen that the sign of λ controls the sign of the average torque for each of the spacecraft dampers, and the sign of $\lambda - \sigma$ determines the sign of the average torque for each of the wheel dampers. These quantities represent the rotation rate of the transverse angular velocity vector in a reference frame fixed in the respective body. In general, then, damping in a particular body increases the spacecraft spin rate if the transverse angular velocity vector moves counterclockwise in that body. For lack of a better word, this type of motion will be called a positive nutation rate.

Earlier in this chapter, we showed that spin rate increases imply cone angle decreases. Thus, damping in a particular body decreases the cone angle if the nutation rate in that body is positive. For

a single-spin spacecraft, the nutation rate λ, the spin rate Ω, and the moments of inertia C and A are related by $\lambda = (C/A - 1)\Omega$. The spin rate and the cone angle are related by $C\Omega = H \cos\theta$, where H is the total angular momentum, which we take as a positive quantity that is a constant of the motion for a system free of external torques. For θ near 0°, stability would involve a decreasing cone angle, and for motion near 180°, an increasing θ would indicate stability. In either case, stability can be seen to require $C > A$, the usual moment of inertia constraint for spinning bodies.

Nutation (as defined above) is a measurable quantity in a spinning body, but it is not an obvious characteristic of torque-free motion to an outside observer. The spin rate is observable, of course, and if there is any cone angle present, another quantity, the precession rate, can be seen. This is the rate at which the nominal spin axis actually moves around the inertially fixed angular momentum vector, and it is one of the usual "Euler angle" rates in textbook descriptions of rigid body motion ($\dot{\psi}_1$ in Figure 6.2). If the system angular momentum is expressed in terms of the Euler angle rate vectors, it can be easily shown that $\dot{\psi}_1 = H/A$, if $\dot{\theta}$ vanishes, as it does for the torque-free motion of a symmetric body.

The relationship $\dot{\psi}_1 = H/A$ holds for dual-spin systems as well, since the transverse angular momentum is still $A\omega$. For the dual-spin system, we have the relationships

$$C\Omega + J_3'\sigma = H \cos\theta ,$$

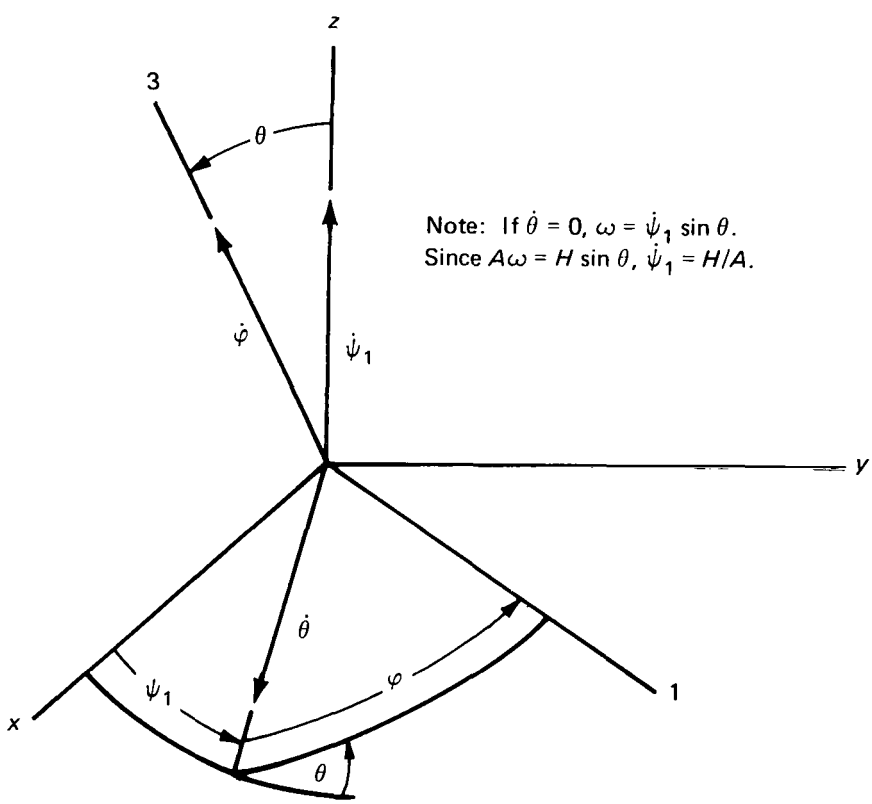

Figure 6.2—Orientation of a rigid body by a 3-1-3 transformation of angles ψ_1, θ, and φ.

$$\lambda = \left(\frac{C}{A} - 1\right)\Omega + \frac{J'_3}{A}\sigma ,$$

and

$$\dot{\psi}_1 = \frac{H}{A} ,$$

which can be combined to yield

$$\lambda = \dot{\psi}_1 \cos\theta - \Omega .$$

For the case of small cone angles, $\lambda \approx \dot{\psi}_1 - \Omega$. Spacecraft damping is stabilizing if $\lambda > 0$, or in this case, if $\dot{\psi}_1 > \Omega$; wheel damping is stabilizing if $\lambda - \sigma > 0$, which in this case requires $\dot{\psi}_1 > \Omega + \sigma$. Thus, we deduce that damping on a particular body is stabilizing if that body precesses faster than it spins.

J. Energy Dissipation

The damper equations just considered were all of the general form

$$\ddot{\rho}_1 + \frac{c}{m}\dot{\rho}_1 + K_1\rho_1 = a + \beta_1 \sin(\gamma t + \varphi_1) ,$$

with a steady-state solution of the form

$$\rho_1 = A' + B' \sin(\gamma t + \varphi_1) + C' \cos(\gamma t + \varphi_1) .$$

The energy dissipation rate for the damper is

$$P = c\dot{\rho}^2 ,$$

and the average rate is given by

$$\bar{P} = \tfrac{1}{2}c\gamma^2(B'^2 + C'^2) .$$

It can be easily shown that

$$B'^2 + C'^2 = \frac{\beta_1^2}{\left(K - \gamma^2\right)^2 + \left(\frac{c}{m}\gamma\right)^2} .$$

Thus

$$\bar{P} = \tfrac{1}{2}c\frac{\gamma^2\beta_1^2}{\left(K - \gamma^2\right)^2 + \left(\frac{c}{m}\gamma\right)^2} .$$

Term-by-term inspection of the average spin-axis torque expressions, Equations 6.11 through 6.16, shows that in every case they are of the form

$$\bar{T}_S = \frac{\bar{P}}{\gamma}.$$

If a dual-spin system containing any arbitrary combination of the above types of dampers is considered, all of the spacecraft dampers will be driven at the frequency λ, and the wheel dampers at the frequency $\lambda - \sigma$. The average torques in the system will combine linearly, and we can say in general that

$$\bar{T}_S = \frac{P_S}{\lambda} + \frac{P_W}{\lambda - \sigma}, \tag{6.17}$$

where P_S and P_W represent the rates of energy dissipation in the spacecraft and the wheel, respectively, and are inherently positive quantities.

Since an increasing spin rate implies a decreasing cone angle, stability for an arbitrary initial state requires

$$\bar{T}_S \cos\theta_0 > 0, \tag{6.18}$$

where θ_0 is either 0° or 180°.

Equations 6.17 and 6.18 are of a form reminiscent of a result presented by Likins (Reference 13) after an "energy sink" analysis of the attitude stability of a similar dual-spin system. In fact, with allowances for differences in notation, the conclusions are identical.

Working with linearized equations, Likins ignored equations "involving the changes in rotation rates of the two bodies about their common axis ... under the assumption of small motor and bearing friction torques" and assumed that any damping present would decrease the kinetic energy of the system, i.e., $T < 0$. Then, recognizing the conservation of angular momentum in the system, he manipulated appropriate equations to deduce that the decreasing energy implies a stability criterion equivalent to that deduced here.

Now, with the assumption of a constant wheel rate, it can be shown that in the case of prime interest in dual-spin stabilization (i.e., the stability of pure rotations about the axis of minimum moment of inertia), stable equilibrium involves a maximum energy state. That is, stable behavior implies an increasing kinetic energy for the system. This can be seen by combination of the equations

$$T = \tfrac{1}{2}A\omega^2 + \tfrac{1}{2}(C - J_3')\Omega^2 + \tfrac{1}{2}J_3'(\Omega + \sigma)^2,$$

$$A\omega = H \sin\theta,$$

and

$$C\Omega + J_3'\sigma = H \cos\theta$$

to obtain

$$T = \frac{C - A}{2AC} \sin^2 \theta + \text{constant} . \tag{6.19}$$

Equation 6.19 shows that, for the dual-spin system, 0°, 90°, and 180° will always represent extrema in kinetic energy. For "favorable" systems (i.e., $C > A$) pure spins about the nominal spin axis will be minimum-energy states. In this, the dual-spin system is similar to a single-spin body, but static equilibrium might involve any cone angle ($0° \leqslant \theta_0 \leqslant 180°$). Thus, in terms of kinetic energy, maximum, minimum, or even intermediate energy states can be stable.

In light of the above considerations, the previously mentioned agreement with Likins' result is somewhat surprising. In fact, one might reasonably reject *a priori* "energy sink" analyses in the area of dual-spin stabilization.

However, it has been shown that our stability criterion takes on a simple form when expressed in terms of the amount of energy dissipated on each of the bodies, although we have not said anything about the overall system kinetic energy. Our result, as given by Equation 6.17, can be interpreted in terms of a dimensionless stability diagram [in the $(\sigma/\Omega_0)q$-plane representation used earlier].

Again, for definiteness of cone angle only, it is assumed that $\Omega_0 > 0$. The initial-state plane (Figure 6.3) then becomes divided into various regions characterized by the signs of the quantities $\cos\theta_0$,

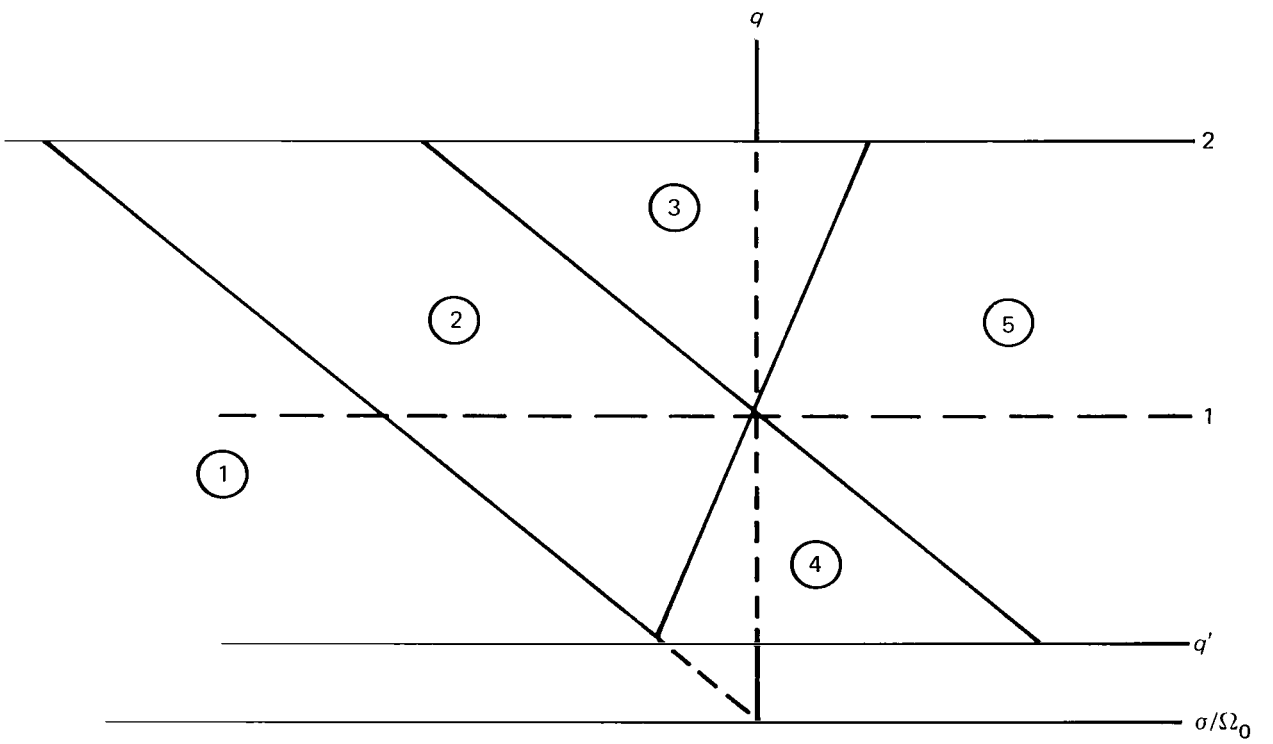

Figure 6.3—Subdivided initial-state plane.

λ, and $\lambda - \sigma$. Quantities pertinent to the subdivision of the initial-state plane shown are repeated here for reference.

$$q = \frac{C}{A},$$

$$q' = \frac{J_3'}{A},$$

$$\lambda = (q - 1)\Omega_0 + q'\sigma,$$

and

$$q\Omega_0 + q'\sigma = \frac{H}{A}\cos\theta_0 .$$

With the previously mentioned assumption that $\Omega_0 > 0$, these regions represent the combination of variables shown in Table 6.1.

Regions 3 and 4 are seen to be always stable and always unstable, respectively. In the other regions, however, stability or instability depends on the relative dissipation in the two bodies, and the requirement for stability becomes

(1) $\frac{P_S}{P_W} > \frac{\lambda}{\sigma - \lambda}$ for Region 1.

(2) $\frac{P_S}{P_W} < \frac{\lambda}{\sigma - \lambda}$ for Region 2.

(3) $\frac{P_S}{P_W} > \frac{\lambda}{\sigma - \lambda}$ for Region 3.

Thus, the quantity $k_1 = \lambda/(\sigma - \lambda)$ represents either an upper or lower limit for the ratio P_S/P_W for stability. Lines of constant k_1 can be determined algebraically and simply as follows:

Table 6.1–Characteristics of initial state regions.

Region	Cone Angle	Sgn (λ)	Sgn ($\lambda - \sigma$)	Effect of Damping	
				Spacecraft	Wheel
1	180°	−	+	Stabilizing	Destabilizing
2	0°	−	+	Destabilizing	Stabilizing
3	0°	+	+	Stabilizing	Stabilizing
4	0°	−	−	Destabilizing	Destabilizing
5	0°	+	−	Stabilizing	Destabilizing

$$\frac{\lambda}{\sigma - \lambda} = k_1 \quad \Rightarrow \quad \lambda = \frac{k_1}{1 + k_1}\sigma ,$$

but

$$\lambda = (q - 1)\Omega_0 + q'\sigma .$$

Thus

$$q + q'\frac{\sigma}{\Omega_0} - 1 = \frac{k_1}{1 + k_1}\frac{\sigma}{\Omega_0} ,$$

or

$$q = 1 + \left(\frac{k_1}{1 + k_1} - q'\right)\frac{\sigma}{\Omega_0} .$$

These lines all pass through the point (0, 1) and are obviously straight lines with a slope of $k_1/(1 + k_1) - q'$.

In the limiting cases of $k_1 = 0$ and $k_1 = \infty$, these lines are $q + q'(\sigma/\Omega_0) = 1$ and $q + q'(\sigma/\Omega_0) = 1 + \sigma/\Omega_0$. The line will be horizontal when $k_1 = q'/(1 - q')$. Figure 6.4 shows this overall result.

The above result suggests that the transformation of the stability diagram, discussed earlier in terms of the parameters δ and δ' for the specific system analyzed, can be understood quite simply in terms of the quantity k_1, which measures the relative energy dissipation in the spacecraft and the wheel. Figure 6.5 shows how the transformation progresses.

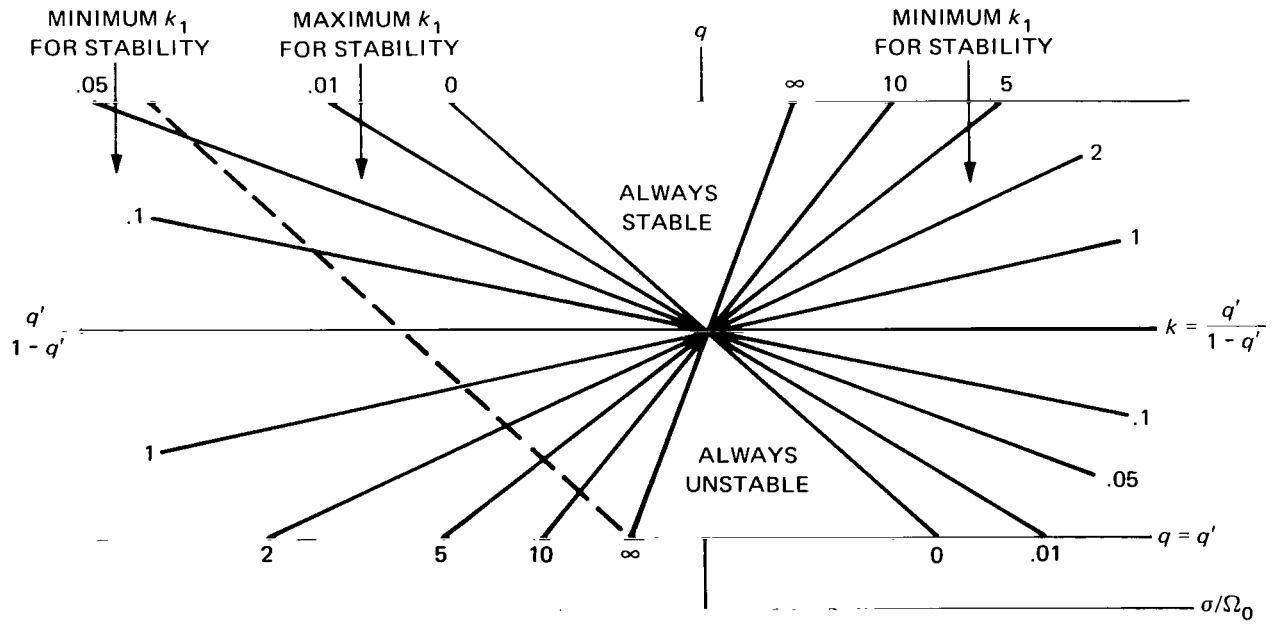

Figure 6.4—Stability diagram with damping on both bodies in terms of the energy dissipation ratio k_1.

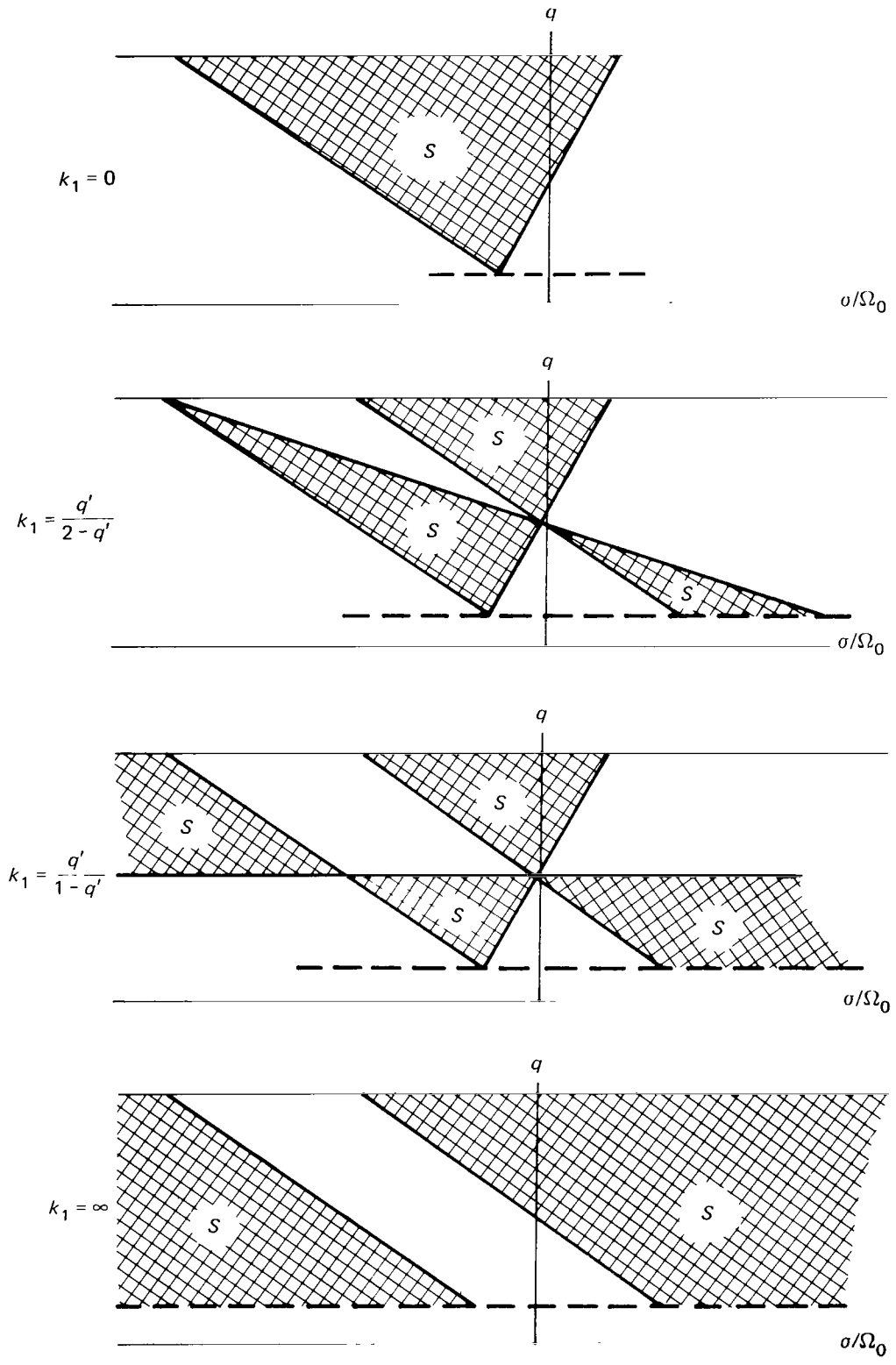

Figure 6.5—Transformation of stability diagram in terms of k_1.

CHAPTER 7

SUMMARY AND CONCLUDING REMARKS

The research reported here concerns the attitude stability of a dual-spin spacecraft whose behavior is described by a seventh-order, nonlinear, nonautonomous set of ordinary differential equations, inconveniently coupled even in the highest derivatives.

In the recent literature, this and similar systems are analyzed by linearization of the equations of motion about a reference motion that is a pure rotation about the nominal spin axis, or equivalently, linearization in six of the seven dependent variables. One of the resulting equations integrates trivially, reducing the order to six. The remaining equations have periodic coefficients and are studied by numerical Floquet analyses of very special cases.

With damping on one body only, however, the linearized equations have constant coefficients, and the order of the system is reduced to four. More general results are then obtainable by a Routhian analysis of the characteristic equation for the system. Five Routhian inequalities necessary and sufficient for stability are produced by this procedure. Two are trivially satisfied for practical systems, one is a somewhat general criterion not related to the damper mass sizes, and the other two impose damper size limitations.

The initial motivation for this work was a curiosity about the nature of instabilities in such a dual-spin system. Unstable single-spin spacecraft are subject to the well-known flat-spin or tumble instability, but nothing could be found in the literature concerning analogous behavior for dual-spin systems.

In the approach to this problem, gross linearization of the equations of motion was rejected *a priori*, since "large angle" motion of the system was anticipated where instabilities occur. Physical insight eventually led to the perturbation technique applied to this problem.

Through consideration of the nonlinear equations of motion with the damper masses vanishingly small, the "rigid body" behavior of the system was revealed, and the unperturbed motion of the system was found to be similar to the general precession of the torque-free, symmetric, rigid body in classical mechanics. Then, with the retention of all terms up to the first order in the damper masses, equations were produced that represented the first-order behavior of the dampers, and these were solvable in closed form.

Since an inertially fixed angular momentum vector is necessarily a constant of the motion for the system, in spite of the complicated nature of the equations, the spin component of this momentum

and the equations of motion were used to deduce an exact differential equation controlling the behavior of the system cone angle. This equation is of a form amenable to analysis by an averaging technique, which produced an equation of the form $\dot{\theta} = f(\theta)$ governing secular changes in the cone angle.

Since in spin-stabilized systems the behavior of the cone angle alone often represents all one wishes to know about stability, the perturbation analysis had, in effect, determined the essential behavior of a system characterized by a seventh-order, nonlinear, nonautonomous set of differential equations with arbitrary initial conditions in terms of a first-order equation. Plotting the function $f(\theta)$ for a particular configuration immediately reveals the stability characteristics of the system, indicates "zones of attraction" for particular stable equilibrium points, and shows the "time constant" associated with cone-angle buildup or decay near equilibrium states.

In appropriately reduced form, the general stability criterion developed was compared to pertinent results in the recent literature, all of which treat "small-angle" stability as mentioned before, and generally good agreement was found. In addition, however, analytical stability boundaries were established where only numerical Floquet results were found in the literature, and the nature of possible instabilities was revealed.

Two general types of instability were found—complete inversions of the system and an eventual steady-state cone angle. In the former case, the spacecraft literally turns upside down in reaching a stable equilibrium state, and in the latter, calculable stable cone angles ranging from 0° to 180° are found. The inversion phenomenen is unreported in the literature, if known at all, and the flat-spin instability of single-spin spacecraft is a special case of the other type of instability.

Fairly general stability diagrams appear in the literature for the special cases of damping on only one of the bodies. These diagrams are shown to be consistent with the general first-order stability criteria developed here, and, in addition, unstable regions are divided according to the nature of the instability. Also, these diagrams are generalized to cases with damping on both bodies, and the transformation of the stability diagram as damping is gradually shifted from one of the bodies to the other is revealed.

Certain possible instabilities revealed by Routhian and Floquet analyses in the literature were undetected in the perturbation analysis reported here. These are characterized by inequalities which limit the sizes of the damper masses. The significance of these limitations is greatly enhanced in cases where one attempts to "tune" the dampers to very low excitation frequencies. In practice, these instabilities are unlikely, due to the unrealistically low spring constants required for tuning. Since the pertinent inequalities are related to the sizes of the damper masses, it is felt that they represent second-order effects relative to the perturbation analysis reported here. They arise because of the coupling between equations and were undetected here because the equations uncoupled in this first-order perturbation analysis.

Possible generalizations of the results obtained are sought by a determination of the effect of an arbitrarily positioned and arbitrarily oriented spring-mass-dashpot damper in a dual-spin system. In general, the damper equations derived are of the Mathieu type, so that instabilities within the dampers themselves can occur. For small-angle motion, however, all of the equations reduce to constant-coefficient linear equations solvable in closed form, and the spin-axis torques generated by their

motions can be found. Although quantitative differences exist for various damper locations and orientations, all have in common the characteristic that damping on a particular body is stabilizing if that body precesses faster than it spins. For a single-spin body, this statement is equivalent to the maximum-inertia axis rule for stability of rotations in the presence of energy dissipation.

The average spin-axis torque generated by a particular damper is found to be simply related to the average rate of energy dissipation in that damper and the excitation rate at which it is driven. This fact permits a generalization to a simple stability criterion applicable to a system with any number of arbitrarily positioned and arbitrarily oriented spring mass-dashpot dampers. This criterion is consistent with a result obtained in the literature by an "energy sink" approach to dual-spin stabilization, but the agreement is, in principle, puzzling. The energy sink approach assumes a monotonically decreasing kinetic energy, but, in the case of our system, stable behavior often involves a move to a maximum energy state.

Goddard Space Flight Center
National Aeronautics and Space Administration
Greenbelt, Maryland, May 29, 1970
877-11-75-01-51

REFERENCES

1. Thomson, W. T., and Reiter, G. S., "Attitude Drift of Space Vehicles," *J. Astronautical Sci.* 7, p. 29, 1960.

2. Thomson, W. T., "Introduction to Space Dynamics," New York: John Wiley and Sons, 1961.

3. Huston, R. L., "Gyroscopic Stabilization of Space Vehicles," *American Institute of Aeronautics and Astronautics J.* 1(7), p. 1694, 1963.

4. Landon, V. D., and Stewart, B., "Nutational Stability of an Axisymmetric Body Containing a Rotor," *J. Spacecr. Rockets* 1(6), p. 682, 1964.

5. "Proceedings of the Symposium on Attitude Stabilization and Control of Dual-Spin Spacecraft," Aerospace Corporation TR-0158(3307-01)-16, Los Angeles, Calif., 1967.

6. Fang, B. T., "Energy Considerations for Attitude Stability of Dual-Spin Spacecraft," *J. Spacecr. Rockets* 5(10), p. 1241, 1968.

7. Fang, B. T., "Additional Results on Attitude Stability of Dual-Spin Spacecraft," The Catholic University of America Report No. 68-010, Washington, D.C., 1968.

8. Cloutier, G. J., "Stable Rotation States of Dual-Spin Spacecraft," *J. Spacecr. Rockets* 5(4), p. 490, 1968.

9. Cloutier, G. J., "Nutation Damper Design Principles for Dual-Spin Spacecraft," *J. Astronautical Sci.* 16(2), p. 79, 1969.

10. Cloutier, G. J., "Nutation Damper Instability on Spin-Stabilized Spacecraft," *American Institute of Aeronautics and Astronautics J.* 7(11), p. 2110, 1969.

11. Mingori, D. L., "Effects of Energy Dissipation on the Attitude Stability of Dual-Spin Satellites," *American Institute of Aeronautics and Astronautics J.* 7(1), p. 20, 1969.

12. Bogoliubov, N. N., and Mitropolsky, Y. A., "Asymptotic Methods in the Theory of Nonlinear Oscillations," Delhi, India: Hindustan Publishing Corporation, 1961.

13. Likins, P. W., "Attitude Stability Criteria for Dual-Spin Spacecraft," *J. Spacecr. Rockets* 4(12), p. 1638, 1967.

SELECTED BIBLIOGRAPHY

Fang, B. T., "Reply by Author to D. L. Mingori and W. J. Russell," *J. Spacecr. Rockets* 6(3), p. 352, 1969.

Likins, P. W., and Mingori, D. L., "Liapunov Stability Analysis of Freely Spinning Systems," Proceedings of the 18th International Astronautical Federation Congress, Belgrade, Yugoslavia, 1967.

Mingori, D. L., "Comments on 'Energy Considerations for Attitude Stability of Dual-Spin Spacecraft'," *J. Spacecr. Rockets* 6(3), p. 350, 1969.

Pringle, R., Jr., "On the Stability of a Body with Connected Moving Parts," *American Institute of Astronautics and Aeronautics J.* 4(8), p. 1395, 1966.

Pringle, R., Jr., "The Stability of the Force-Free Motions of a Dual-Spin Spacecraft," *American Institute of Astronautics and Aeronautics J.* 7(6), p. 1054, 1969.

Puri, N. N., and Gido, J. F., "Nutational Stability Criteria for a Dual-Spin Spacecraft–The Damper Reaction Torque and Quadratic Function Method," 19th Congress of the International Astronautical Federation, International Astronautical Federation Paper No. AT-103, 1968.

Russell, W. J., "Comments on 'Energy Considerations for Attitude Stability of Dual-Spin Spacecraft'," *J. Spacecr. Rockets* 6(3), p. 351, 1969.

Velman, J. R., "Attitude Dynamics of Dual-Spin Satellites," Hughes Aircraft Company SSD 60419R, Culver City, Calif., 1966.

Appendix I

Derivation of the Equations of Motion for the System

First, the Lagrangian will be determined for the system. It will then be substituted into Lagrange's equations of motion with the angular velocities in the spacecraft-fixed coordinate system as quasi-generalized velocities and the displacements of the dampers' active masses as generalized coordinates:

$$\frac{d}{dt}\left(\frac{\partial \mathcal{L}}{\partial \omega_1}\right) + \omega_2 \frac{\partial \mathcal{L}}{\partial \omega_3} - \omega_3 \frac{\partial \mathcal{L}}{\partial \omega_2} = 0 ,$$

$$\frac{d}{dt}\left(\frac{\partial \mathcal{L}}{\partial \omega_2}\right) + \omega_3 \frac{\partial \mathcal{L}}{\partial \omega_1} - \omega_1 \frac{\partial \mathcal{L}}{\partial \omega_3} = 0 ,$$

$$\frac{d}{dt}\left(\frac{\partial \mathcal{L}}{\partial \omega_3}\right) + \omega_1 \frac{\partial \mathcal{L}}{\partial \omega_2} - \omega_2 \frac{\partial \mathcal{L}}{\partial \omega_1} = 0 ,$$

$$\frac{d}{dt}\left(\frac{\partial \mathcal{L}}{\partial \dot{z}}\right) - \frac{\partial \mathcal{L}}{\partial z} = Q_z ,$$

and

$$\frac{d}{dt}\left(\frac{\partial \mathcal{L}}{\partial \dot{z}'}\right) - \frac{\partial \mathcal{L}}{\partial z'} = Q_{z'} .$$

The kinetic energy T will be developed in three steps:

T_0 = kinetic energy of the system with $z = \dot{z} = z' = \dot{z}' = 0$, rotating about and translating with respect to the true center of mass.

T_1 = additional kinetic energy of the spacecraft damper active mass due to z and $\dot{z} \neq 0$.

T_2 = additional kinetic energy of the wheel damper active mass due to z' and $\dot{z}' \neq 0$.

The total kinetic energy will then be $T = T_0 + T_1 + T_2$.

The center of mass of the system will lie along the nominal spin axis at a distance $\bar{z}$ above the spacecraft center of mass, as depicted in Figure I.1.

Since the total mass of the wheel is $M' + 4m_b'$ and the total mass of the spacecraft is $M + 4m_b$, $\bar{z}$ becomes

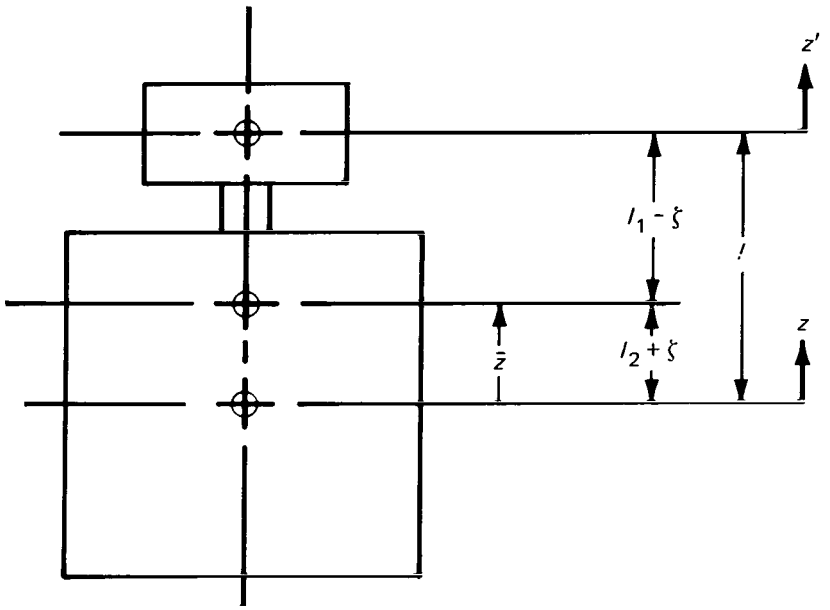

Figure I.1—System center of mass.

$$\bar{z} = \frac{(M' + 4m_b' - m')l + m'(l + z') + mz}{M_T} ,$$

where

$$M_T = M + 4m_b + M' + 4m_b'$$

is the total mass of the system.

If

$$l_1 = \frac{M + 4m_b}{M_T} l$$

and

$$l_2 = \frac{M' + 4m_b'}{M_T} l ,$$

then

$$\bar{z} = l_2 + \frac{mz + m'z'}{M_T}$$

$$= l_2 + \zeta$$

and

$$l - \bar{z} = l_1 - \zeta ,$$

where

$$\rho = \frac{m}{M_T} ,$$

$$\rho' = \frac{m'}{M_T} ,$$

and

$$\zeta = \rho z + \rho' z' .$$

Translation of the system relative to the center of mass is along the nominal spin axis at a rate $\dot{\zeta}$. Thus, the translational kinetic energy is simply $\frac{1}{2}M_T\dot{\zeta}^2$.

The transverse moment of inertia of the nominal system about the true center of mass is

$$I_1 + 2m_b a^2 + (M + 4m_b)(l_2 + \zeta)^2 + I_1' + 2m_b' a'^2 + (M' + 4m_b')(l_1 - \zeta)^2 = A + M_T\zeta^2 .$$

In the above equation,

$$A = I_1 + I_1' + 2m_b a^2 + 2m_b' a'^2 + (M' + 4m_b')(1 - \nu)l^2 ,$$

where

$$\nu = \frac{M' + 4m_b'}{M_T} .$$

The transverse kinetic energy of rotation of the system is thus $\frac{1}{2}(A + M_T\zeta^2)(\omega_1^2 + \omega_2^2)$.

The kinetic energy of rotation about the nominal spin axis is

$$\tfrac{1}{2}(I_3 + 4m_b a^2)\omega_3^2 + \tfrac{1}{2}(I_1' + 4m_b' a'^2)(\omega_3 + \sigma)^2 = \tfrac{1}{2}C\omega_3^2 + \tfrac{1}{2}J_3'\sigma(2\omega_3 + \sigma) ,$$

where

$$C = I_3 + 4m_b a^2 + I_3' + 4m_b' a'^2$$

and

$$J_3' = I_3' + 4m_b' a'^2 .$$

Combining the above quantities yields

$$T_0 = \tfrac{1}{2}M_T\dot{\zeta}^2 + \tfrac{1}{2}C\omega_3^2 + \tfrac{1}{2}J_3'\sigma(2\omega_3 + \sigma) + \tfrac{1}{2}(A + M_T\zeta^2)(\omega_1^2 + \omega_2^2) .$$

Determination of T_1

Now, $T_1 = \frac{1}{2}m(v^2 - v_0^2)$, where v is the actual velocity of the active mass of the spacecraft damper and v_0 is the velocity of the same mass if $z = \dot{z} = 0$. Let $\mathbf{r}_m$ be the position vector for the mass m. Expressed as a column matrix,

$$\mathbf{r}_m = \begin{pmatrix} a \\ 0 \\ z - l_2 - \zeta \end{pmatrix}.$$

Figure I.2 shows the positions of the mass m, the system center of mass, and the total angular velocity vector $\boldsymbol{\omega}_T$ in a spacecraft-fixed coordinate frame.

Now,

$$\boldsymbol{\omega}_T \times \mathbf{r}_m = \begin{vmatrix} \mathbf{i} & \mathbf{j} & \mathbf{k} \\ \omega_1 & \omega_2 & \omega_3 \\ a & 0 & z - l_2 - \zeta \end{vmatrix}.$$

Thus,

$$\mathbf{v} = \begin{pmatrix} \omega_2(z - l_2 - \zeta) \\ a\omega_2 - \omega_1(z - l_2 - \zeta) \\ \dot{z} - \dot{\zeta} \end{pmatrix},$$

and

$$\mathbf{v}_0 = \begin{pmatrix} \omega_2(-l_2 - \zeta) \\ a\omega_2 - \omega_1(-l_2 - \zeta) \\ -\dot{\zeta} \end{pmatrix}.$$

Then,

$$\mathbf{v} = \mathbf{v}_0 + \delta\mathbf{v},$$

where

$$\delta\mathbf{v} = \begin{pmatrix} z\omega_2 \\ -z\omega_1 \\ \dot{z} \end{pmatrix}.$$

Hence,

$$v^2 - v_0^2 = 2\mathbf{v}_0 \cdot \delta\mathbf{v} + (\delta\mathbf{v})^2$$

$$= 2\left\{[\omega_2(-l_2 - \zeta)z\omega_2] + [a\omega_2 - \omega_1(-l_2 - \zeta)](-z\omega_1) + (-\dot{\zeta})\dot{z}\right\} + z^2\omega_2^2 + z^2\omega_1^2 + \dot{z}^2$$

and

$$T_1 = \tfrac{1}{2}m\left\{2\omega_2 z[-\omega_2(l_2 + \zeta)] + \omega_2^2 z^2 - 2\omega_1 z[a\omega_3 + \omega_1(l_2 + \zeta)] + \omega_1^2 z^2 - 2\dot{z}(\dot{\zeta} + a\omega_2) + \dot{z}^2\right\}.$$

Determination of T_2

Now, $T_2 = \frac{1}{2}m'(v'^2 - v_0'^2)$, where v' is the actual velocity of the active mass of the wheel damper and v_0' is the velocity of the same mass if $z' = \dot{z}' = 0$. Let $\mathbf{r}'$ be the position vector for the mass m' (Figure I.3). Then,

$$\mathbf{r}' = \begin{pmatrix} a' \cos\psi \\ a' \sin\psi \\ z' + l_1 - \zeta \end{pmatrix}$$

and

$$\boldsymbol{\omega}_T \times \mathbf{r}' = \begin{vmatrix} \mathbf{i} & \mathbf{j} & \mathbf{k} \\ \omega_1 & \omega_2 & \omega_3 \\ a' \cos\psi & a' \sin\psi & z' + l_1 - \zeta \end{vmatrix}.$$

Thus,

$$\mathbf{v}' = \begin{pmatrix} -a'\sigma \sin\psi + \omega_2(z' + l_1 - \zeta) - \omega_3 a' \sin\psi \\ a'\sigma \cos\psi + \omega_3 a' \cos\psi - \omega_1(z' + l_1 - \zeta) \\ \dot{z}' - \dot{\zeta} + \omega_1 a' \sin\psi - \omega_2 a' \cos\psi \end{pmatrix},$$

$$\mathbf{v}_0' = \begin{pmatrix} -a'\sigma \sin\psi + \omega_2(l_1 - \zeta) - \omega_3 a' \sin\psi \\ a'\sigma \cos\psi + \omega_3 a' \cos\psi - \omega_1(l_1 - \zeta) \\ -\dot{\zeta} + \omega_1 a' \sin\psi - \omega_2 a' \cos\psi \end{pmatrix},$$

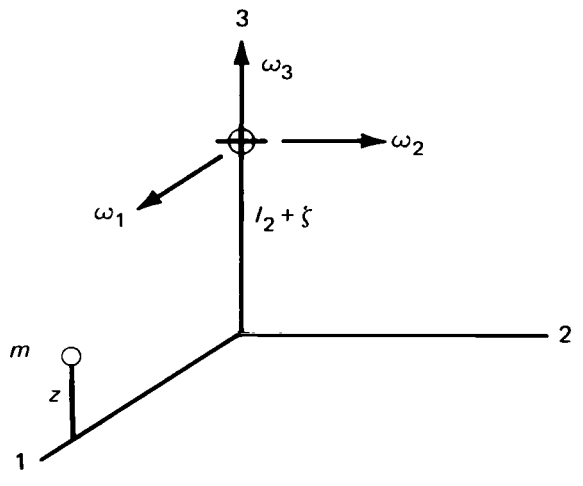

Figure I.2—Spacecraft damper position.

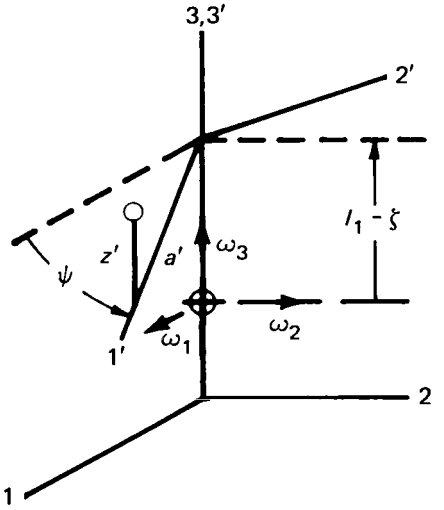

Figure I.3—Wheel damper position.

and

$$\mathbf{v}' = \mathbf{v}_0' + \delta\mathbf{v}' ,$$

where

$$\delta\mathbf{v}' = \begin{pmatrix} z'\omega_2 \\ -z'\omega_1 \\ \dot{z}' \end{pmatrix} .$$

Thus,

$$\begin{aligned} v'^2 - v_0'^2 &= 2\mathbf{v}_0' \cdot \delta\mathbf{v}' + (\delta\mathbf{v}')^2 \\ &= 2\{[-a'\sigma \sin\psi + \omega_2(l_1 - \zeta) - \omega_3 a' \sin\psi](z'\omega_2) \\ &\quad + [a'\sigma \cos\psi + \omega_3 a' \cos\psi - \omega_1(l_1 - \zeta)](-z'\omega_1) \\ &\quad + (-\dot{\zeta} + \omega_1 a' \sin\psi - \omega_2 a' \cos\psi)\dot{z}'\} + z'^2\omega_2^2 + z'^2\omega_1^2 + \dot{z}'^2 . \end{aligned}$$

Thus, T_2 becomes

$$\begin{aligned} T_2 = \tfrac{1}{2}m'\{&2z'\omega_2[-a'\sigma \sin\psi + \omega_2(l_1 - \zeta) - \omega_3 a' \sin\psi] + z'^2\omega_2^2 \\ &- 2z'\omega_1[a'\sigma \cos\psi + \omega_3 a' \cos\psi - \omega_1(l_1 - \zeta)] + z'^2\omega_1^2 \\ &+ 2\dot{z}'[-\dot{\zeta} + \omega_1 a' \sin\psi - \omega_2 a' \cos\psi] + \dot{z}'^2\} , \end{aligned}$$

and the total kinetic energy of the system is

$$\begin{aligned} T = \tfrac{1}{2}M_T\dot{\zeta}^2 &+ \tfrac{1}{2}C\omega_3^2 + \tfrac{1}{2}J_3'\sigma(2\omega_3 + \sigma) + \tfrac{1}{2}(A - M_T\zeta^2)(\omega_1^2 + \omega_2^2) \\ &+ \tfrac{1}{2}m\{2\omega_2 z[-\omega_2(l_2 + \zeta)] + \omega_2^2 z^2 - 2\omega_1 z[a\omega_3 + \omega_1(l_2 + \zeta)] + \omega_1^2 z \\ &- 2\dot{z}(\dot{\zeta} + a\omega_2) + \dot{z}^2\} + \tfrac{1}{2}m'\{2z'\omega_2[-a'\sigma \sin\psi + \omega_2(l_1 - \zeta) - \omega_3 a' \sin\psi] \\ &+ z'^2\omega_2^2 - 2z'\omega_1[a'\sigma \cos\psi + \omega_3 a' \cos\psi - \omega_1(l_1 - \zeta)] + z'^2\omega_1^2 \\ &+ 2\dot{z}'(-\dot{\zeta} + \omega_1 a' \sin\psi - \omega_2 a' \cos\psi) + \dot{z}'^2\} . \end{aligned}$$

The potential energy of the system is that energy stored in the damper springs, i.e., $V = \tfrac{1}{2}kz^2 + \tfrac{1}{2}k'z'^2$; and the generalized forces associated with the coordinates z and z' are the viscous drag forces $Q_z = -c\dot{z}$ and $Q_{z'} = -c'\dot{z}'$. The Lagrangian is, of course, $\mathcal{L} = T + V$, and the partial derivatives (and their time derivatives) necessary for construction of the equations of motion for the system are as follows:

$$\frac{\partial \mathcal{L}}{\partial \omega_1} = \frac{\partial T}{\partial \omega_1}$$

$$= (A + M_T\zeta^2)\omega_1 + m\{\omega_1[z^2 - 2z(l_2 + \zeta)] - za\omega_3\} - m'[z'a' \cos\psi\,(\omega_3 + \sigma) - \dot{z}'a' \sin\psi]$$

$$+ m'\omega_1[z'^2 + 2z'(l_1 - \zeta)]\,,$$

$$\frac{d}{dt}\frac{\partial \mathcal{L}}{\partial \omega_1} = \{A + M_T\zeta^2 + m[z^2 - 2z(l_2 + \zeta)] + m'[z'^2 + 2z'(l_1 - \zeta)]\}\dot{\omega}_1 + \omega_1\{2M_T\zeta\dot{\zeta}$$

$$+ m[2z\dot{z} - 2z\dot{\zeta} - 2\dot{z}(l_2 + \zeta)] + m'[2z'\dot{z}' - 2z'\dot{\zeta} + 2\dot{z}'(l_1 - \zeta)]\} + m'a' \sin\psi\,\ddot{z}' - maz\dot{\omega}_3$$

$$- ma\dot{z}\omega_3 - m'[z'a' \cos\psi\,\dot{\omega}_3 - \dot{z}'a'\sigma \cos\psi + (\omega_3 + \sigma)(\dot{z}'a' \cos\psi - z'a'\sigma \sin\psi)]\,,$$

$$\frac{\partial \mathcal{L}}{\partial \omega_2} = \frac{\partial T}{\partial \omega_2}$$

$$= [A + M_T\zeta^2 + mz^2 - 2mz(l_2 + \zeta) + m'z'^2 + 2m'z'(l_1 - \zeta)]\omega_2 - ma\dot{z} - m'a'z' \sin\psi\,(\omega_3 + \sigma)$$

$$- m'a' \cos\psi\,\dot{z}'\,,$$

$$\frac{d}{dt}\frac{\partial \mathcal{L}}{\partial \omega_2} = [A + M_T\zeta^2 + mz^2 - 2mz(l_2 + \zeta) + m'z'^2 + 2m'z'(l_1 - \zeta)]\dot{\omega}_2 + \omega_2[2M_T\zeta\dot{\zeta} + 2mz\dot{z}$$

$$- 2mz\dot{\zeta} - 2m\dot{z}(l_2 + \zeta) + 2m'z'\dot{z}' + 2m'\dot{z}'(l_1 - \zeta) - 2m'z'\dot{\zeta}] - ma\ddot{z} - m'a'z' \sin\psi\,\dot{\omega}_3$$

$$- m'a'(\omega_3 + \sigma)(\dot{z}' \sin\psi + z'\sigma \cos\psi) - m'a' \cos\psi\,\ddot{z}' + m'a'\dot{z}'\sigma \sin\psi\,,$$

$$\frac{\partial \mathcal{L}}{\partial \omega_3} = \frac{\partial T}{\partial \omega_3}$$

$$= C\omega_3 + J_3'\sigma - maz\omega_1 - m'a'z'(\omega_2 \sin\psi + \omega_1 \cos\psi)\,,$$

$$\frac{d}{dt}\frac{\partial \mathcal{L}}{\partial \omega_3} = C\dot{\omega}_3 - ma(z\dot{\omega}_1 + \dot{z}\omega_1) - m'a'\dot{z}'(\omega_2 \sin\psi + \omega_1 \cos\psi) - m'a'z'(\sin\psi\,\dot{\omega}_2 - \cos\psi\,\sigma\omega_2$$

$$+ \cos\psi\,\dot{\omega}_1 - \sin\psi\,\sigma\omega_1)\,,$$

$$\frac{\partial \mathcal{L}}{\partial \dot{z}} = \frac{\partial T}{\partial \dot{z}}$$

$$= -m'\dot{z}'\rho + m\dot{z} - m\rho\dot{z} - ma\omega_2\,,$$

$$\frac{d}{dt}\frac{\partial \mathcal{L}}{\partial \dot{z}} = -m'\ddot{z}'\rho + m(1 - \rho)\ddot{z} - ma\dot{\omega}_2\,,$$

$$\frac{\partial \mathcal{L}}{\partial z} = \frac{\partial T}{\partial z} - \frac{\partial V}{\partial z}$$

$$= mz(\omega_1^2 + \omega_2^2) - m(l_2 + \rho' z')(\omega_1^2 + \omega_2^2) - m\rho z(\omega_1^2 + \omega_2^2) - ma\omega_1\omega_3 - kz \ ,$$

$$\frac{\partial \mathcal{L}}{\partial \dot{z}'} = \frac{\partial T}{\partial \dot{z}'}$$

$$= m'\dot{z}' + m'(-\rho\dot{z} - \rho'\dot{z}' + \omega_1 a' \sin\psi - \omega_2 a' \cos\psi) \ ,$$

$$\frac{d}{dt}\frac{\partial \mathcal{L}}{\partial \dot{z}'} = m'[(1-\rho')\ddot{z}' - \rho\ddot{z} + \dot{\omega}_1 a' \sin\psi - \omega_1 a' \cos\psi\, \sigma - \dot{\omega}_2 a' \cos\psi + \omega_2 a' \sin\psi\, \sigma] \ ,$$

and

$$\frac{\partial \mathcal{L}}{\partial z'} = \frac{\partial T}{\partial z'} - \frac{\partial V}{\partial z'}$$

$$= m'\omega_2[-a'\sigma \sin\psi + \omega_2(l_1 - \rho z) - \omega_3 a' \sin\psi] - m'\rho' z'\omega_2^2 + m'z'(\omega_1^2 + \omega_2^2) - m'\rho' z'\omega_1^2 - k'z'$$

$$- m'\omega_1[a'\sigma \cos\psi + \omega_3 a' \cos\psi - \omega_1(l_1 - \rho z)] \ .$$

The resulting equations of motion are

$$[A + M_T\xi^2 + mz^2 - 2m(\xi + l_2)z + m'z'^2 - 2m'(\xi - l_1)z']\dot{\omega}_1 - (maz + m'a'z' \cos\psi)\dot{\omega}_3 + m'a' \sin\psi\, \ddot{z}'$$

$$= (A - C)\omega_2\omega_3 - J_3'\sigma\omega_2 - 2M_T\xi\dot{\xi}\omega_1 + M_T\xi^2\omega_2\omega_3 + 2m(\xi + l_2)(\dot{z}\omega_1 - z\omega_2\omega_3)$$

$$+ mz(2\dot{\xi}\omega_1 - 2\dot{z}\omega_1 + z\omega_2\omega_3 + a\omega_1\omega_2) + 2m'(\xi - l_1)(\dot{z}'\omega_1 - z'\omega_2\omega_3)$$

$$+ m'z'(2\dot{\xi}\omega_1 - 2\dot{z}'\omega_1 + z'\omega_2\omega_3 + a' \cos\psi\, \omega_1\omega_2) - m'a' \sin\psi\, z'[(\omega_3 + \sigma)^2 - \omega_2^2] \ , \quad (2.1)$$

$$[A + M_T\xi^2 + mz^2 - 2m(\xi + l_2)z + m'z'^2 - 2m'(\xi - l_1)z']\dot{\omega}_2 - m'a' \sin\psi\, z'\dot{\omega}_3 - ma\ddot{z} - m'a' \cos\psi\, \ddot{z}'$$

$$= (C - A)\omega_1\omega_3 + J_3'\sigma\omega_1 - 2M_T\xi\dot{\xi}\omega_2 - M_T\xi^2\omega_1\omega_3 + 2m(\xi + l_2)(\dot{z}\omega_2 + z\omega_1\omega_3)$$

$$+ mz(2\dot{\xi}\omega_2 - 2\dot{z}\omega_2 - z\omega_1\omega_3) + maz(\omega_3^2 - \omega_1^2) + 2m'(\xi - l_1)(z'\omega_1\omega_3 + \dot{z}'\omega_2)$$

$$+ m'z'(2\dot{\xi}\omega_2 - 2\dot{z}'\omega_2 - z'\omega_1\omega_3) + m'z'[(\omega_3 + \sigma)^2 - \omega_1^2]a' \cos\psi - m'a' \sin\psi\, z'\omega_1\omega_2 \ , \quad (2.2)$$

$$-(maz + m'a'z' \cos\psi)\dot{\omega}_1 - m'a' \sin\psi\, z'\dot{\omega}_2 + C\dot{\omega}_3$$

$$= ma(2\dot{z}\omega_1 - z\omega_2\omega_3) + m'a' \sin\psi\, (2\dot{z}'\omega_2 + z'\omega_1\omega_3) + m'a' \cos\psi\, (2\dot{z}'\omega_1 - z'\omega_2\omega_3) \ , \quad (2.3)$$

$$-ma\dot{\omega}_2 + m(1-\rho)\ddot{z} - m'\rho\ddot{z}' = -ma\omega_1\omega_3 + m(\omega_1^2 + \omega_2^2)[z(1-\rho) - l_2 - \rho' z'] - c\dot{z} - kz \ , \quad (2.4)$$

and

$$m'a' \sin\psi\ \dot{\omega}_1 - m'a' \cos\psi\ \dot{\omega}_2 - m\rho'\ddot{z} + m'(1-\rho')\ddot{z}'$$

$$= -m'a'[\sin\psi\ \omega_2(\omega_3 + 2\sigma) + \cos\psi\ \omega_1(\omega_3 + 2\sigma)]$$

$$+ m'(\omega_1^2 + \omega_2^2)[z'(1-\rho') + l_1 - \rho z] - c'\dot{z}' - k'z' \ . \quad (2.5)$$

Appendix II

Damper Size Limitations Imposed by Routhian Analyses When Dampers Are Tuned

In Reference 11, Mingori explored a parameter space with $\delta = ma^2/A$ and $\delta' = m'a'^2/A$ in the range from 0.001 to 0.100. Of additional interest, however, is the behavior of the system when one or the other of these parameters vanishes, i.e., on the δ and δ' axes. The results of Mingori's Routhian analysis are then applicable, and we deduce that three of the five inequalities produced by this analysis are not of particular concern to us here. Two of them are trivially satisfied for practical systems, and the other represents the stability criteria which have been shown to be in agreement with that determined for these special cases in the research reported here.

The following inequalities, however, must also be satisfied for stability, and they depend on the size of the damper masses. In Mingori's notation, these are

$$K + \delta^2(\Lambda^2 - r_\Omega^2 - \Lambda r_\Omega) > 0 \tag{II.1}$$

and

$$\Lambda(\Lambda K - \delta^2 r_\Omega^3) > 0 \,, \tag{II.2}$$

for damping on the spacecraft only, and

$$K' + \delta'^2[(\Lambda - r_\sigma)^2 - (\Lambda + r_\Omega)(r_\sigma + r_\Omega)] > 0 \tag{II.3}$$

and

$$(\Lambda - r_\sigma)[(\Lambda - r_\sigma)K' - \delta'^2(r_\Omega + r_\sigma)^3] > 0 \,, \tag{II.4}$$

for damping on the wheel only.

Before attempting a Floquet analysis of the general case (i.e., damping on both bodies), Mingori made the assumptions that $\rho = \delta$ and $\rho' = \delta'$ and tuned the dampers such that

$$K = \delta(1 - \delta)\Lambda^2 \tag{II.5}$$

and

$$K' = \delta'(1 - \delta')(\Lambda - r_\sigma)^2 \,. \tag{II.6}$$

Substituting Equations II.5 and II.6 into Equations II.1 through II.4 produces the modified Routhian inequalities

$$\Lambda^2 - \delta r_\Omega (r_\Omega + \Lambda) > 0 \,, \tag{II.7}$$

$$\Lambda^4 - \delta\Lambda(\Lambda^3 + r_\Omega^3) > 0 \,, \tag{II.8}$$

$$(\Lambda - r_\sigma)^2 - \delta'(\Lambda + r_\Omega)(r_\sigma + r_\Omega) > 0 \,, \tag{II.9}$$

and

$$(\Lambda - r_\sigma)^4 - \delta'[(\Lambda - r_\sigma)^3 + (r_\Omega + r_\sigma)^3] > 0 \,, \tag{II.10}$$

where

$$\Lambda = \frac{(q-1)\Omega_0 + q'\sigma}{\eta}$$

$$= \frac{\lambda_0}{\eta} \,,$$

$$r_\Omega = \frac{\Omega_0}{\eta} \,,$$

$$r_\sigma = \frac{\sigma}{\eta} \,,$$

and

$$\eta = |q\Omega_0 + q'\sigma| \,.$$

In terms of more familiar quantities, we have

$$\lambda_0^2 - \delta\Omega_0(\Omega_0 + \lambda_0) > 0 \,, \tag{II.11}$$

$$\lambda_0^4 - \delta\lambda_0(\lambda_0^3 + \Omega_0^3) > 0 \,, \tag{II.12}$$

$$(\lambda_0 - \sigma)^2 - \delta'(\lambda_0 + \Omega_0)(\Omega_0 + \sigma) > 0 \,, \tag{II.13}$$

and

$$(\lambda_0 - \sigma)^4 - \delta'(\lambda_0 - \sigma)[(\lambda_0 - \sigma)^3 + (\Omega_0 + \sigma)^3] > 0 \,. \tag{II.14}$$

Rearranging to see the corresponding damper size limitations, we have

$$\delta\left[\frac{1 + \dfrac{\lambda_0}{\Omega_0}}{\left(\dfrac{\lambda_0}{\Omega_0}\right)^2}\right] < 1 \,, \tag{II.15}$$

$$\delta\left[\frac{1+\left(\frac{\lambda_0}{\Omega_0}\right)^3}{\left(\frac{\lambda_0}{\Omega_0}\right)^3}\right]<1\,, \tag{II.16}$$

$$\delta'\left[\frac{\left(1+\frac{\lambda_0}{\Omega_0}\right)\left(1+\frac{\sigma}{\Omega_0}\right)}{\left(\frac{\lambda_0}{\Omega_0}-\frac{\sigma}{\Omega_0}\right)^2}\right]<1\,, \tag{II.17}$$

and

$$\delta'\left[\frac{\left(\frac{\lambda_0}{\Omega_0}-\frac{\sigma}{\Omega_0}\right)^3+\left(1+\frac{\sigma}{\Omega_0}\right)^3}{\left(\frac{\lambda_0}{\Omega_0}-\frac{\sigma}{\Omega_0}\right)^3}\right]<1\,. \tag{II.18}$$

Appendix III

Derivation of Quadratic When F = 0

Consider

$$\lambda_0(2\sigma - \lambda_0 + \Omega_0) = \pm\beta(\sigma - \lambda_0)(\lambda - \Omega_0) .$$

Let

$$\lambda_0 = (q - 1)\Omega_0 + q'\sigma .$$

Then

$$\left(q - 1 + q'\frac{\sigma}{\Omega_0}\right)\left[2 - q + (2 - q')\frac{\sigma}{\Omega_0}\right] = \pm\beta\left[(1 - q')\frac{\sigma}{\Omega_0} - q + 1\right]\left(q'\frac{\sigma}{\Omega_0} + q - 2\right) ,$$

or

$$[q'(2 - q') \pm \beta q'(q' - 1)]\left(\frac{\sigma}{\Omega_0}\right)^2 + [(q - 1)(2 - q') - q'(q - 2) \pm \beta q'(q - 1)$$

$$\pm \beta(1 - q')(2 - q)]\frac{\sigma}{\Omega_0} + (q - 1)(2 - q) \pm \beta(1 - q)(2 - q) = 0 .$$

For $q' = 0.2$, this becomes

$$(0.36 \mp 0.16\beta)\left(\frac{\sigma}{\Omega_0}\right)^2 + [1.6q - 1.4 \pm \beta(1.4 - 0.6q)]\frac{\sigma}{\Omega_0} + (1 \pm \beta)(q - 1)(2 - q) = 0 .$$

Appendix IV

Derivation of Equation 6.4

$$\begin{aligned}\mathbf{F}\times\boldsymbol{\rho}-\mathbf{r}_0\times(\mathbf{F}-\mathbf{F}_0) = m\Big\{&-2\boldsymbol{\rho}\times(\boldsymbol{\omega}_T\times\dot{\boldsymbol{\rho}})-\lambda(\mathbf{r}\cdot\mathbf{k})\boldsymbol{\rho}\times\boldsymbol{\omega}+\lambda(\mathbf{r}\cdot\boldsymbol{\omega})\boldsymbol{\rho}\times\mathbf{k}\\&-(\boldsymbol{\omega}_T\cdot\mathbf{r})\boldsymbol{\rho}\times\boldsymbol{\omega}_T+\omega_T^2\boldsymbol{\rho}\times\mathbf{r}-\mathbf{r}_0\times\ddot{\boldsymbol{\rho}}-2\mathbf{r}_0\times(\boldsymbol{\omega}_T\times\dot{\boldsymbol{\rho}})\\&-\lambda(\boldsymbol{\rho}\cdot\mathbf{k})\mathbf{r}_0\times\boldsymbol{\omega}+\lambda(\boldsymbol{\rho}\cdot\boldsymbol{\omega})\mathbf{r}_0\times\mathbf{k}-(\boldsymbol{\omega}_T\cdot\boldsymbol{\rho})\mathbf{r}_0\times\boldsymbol{\omega}_T+\omega_T^2\mathbf{r}_0\times\boldsymbol{\rho}\Big\}\\ = m\Big\{&-2\rho_1\dot{\rho}_1\boldsymbol{\omega}_T+2(\boldsymbol{\rho}\cdot\boldsymbol{\omega}_T)\dot{\boldsymbol{\rho}}-\lambda(\mathbf{r}\cdot\mathbf{k})\boldsymbol{\rho}\times\boldsymbol{\omega}+\lambda(\mathbf{r}\cdot\boldsymbol{\omega})\boldsymbol{\rho}\times\mathbf{k}\\&-(\boldsymbol{\omega}_T\cdot\mathbf{r})\boldsymbol{\rho}\times\boldsymbol{\omega}_T+\omega_T^2\boldsymbol{\rho}\times\mathbf{r}-\mathbf{r}_0\times\ddot{\boldsymbol{\rho}}-2(\mathbf{r}_0\cdot\boldsymbol{\rho})\boldsymbol{\omega}_T+2(\mathbf{r}_0\cdot\boldsymbol{\omega}_T)\dot{\boldsymbol{\rho}}\\&-\lambda(\boldsymbol{\rho}\cdot\mathbf{k})\mathbf{r}_0\times\boldsymbol{\omega}+\lambda(\boldsymbol{\rho}\cdot\boldsymbol{\omega})\mathbf{r}_0\times\mathbf{k}-(\boldsymbol{\omega}_T\cdot\boldsymbol{\rho})\mathbf{r}_0\times\boldsymbol{\omega}_T+\omega_T^2\mathbf{r}_0\times\boldsymbol{\rho}\Big\}\,.\end{aligned}$$

$$\begin{aligned}\mathbf{k}\cdot[\mathbf{F}\times\boldsymbol{\rho}+\mathbf{r}_0\times(\mathbf{F}-\mathbf{F}_0)] = m\Big\{&-2\rho_1\dot{\rho}_1\Omega+2(\boldsymbol{\rho}\cdot\boldsymbol{\omega}_T)\dot{\rho}_1e_3-\rho_1\lambda(z_0+\rho_1e_3)(e_1\omega_2-e_2\omega_1)\\&-(\boldsymbol{\omega}_T\cdot\mathbf{r})(e_1\omega_2-e_2\omega_1)\rho_1-e_2x_0\ddot{\rho}_1-\rho_1\lambda e_3x_0\omega_2\\&-(\boldsymbol{\omega}_T\cdot\boldsymbol{\rho})x_0\omega_2-2(\mathbf{r}_0\cdot\dot{\boldsymbol{\rho}})\Omega+2(\mathbf{r}_0\cdot\boldsymbol{\omega}_T)e_3\dot{\rho}_1\Big\}\,.\end{aligned}$$

"The aeronautical and space activities of the United States shall be conducted so as to contribute . . . to the expansion of human knowledge of phenomena in the atmosphere and space. The Administration shall provide for the widest practicable and appropriate dissemination of information concerning its activities and the results thereof."

—NATIONAL AERONAUTICS AND SPACE ACT OF 1958

NASA SCIENTIFIC AND TECHNICAL PUBLICATIONS

TECHNICAL REPORTS: Scientific and technical information considered important, complete, and a lasting contribution to existing knowledge.

TECHNICAL NOTES: Information less broad in scope but nevertheless of importance as a contribution to existing knowledge.

TECHNICAL MEMORANDUMS: Information receiving limited distribution because of preliminary data, security classification, or other reasons.

CONTRACTOR REPORTS: Scientific and technical information generated under a NASA contract or grant and considered an important contribution to existing knowledge.

TECHNICAL TRANSLATIONS: Information published in a foreign language considered to merit NASA distribution in English.

SPECIAL PUBLICATIONS: Information derived from or of value to NASA activities. Publications include conference proceedings, monographs, data compilations, handbooks, sourcebooks, and special bibliographies.

TECHNOLOGY UTILIZATION PUBLICATIONS: Information on technology used by NASA that may be of particular interest in commercial and other non-aerospace applications. Publications include Tech Briefs, Technology Utilization Reports and Technology Surveys.

Details on the availability of these publications may be obtained from:

SCIENTIFIC AND TECHNICAL INFORMATION OFFICE

NATIONAL AERONAUTICS AND SPACE ADMINISTRATION

Washington, D.C. 20546